



**The Abdus Salam
International Centre for Theoretical Physics**



2142-6

**Advanced Conference on Seismic Risk Mitigation and Sustainable
Development**

10 - 14 May 2010

**Dynamics of earthquake rupture
through branched and offset fault systems**

Renata Dmowska
*University of Harvard
Dept. of Earth and Planetary Sciences
USA*

Seismic Risk Mitigation and Sustainable Development

Abdus Salam International Centre for Theoretical Physics

Trieste, Italy, 10-14 May 2010

***Dynamics of earthquake rupture
through branched and offset fault systems***

Renata Dmowska (Harvard)

coworkers:

Harsha S. Bhat (Univ. So. Calif. & Caltech)

Sonia Fliss (Ecole Polytechnique & ENSTA, Paris)

Nobuki Kame (ERI, Univ. Tokyo)

Marion Olives (Paris)

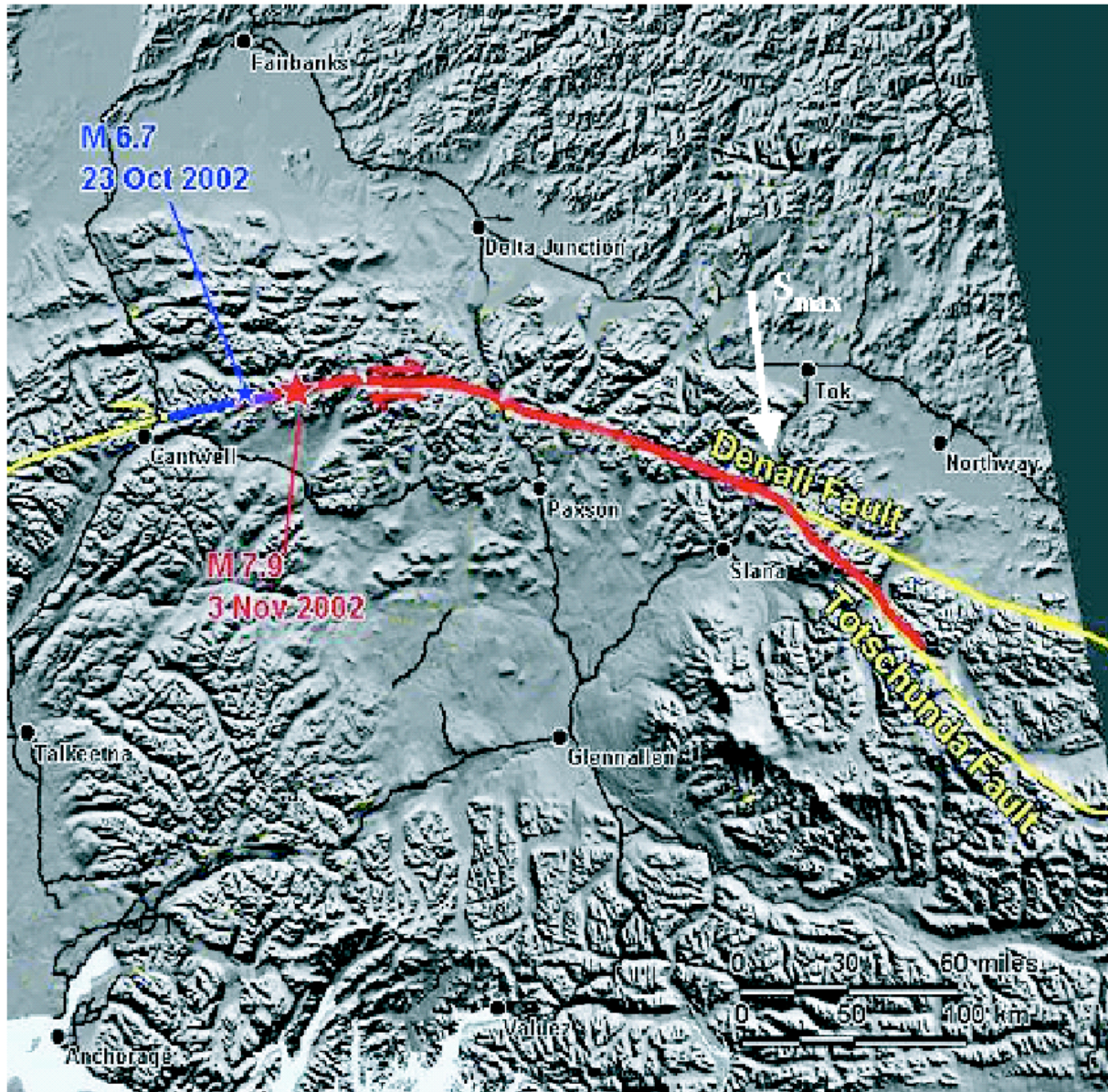
Alexei N. B. Poliakov (Moscow)

James R. Rice (Harvard)

The rupture zones of major earthquakes often involve geometric complexities, like fault bends, branches and stepovers.

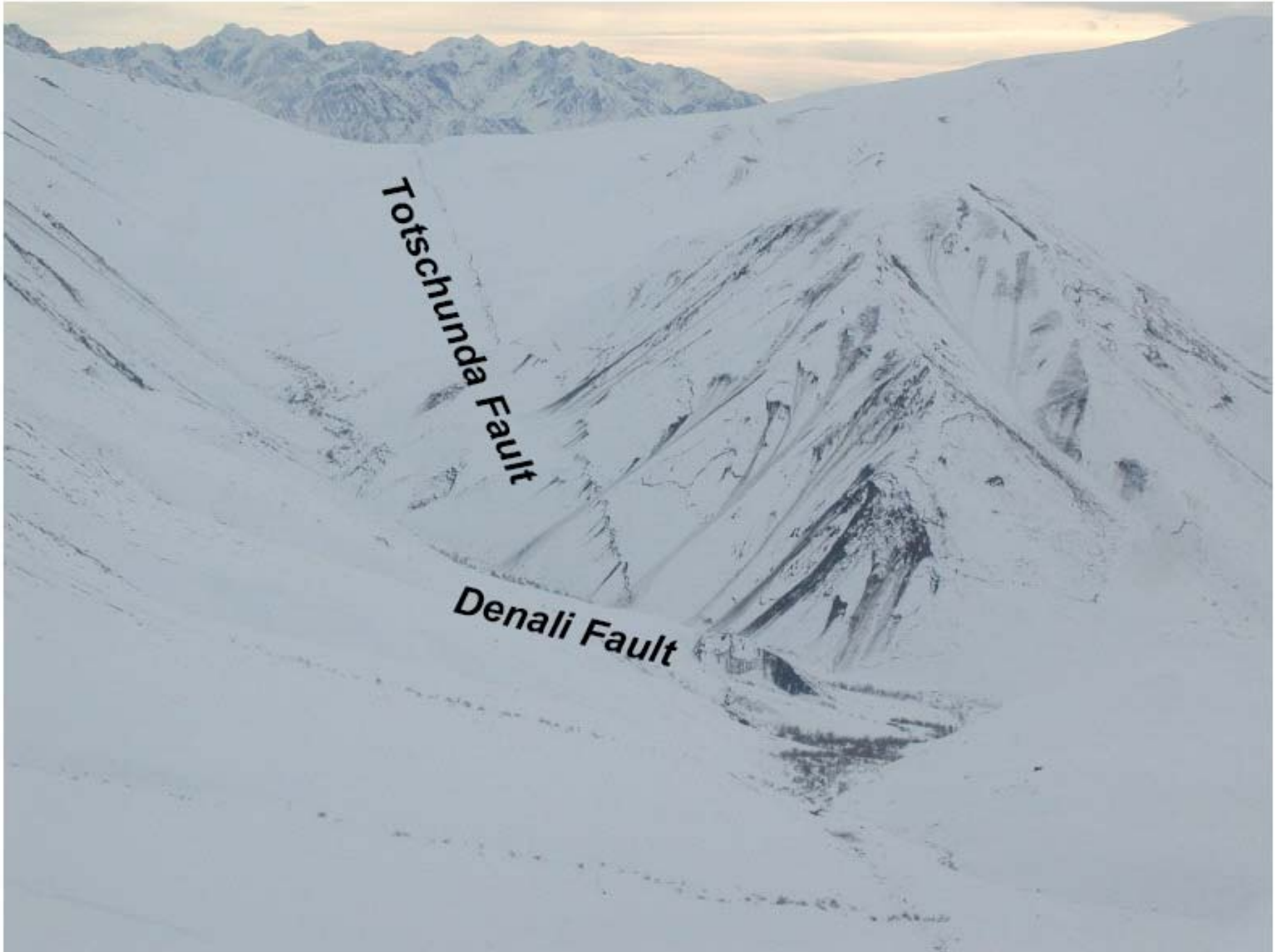
How does an earthquake rupture choose its path through such geometric complexities?

M_w 7.9 Denali Earthquake, 3 Nov 2002



Map provided by
P. Haeussler, *USGS*
Fairbanks, 2002

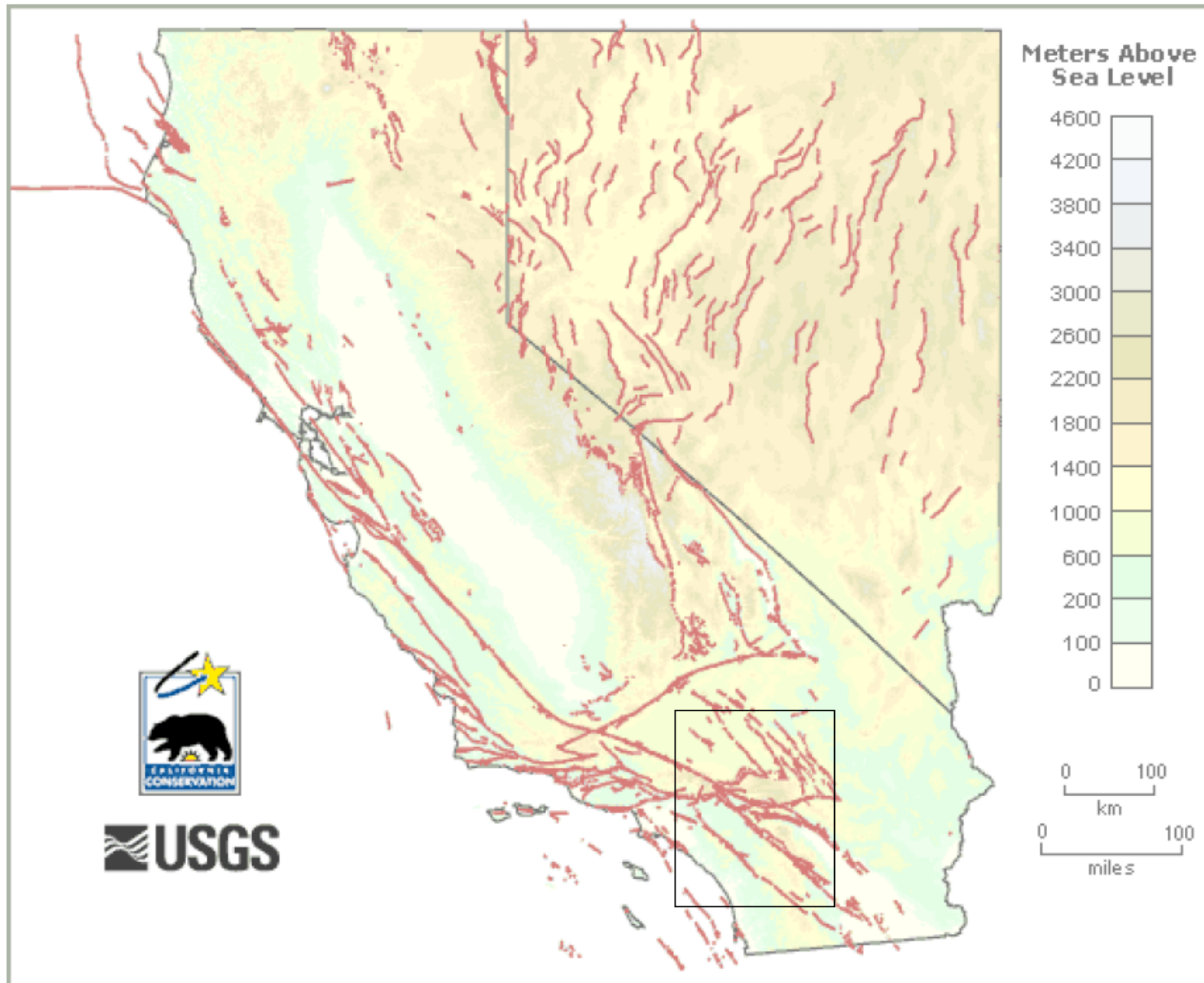
Stress direction at
branch junction
(white arrow) from
Ratchkovski and
Hansen (2002) and
earlier studies.



Totschunda Fault

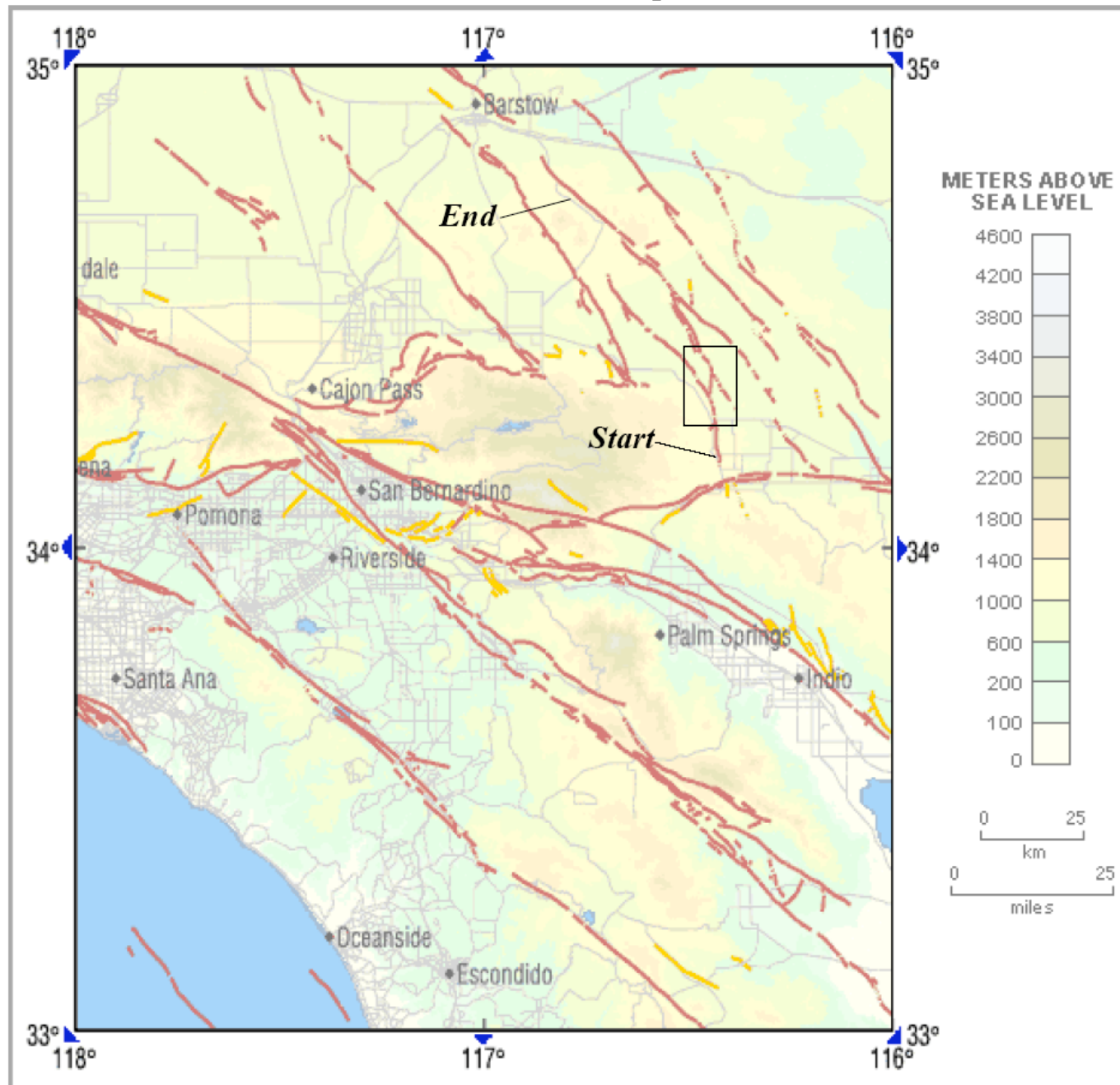
Denali Fault

California and Nevada -- active faults (from USGS)



Faults in Southern California, Mohave Area (from USGS)

Start and End of 1992 Landers rupture shown

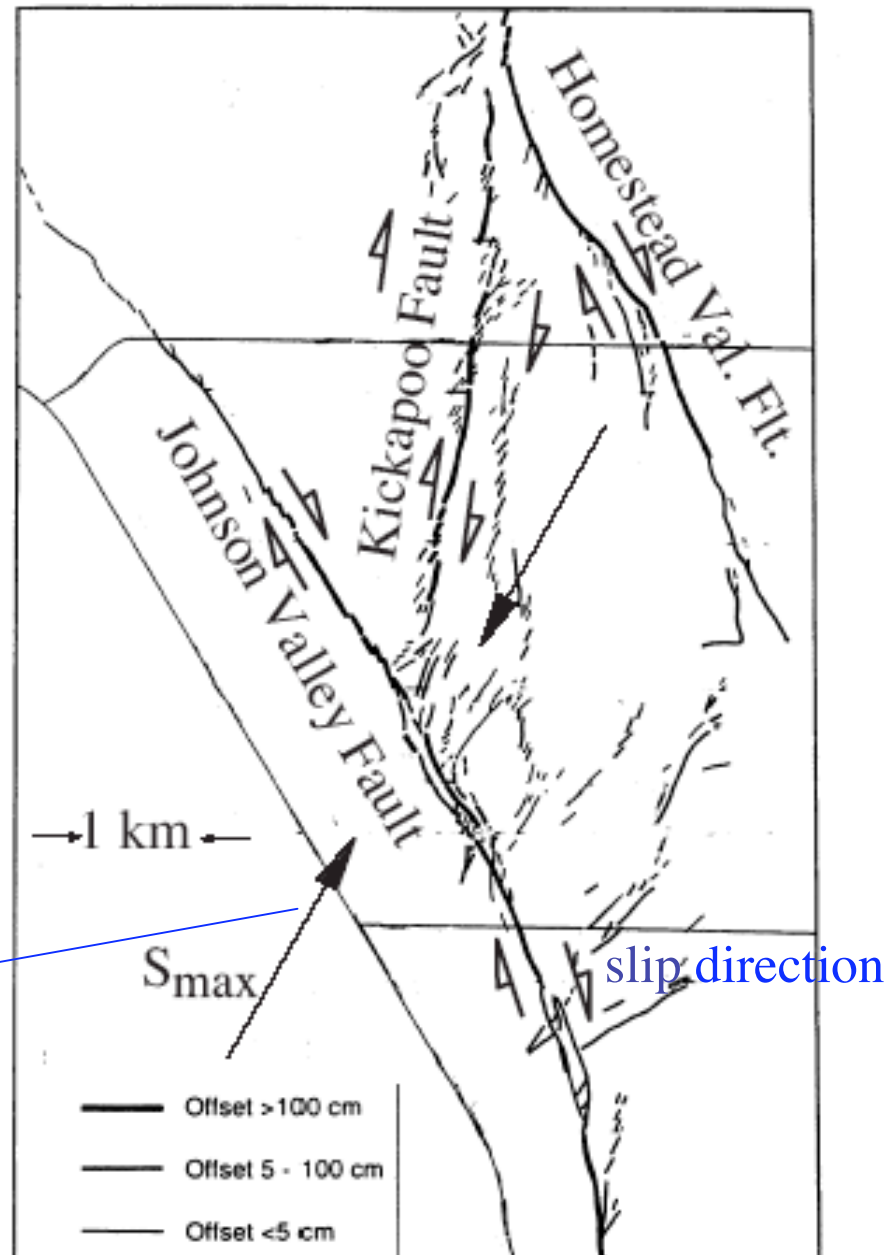


Landers 1992

Portion of 1992
Landers earthquake
rupture path
(transition from
Johnson Valley to
Kickapoo fault,
then to Homestead
Valley fault).

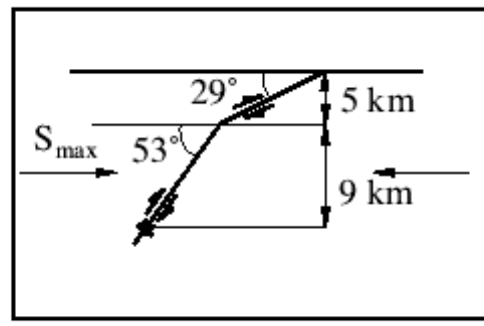
Fault map and slip,
Sowers et al. (1994).

Pre-stress direction,
Hardebeck and
Hauksson (2001).



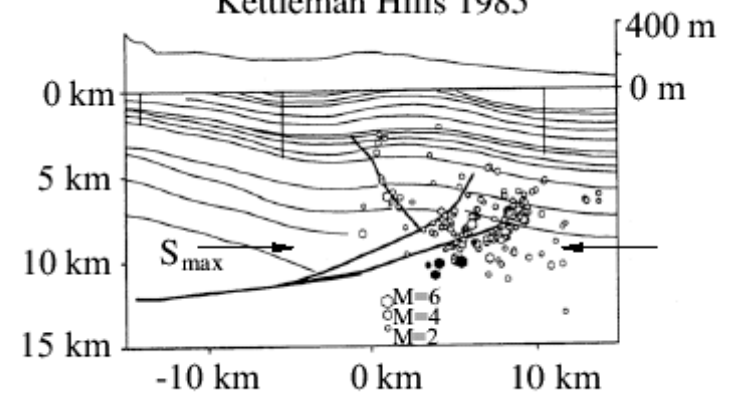
(Poliakov, Dmowska and Rice, *JGR*, 2002; Kame, Rice and Dmowska, *JGR*, 2003)

San Fernando 1971



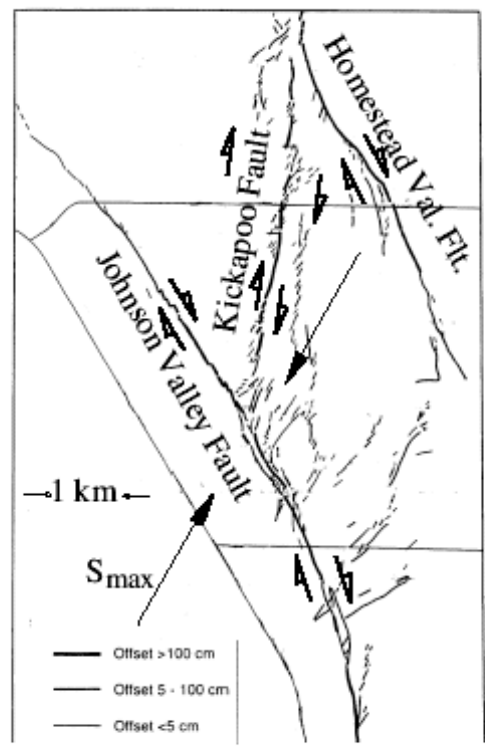
(Heaton and Helmberger, 1979)

Kettleman Hills 1985



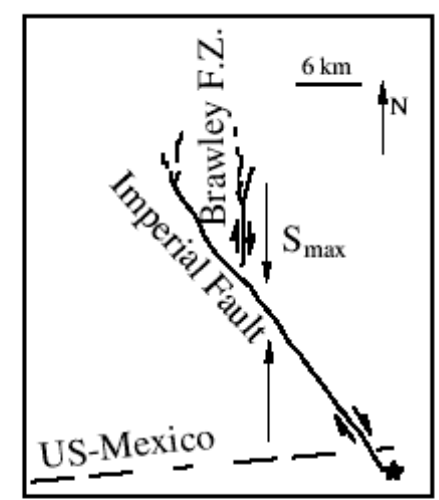
(Ekstrom et al., 1992; fault locations from Meltzer, 1989)

Landers 1992



(fault map from Sowers et al., 1994; stress from Hardebeck and Hauksson, 2001)

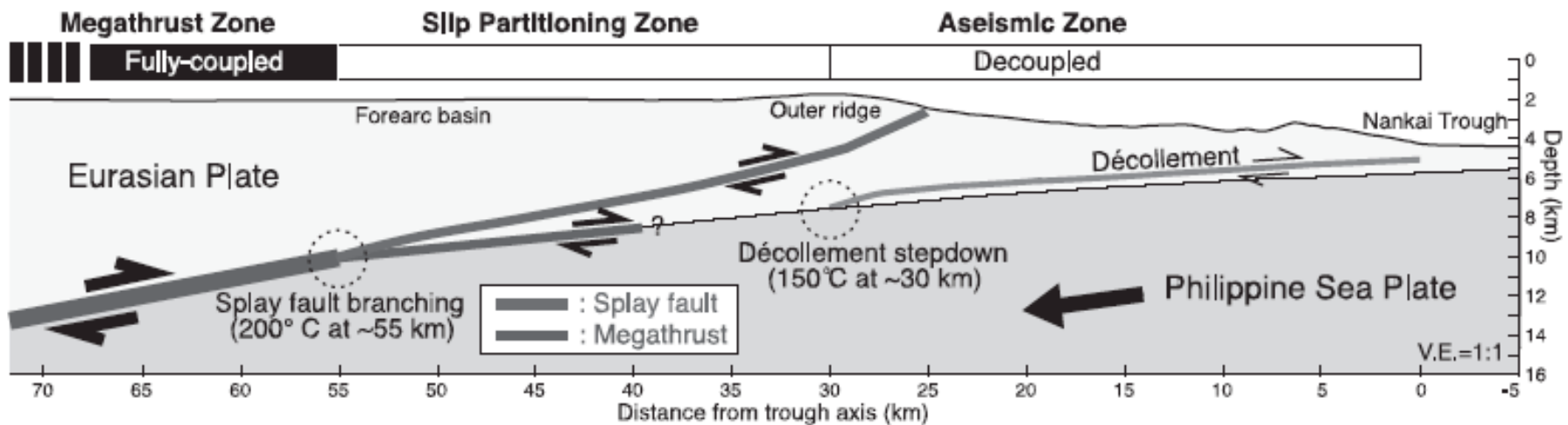
Imperial Valley 1979



(Archuleta, 1984; stress guessed from Hardebeck and Hauksson, 1999, to NW)

Nankai Trough, area of 1944 Mw 8.1 Tonankai earthquake
(Park et al., Sci., 2002; Nakanishi et al., JGR, 2002)

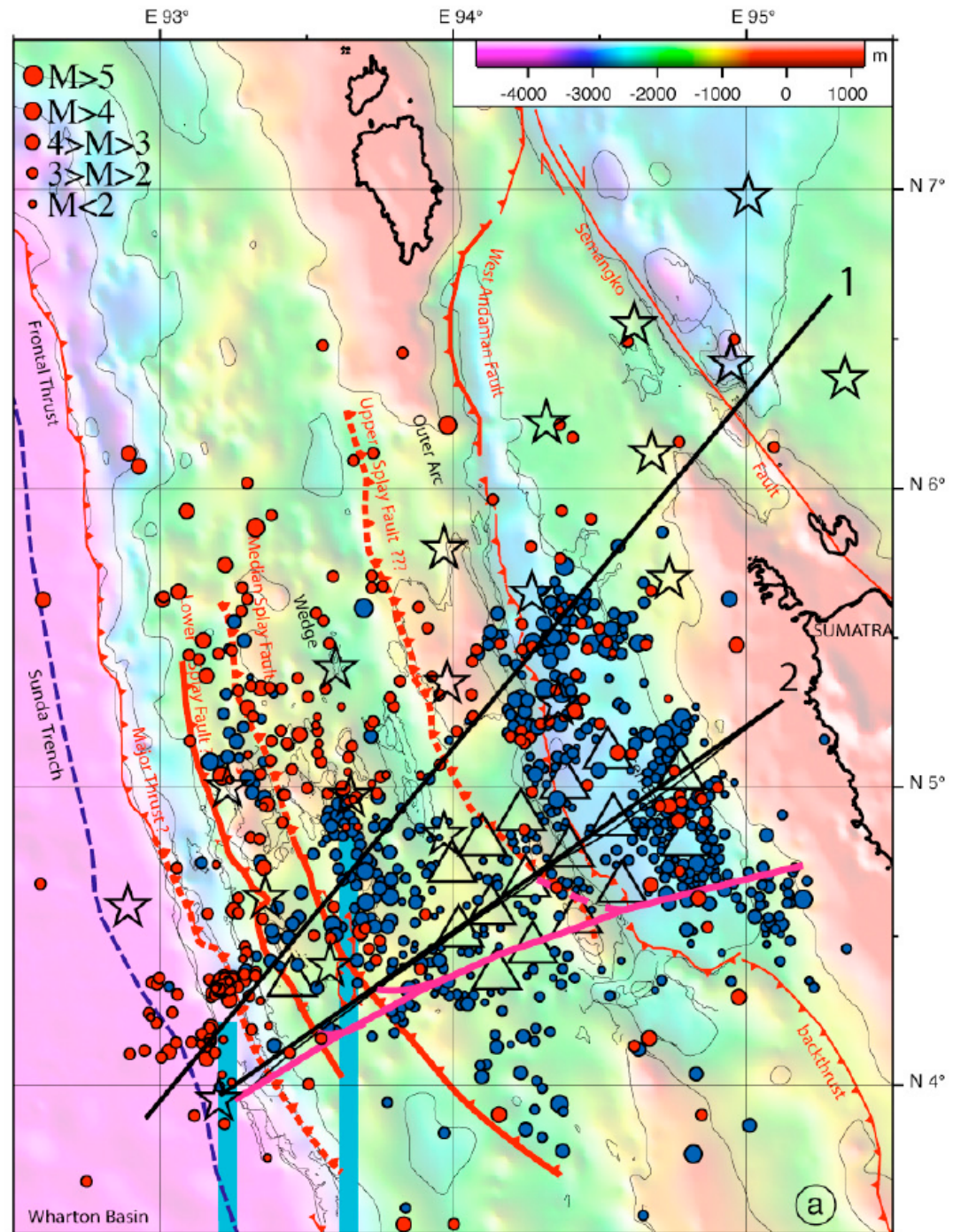
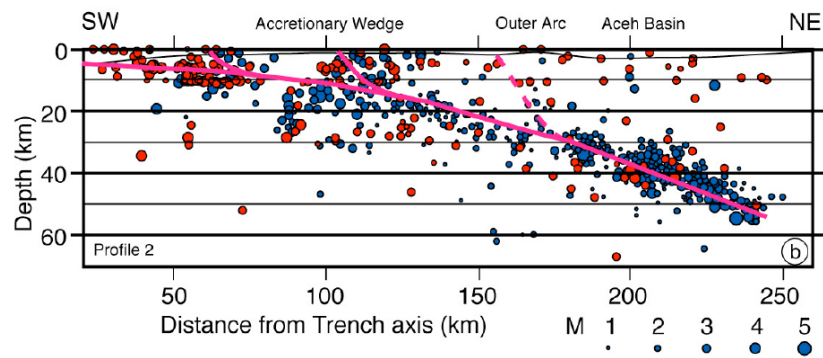
Splay fault branching. Relation to tsunami generation?



Sibuet, Rangin, Le
Pichon, Singh, et al.,

***“26th December 2004
Great Sumatra-
Andaman Earthquake:
Seismogenic Zone and
Active Splay Faults”***,

EPSL, 2007



The rupture zones of major earthquakes often involve geometric complexities, like fault bends, branches and stepovers.

Major questions:

- How the earthquake rupture chooses its path through such geometric complexities? Why do earthquakes stop?
- When and why a fault branch might be preferred? Would the rupture continue as well along the main fault?
- Could the direction of propagation of a complex earthquake be inferred from a pattern of fault branches it ruptured?
- How do small fault branches interact with the main rupture propagation? Could they arrest rupture?
- Can laboratory experiments be used to constrain branching theory?

Our work develops theoretical principles underlying rupture in geometrically complex fault systems.

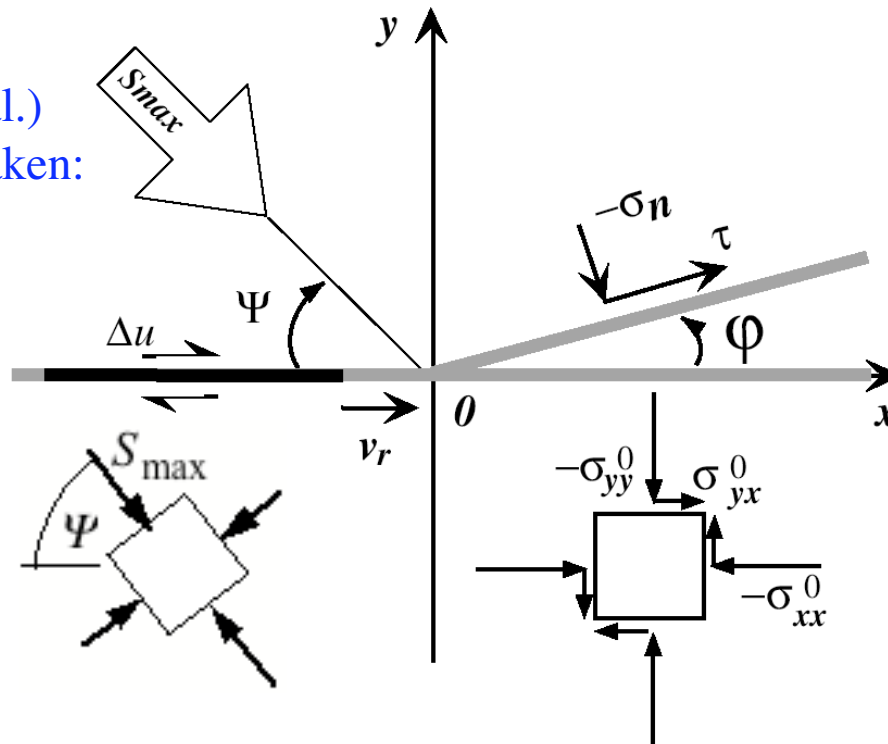
Theory and computational modeling (Poliakov et al., *JGR*, 2002; Kame et al., *JGR*, 2003)

Parameters argued (Poliakov et al.)
to control whether branch path taken:

ϕ -- branch angle

Ψ -- direction of max. pre-stress

v_r -- rupture speed at junction



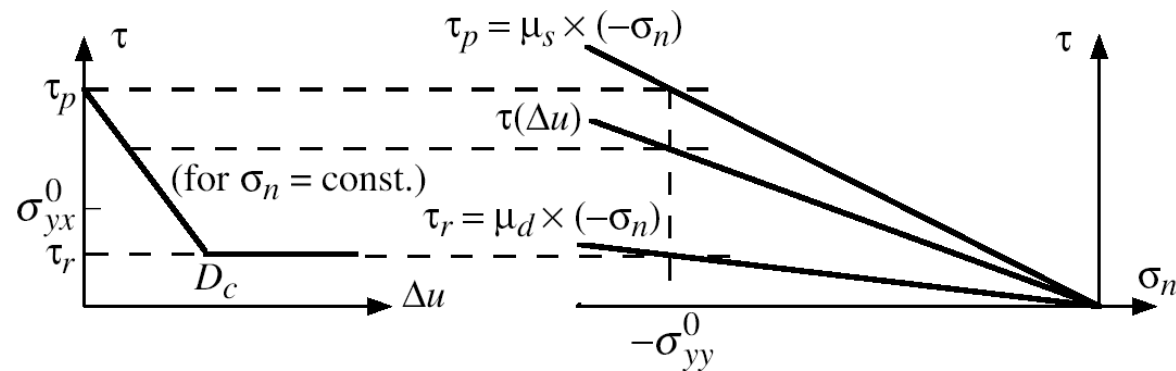
(a)

Slip-weakening model of
frictional failure (Kame et al.);

τ = shear stress,

σ_n = normal stress,

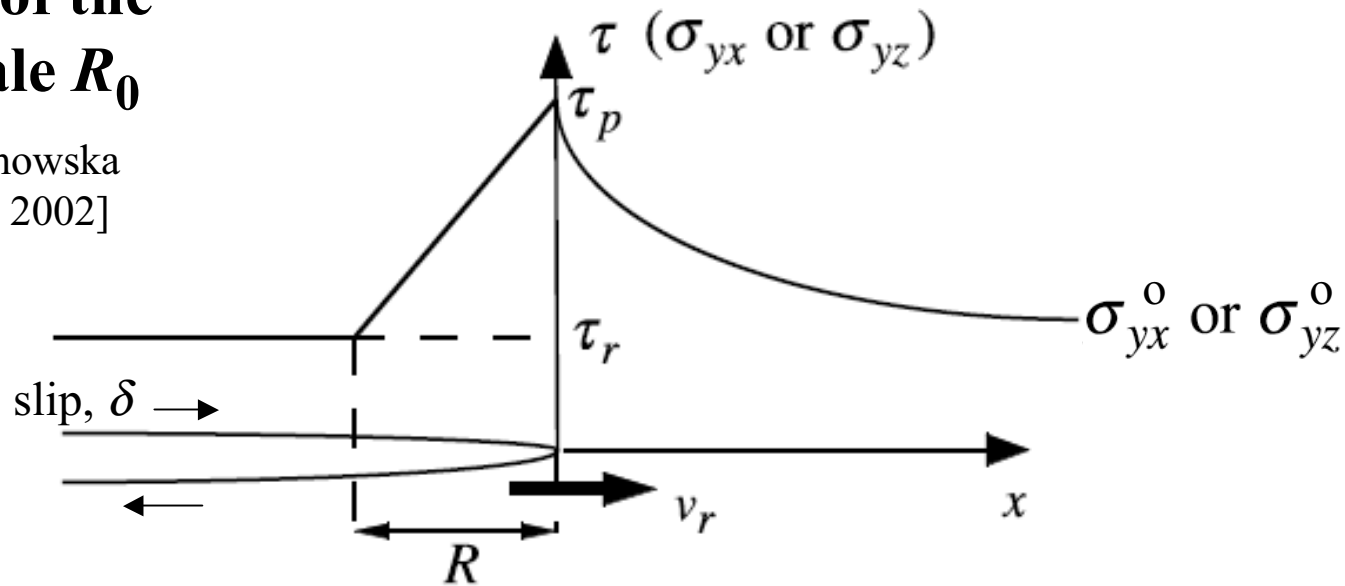
Δu = fault slip.



(b)

Definition of the length scale R_0

[Poliakov, Dmowska & Rice, *JGR*, 2002]



R = length of slip-weakening zone at rupture front;

R_0 = value of R in the low propagation speed ($v_r \ll c_s$),

low stress drop ($\sigma_{yx}^0 - \tau_r \ll \tau_p - \tau_r$) limit.

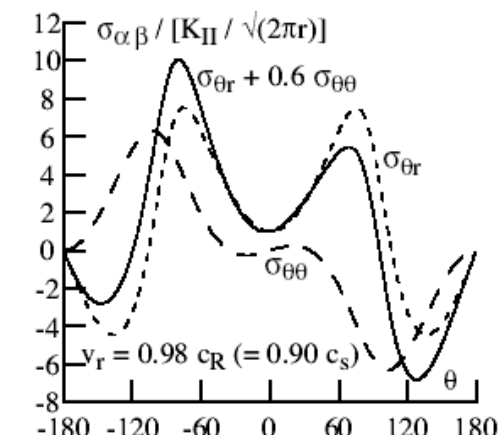
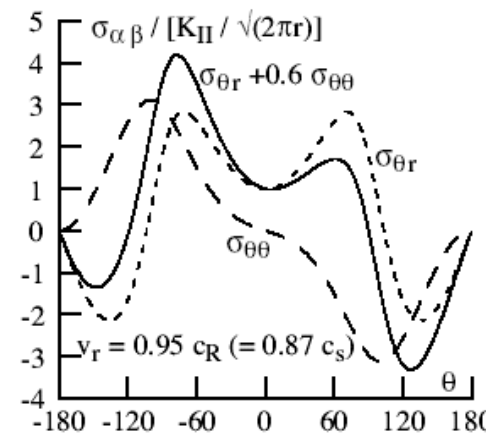
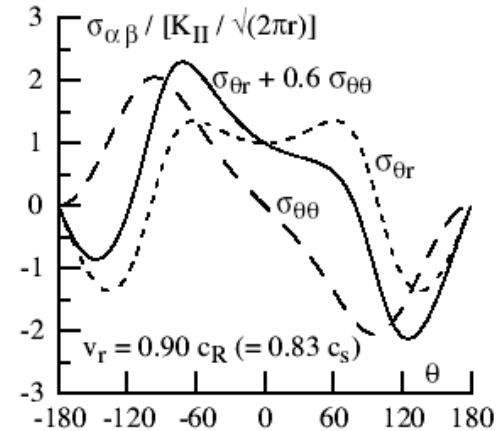
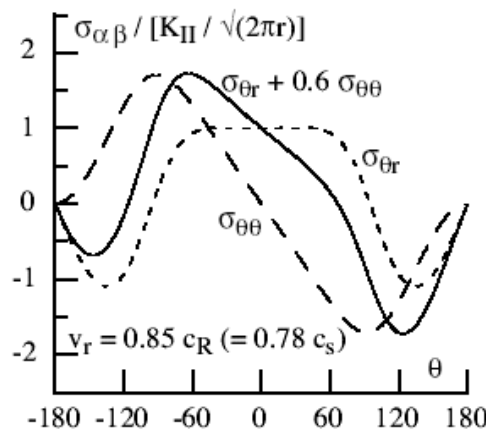
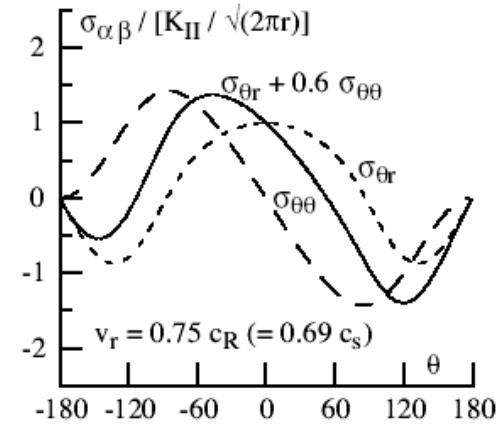
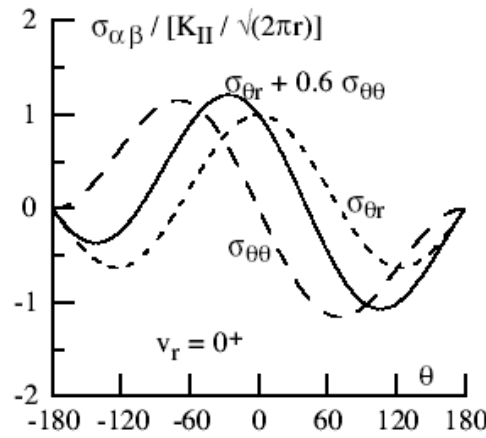
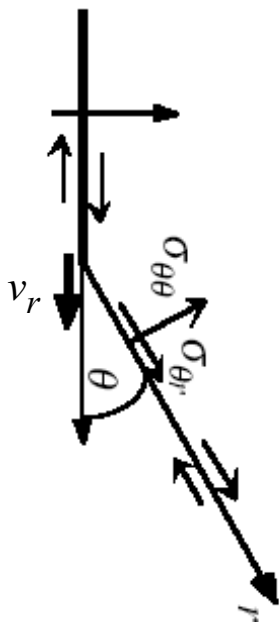
$$R_0 \approx \frac{3\pi}{8} \frac{\mu D_c}{(\tau_p - \tau_r)}$$

[Rice, Sammis and Parsons, *BSSA*, 2005]: Fitting a self-healing pulse model to seismic slip inversions for seven large earthquakes by Heaton [*EPSL*, 1990], R_0 averages ~ 20 - 40 m at mid-depth of crustal seismogenic zone; full range inferred is ~ 1 - 70 m.

Perspective from singular elastic crack theory on the expected importance of rupture propagation speed v_r at the branch junction (Poliakov et al., *JGR*, 2002)

Plotted:

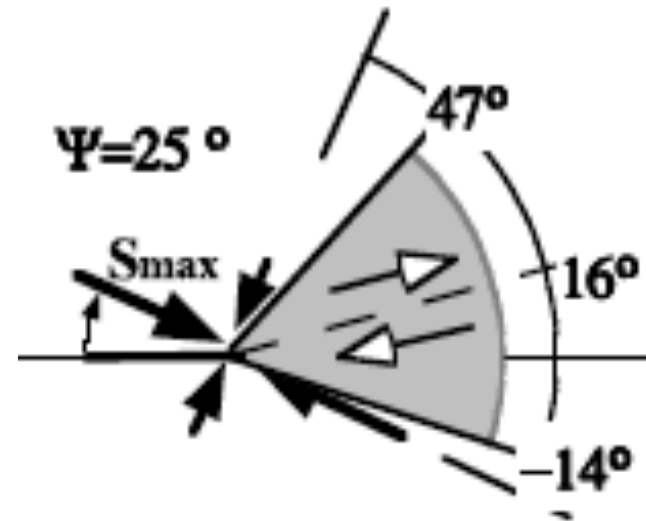
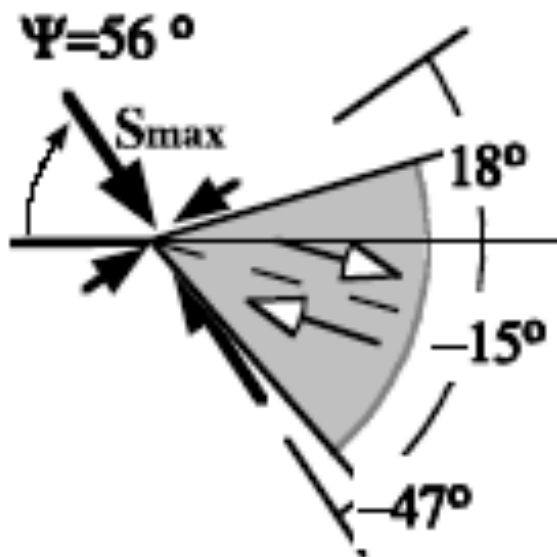
Singular $1/\sqrt{r}$ stress terms, normalized by $K_{II} / \sqrt{(2\pi r)}$ ($=\sigma_{\theta r}|_{\theta=0}$), for various rupture speeds v_r .



Once initiated in the high stress region, can a branched rupture become large?

Importance of direction Ψ of maximum principal compression in pre-stress field

*steep pre-stress angle
favors extensional side*



*shallow pre-stress angle
favors compressional side*

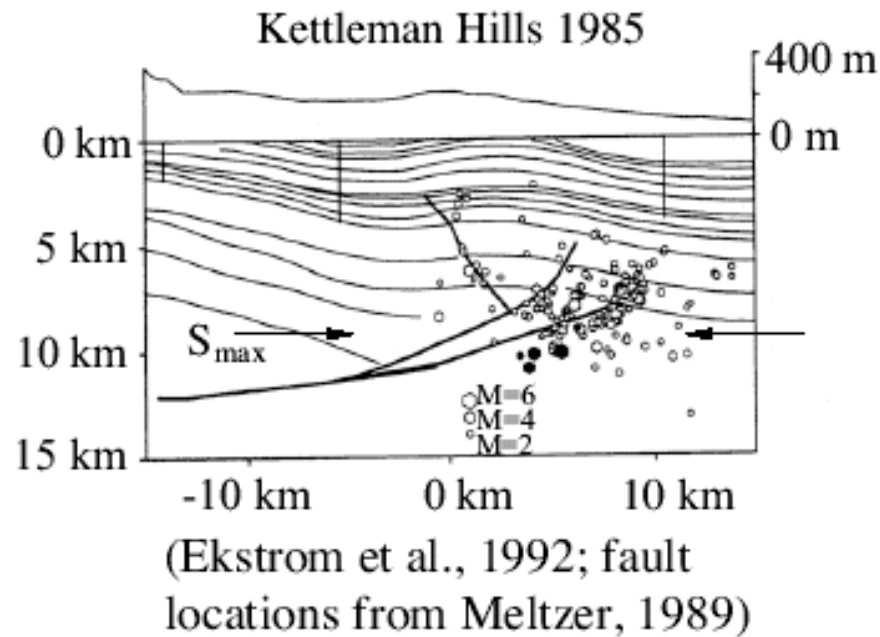
Dashed lines: Directions of maximum $\tau^0 / (-\sigma_n^0)$

Shaded regions: Sectors where $\tau^0 / (-\sigma_n^0) > \mu_d$ (= dynamic friction coef.)

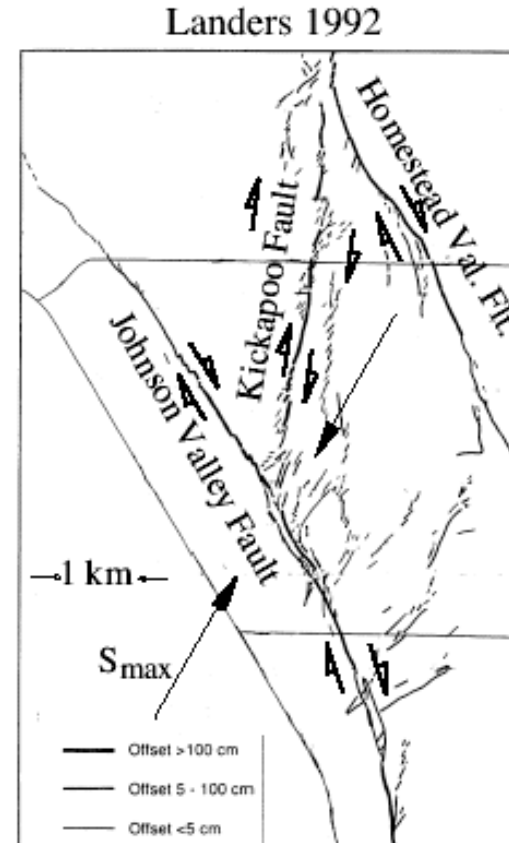
(Poliakov, Dmowska and Rice, *JGR*, 2002)

Correlation with natural examples

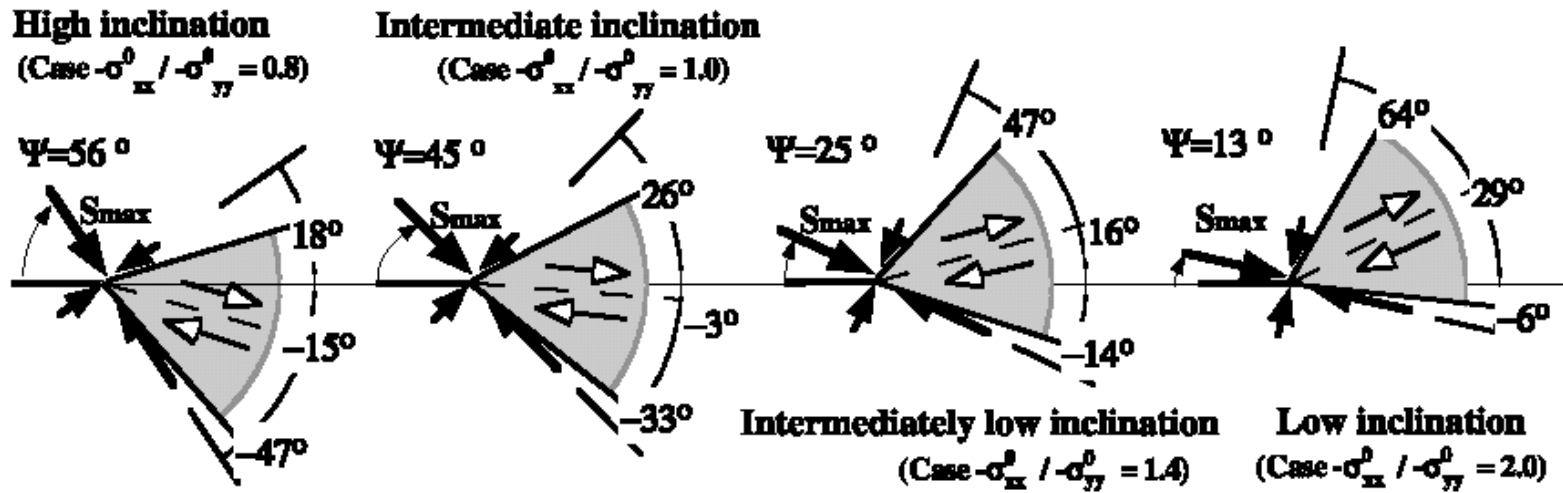
Depth cross-section view: Shallow S_{\max} direction, $\Psi \approx 12-18^\circ$; secondary failures on compressional side:



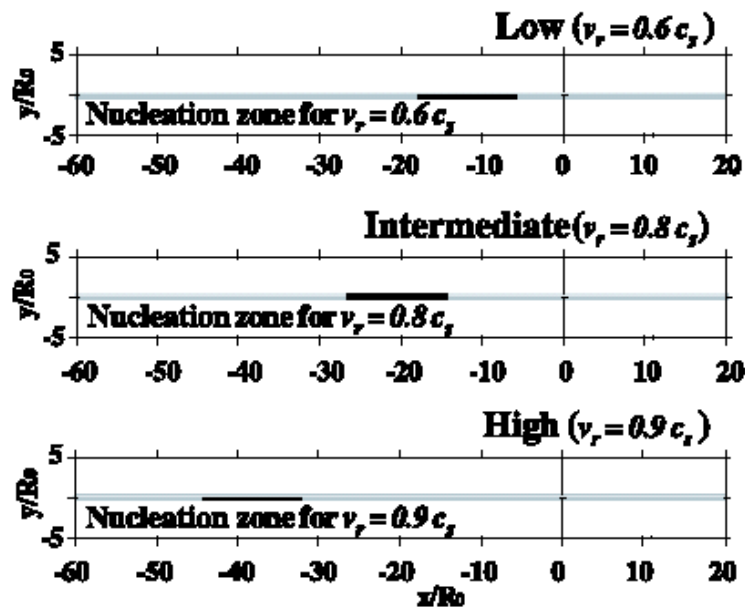
Map view: Steep S_{\max} direction, $\Psi \approx 60^\circ$; secondary failures on extensional side:



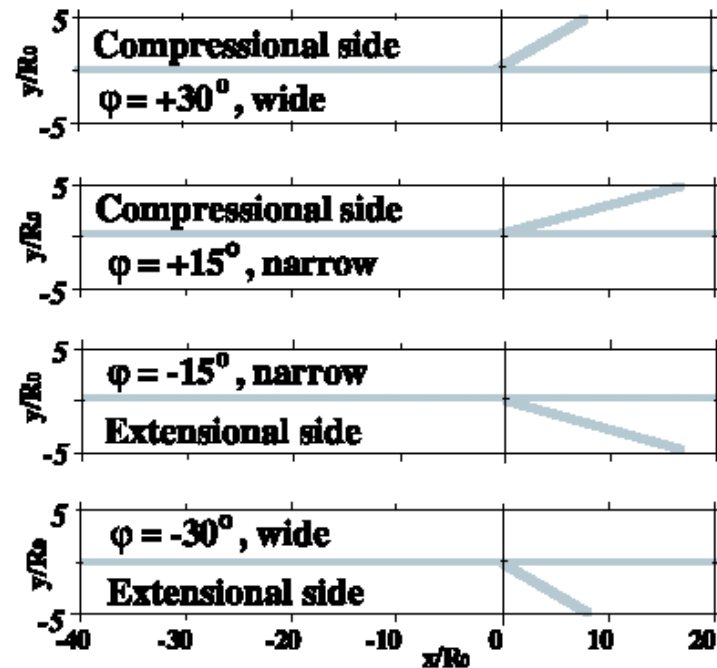
(a) Pre-stress state: Inclination of S_{max}

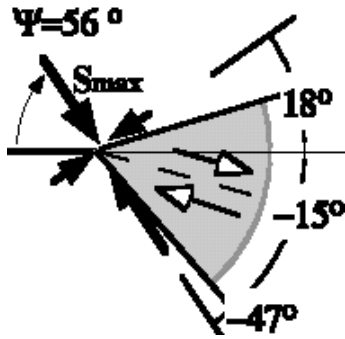


(b) Rupture velocity v_r when reaching the intersection

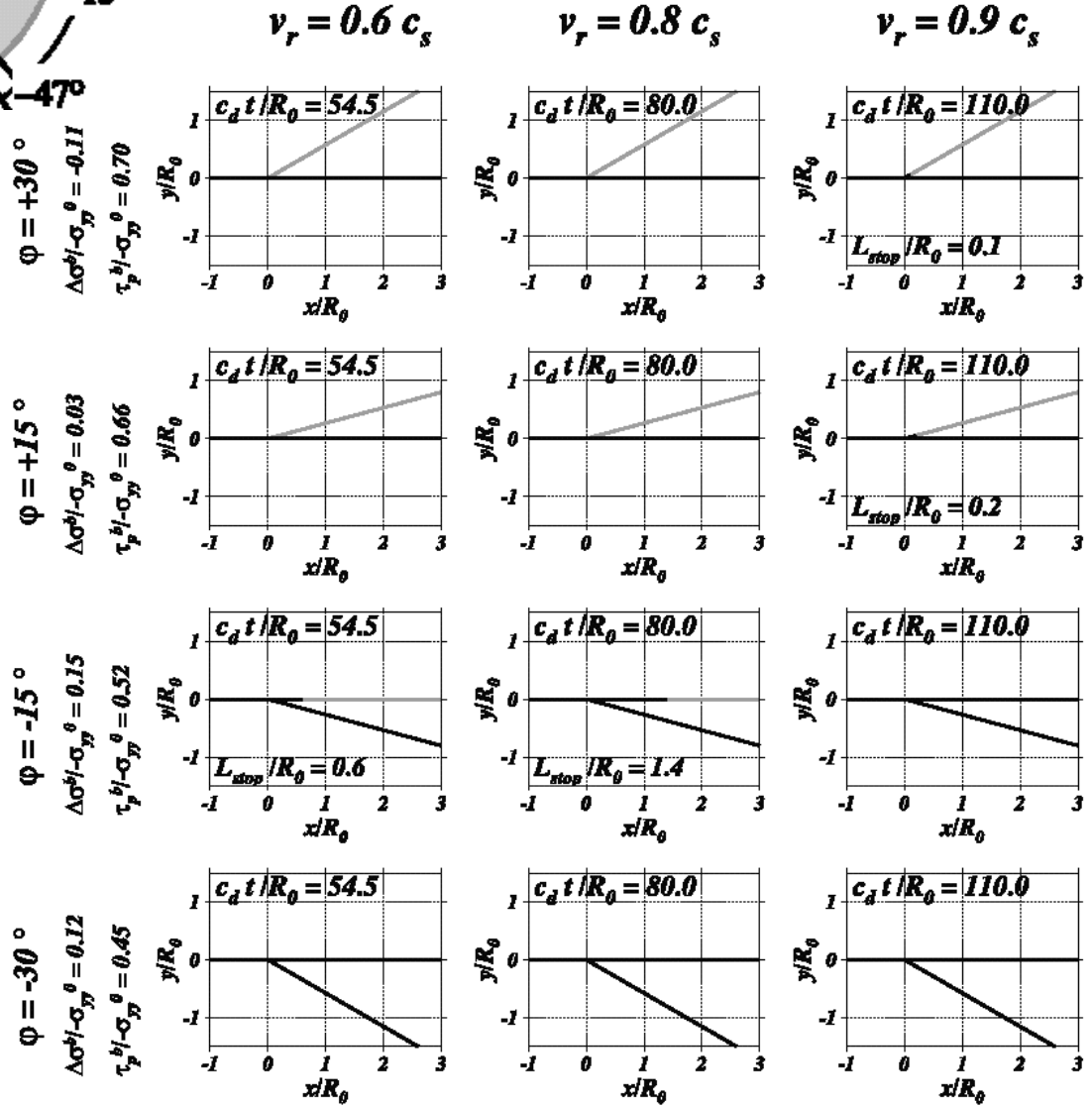
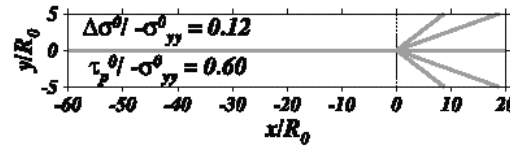


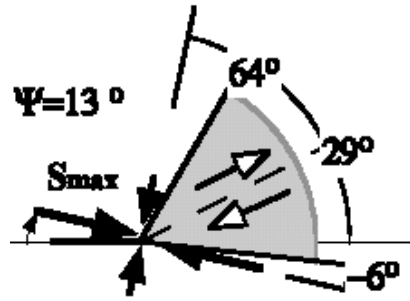
(c) Branching angle ϕ



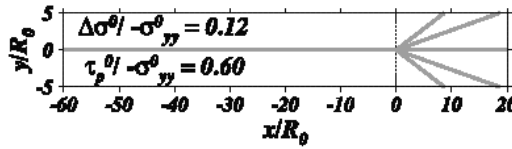


High Inclination of S_{max} , $\Psi = 56^\circ$





Low Inclination of S_{max} , $\Psi = 13^\circ$



$v_r = 0.6 c_s$

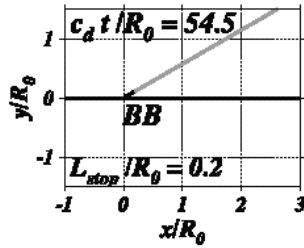
$v_r = 0.8 c_s$

$v_r = 0.9 c_s$

$\Phi = +30^\circ$

$\Delta\sigma^{\theta}/-\sigma_y^{\theta} = 0.38$

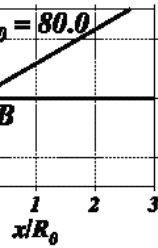
$\tau_p^{\theta}/-\sigma_y^{\theta} = 0.88$



$\Phi = +30^\circ$

$\Delta\sigma^{\theta}/-\sigma_y^{\theta} = 0.38$

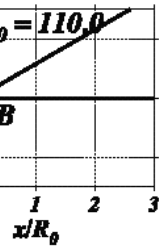
$\tau_p^{\theta}/-\sigma_y^{\theta} = 0.88$



$\Phi = +30^\circ$

$\Delta\sigma^{\theta}/-\sigma_y^{\theta} = 0.38$

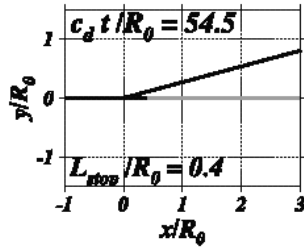
$\tau_p^{\theta}/-\sigma_y^{\theta} = 0.88$



$\Phi = +15^\circ$

$\Delta\sigma^{\theta}/-\sigma_y^{\theta} = 0.31$

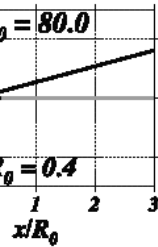
$\tau_p^{\theta}/-\sigma_y^{\theta} = 0.71$



$\Phi = +15^\circ$

$\Delta\sigma^{\theta}/-\sigma_y^{\theta} = 0.31$

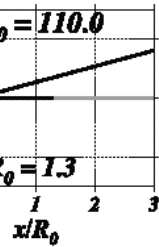
$\tau_p^{\theta}/-\sigma_y^{\theta} = 0.71$



$\Phi = +15^\circ$

$\Delta\sigma^{\theta}/-\sigma_y^{\theta} = 0.31$

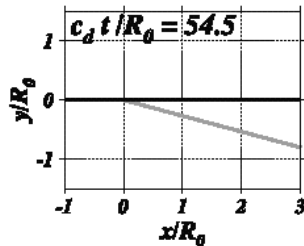
$\tau_p^{\theta}/-\sigma_y^{\theta} = 0.71$



$\Phi = -15^\circ$

$\Delta\sigma^{\theta}/-\sigma_y^{\theta} = -0.16$

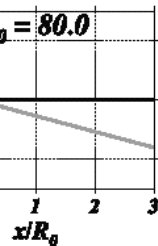
$\tau_p^{\theta}/-\sigma_y^{\theta} = 0.57$



$\Phi = -15^\circ$

$\Delta\sigma^{\theta}/-\sigma_y^{\theta} = -0.16$

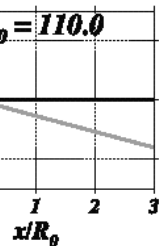
$\tau_p^{\theta}/-\sigma_y^{\theta} = 0.57$



$\Phi = -15^\circ$

$\Delta\sigma^{\theta}/-\sigma_y^{\theta} = -0.16$

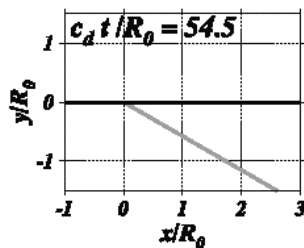
$\tau_p^{\theta}/-\sigma_y^{\theta} = 0.57$



$\Phi = -30^\circ$

$\Delta\sigma^{\theta}/-\sigma_y^{\theta} = -0.44$

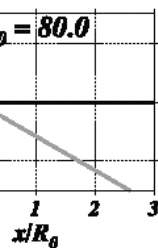
$\tau_p^{\theta}/-\sigma_y^{\theta} = 0.63$



$\Phi = -30^\circ$

$\Delta\sigma^{\theta}/-\sigma_y^{\theta} = -0.44$

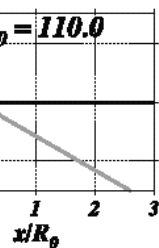
$\tau_p^{\theta}/-\sigma_y^{\theta} = 0.63$



$\Phi = -30^\circ$

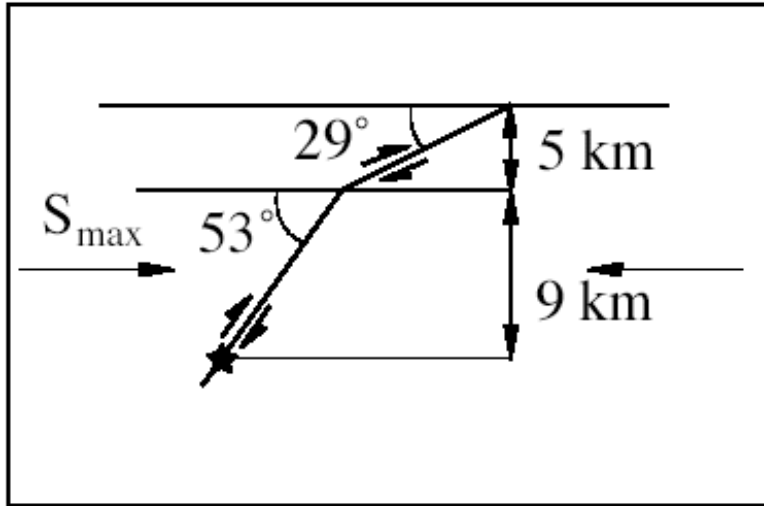
$\Delta\sigma^{\theta}/-\sigma_y^{\theta} = -0.44$

$\tau_p^{\theta}/-\sigma_y^{\theta} = 0.63$



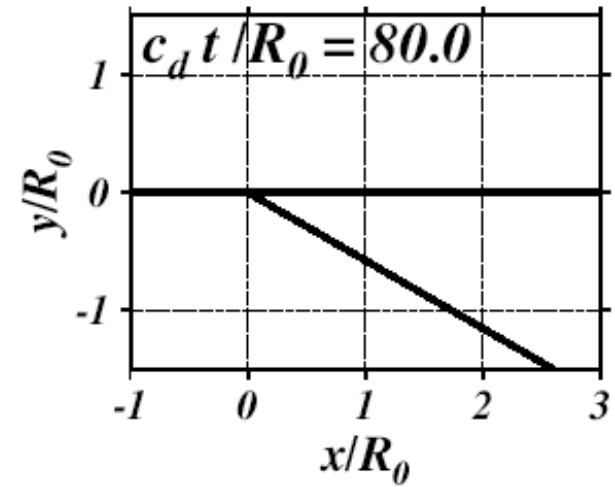
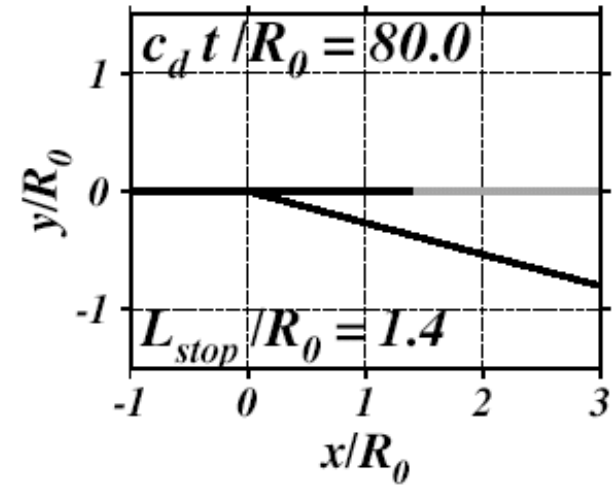
(Kame et al., *JGR*, 2003)

San Fernando 1971

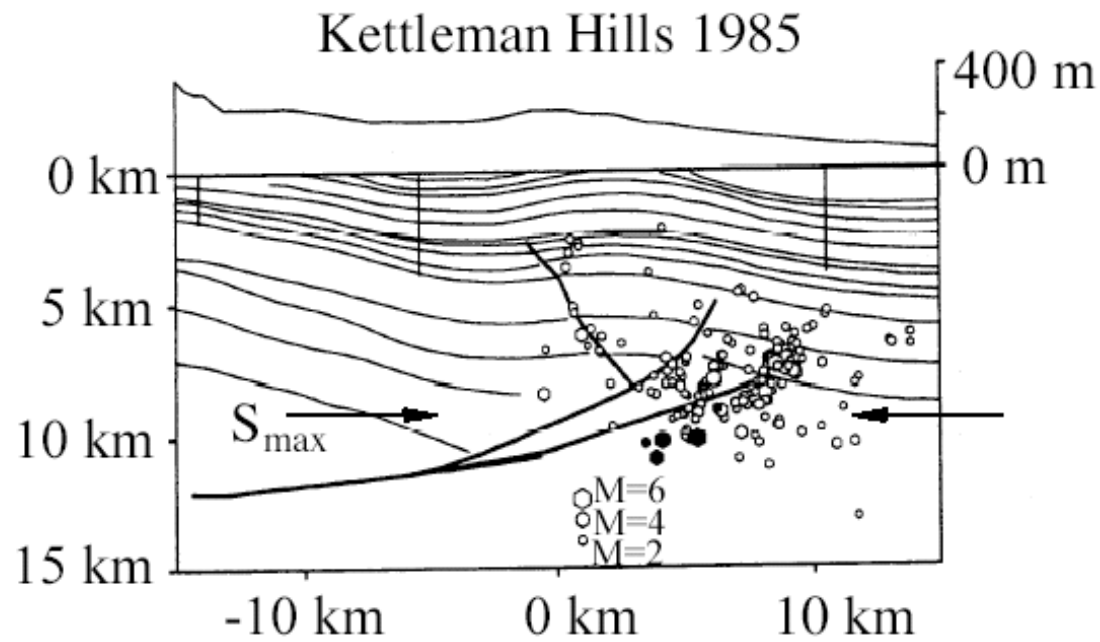


(Heaton and Helmberger, 1979)

$$\Psi = 56^\circ, \nu_r = 0.8 c_s$$

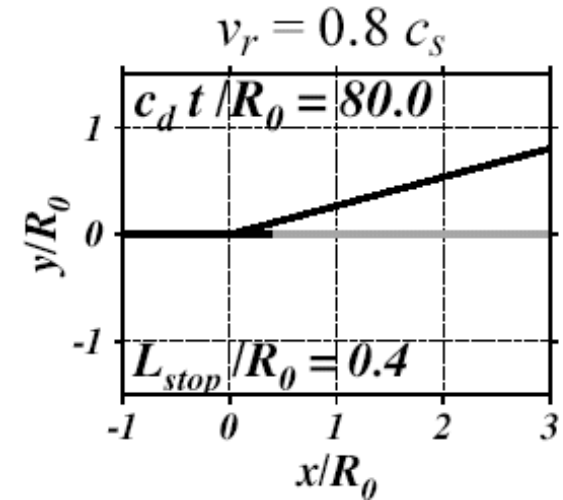
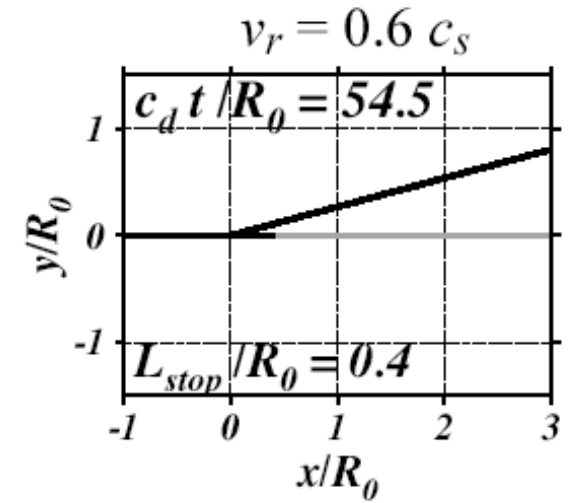


(Kame et al., *JGR*, 2003)



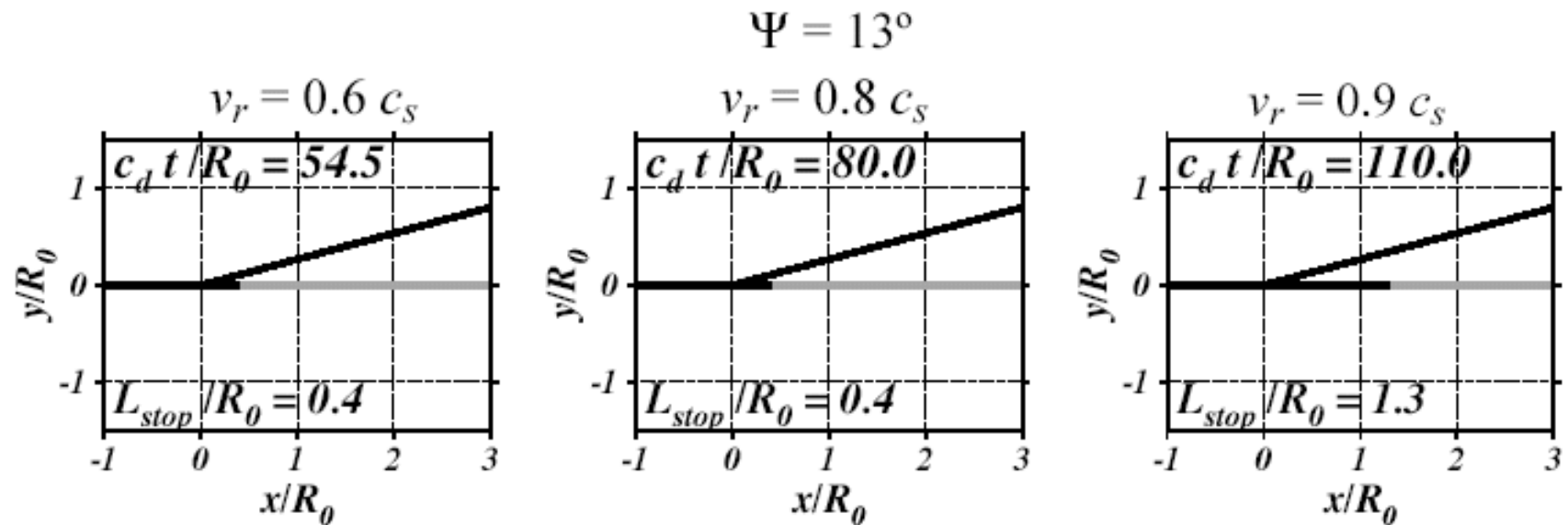
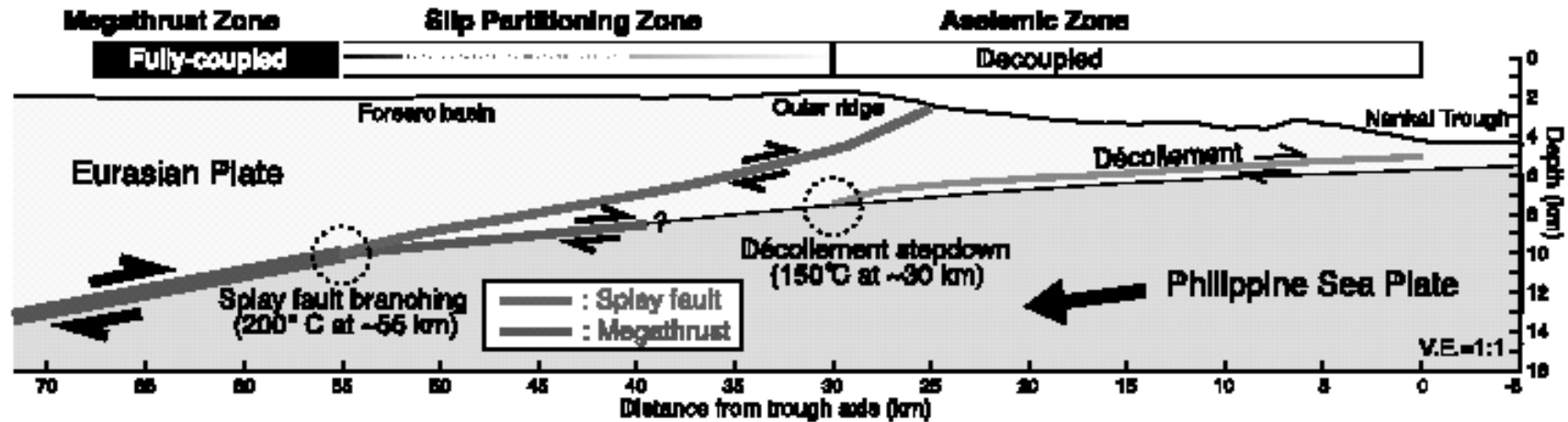
(Ekstrom et al., 1992; fault locations from Meltzer, 1989)

$$\Psi = 13^\circ$$



(Kame et al., *JGR*, 2003)

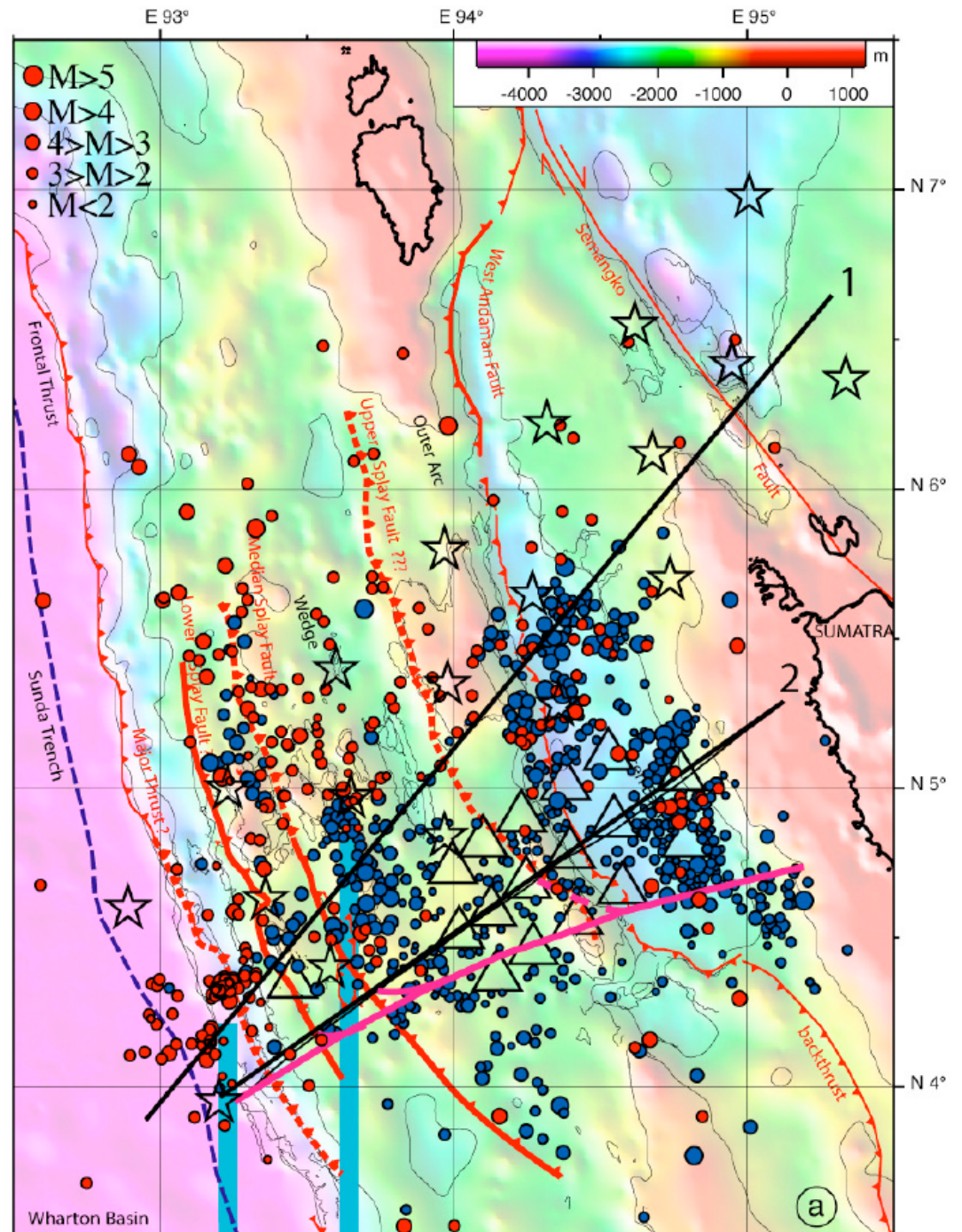
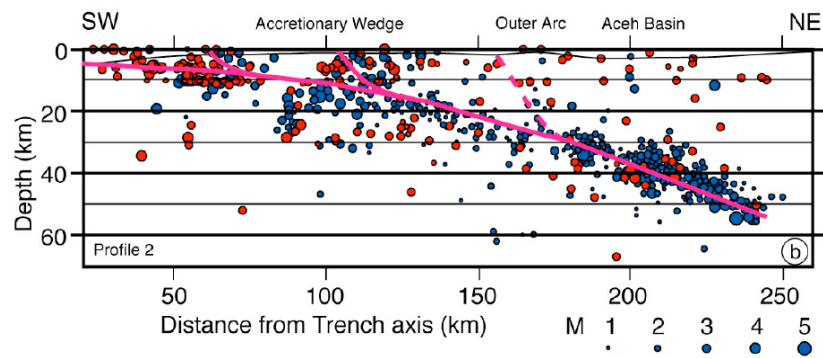
Nankai Trough, area of M 8.1 Tonankai 1944 (Park et al., *Science*, 2002; Nakanishi et al., *JGR*, 2002)

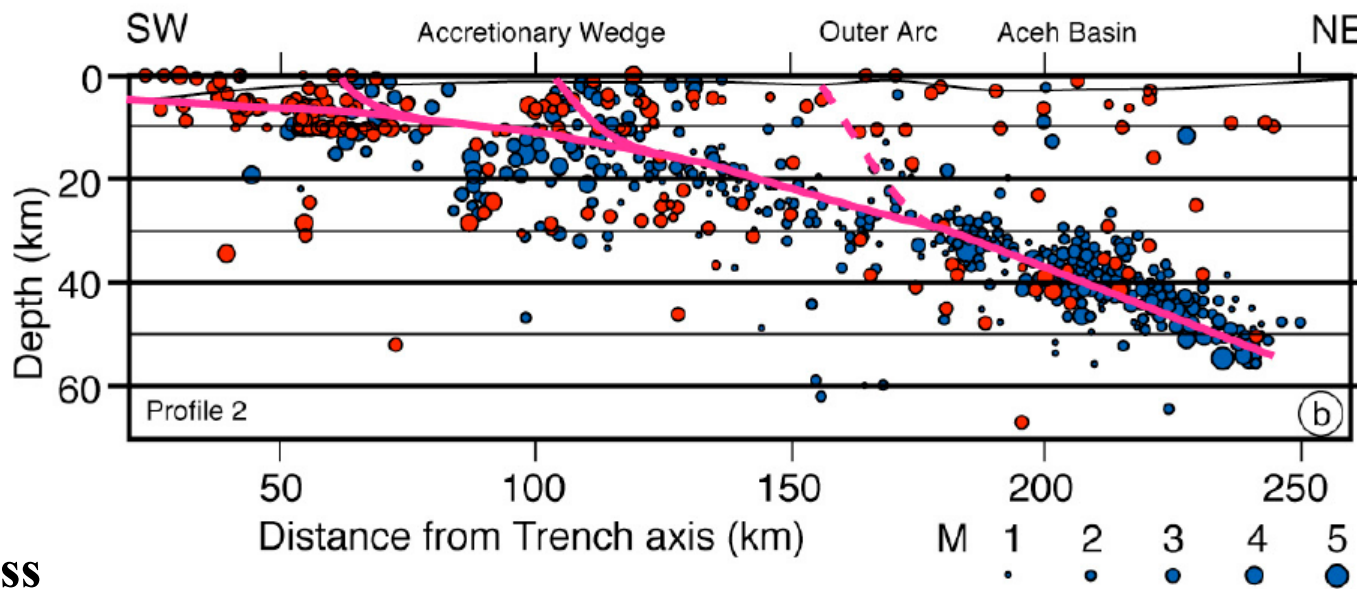


Sibuet, Rangin, Le
Pichon, Singh, et al.,

***“26th December 2004
Great Sumatra-
Andaman Earthquake:
Seismogenic Zone and
Active Splay Faults”***,

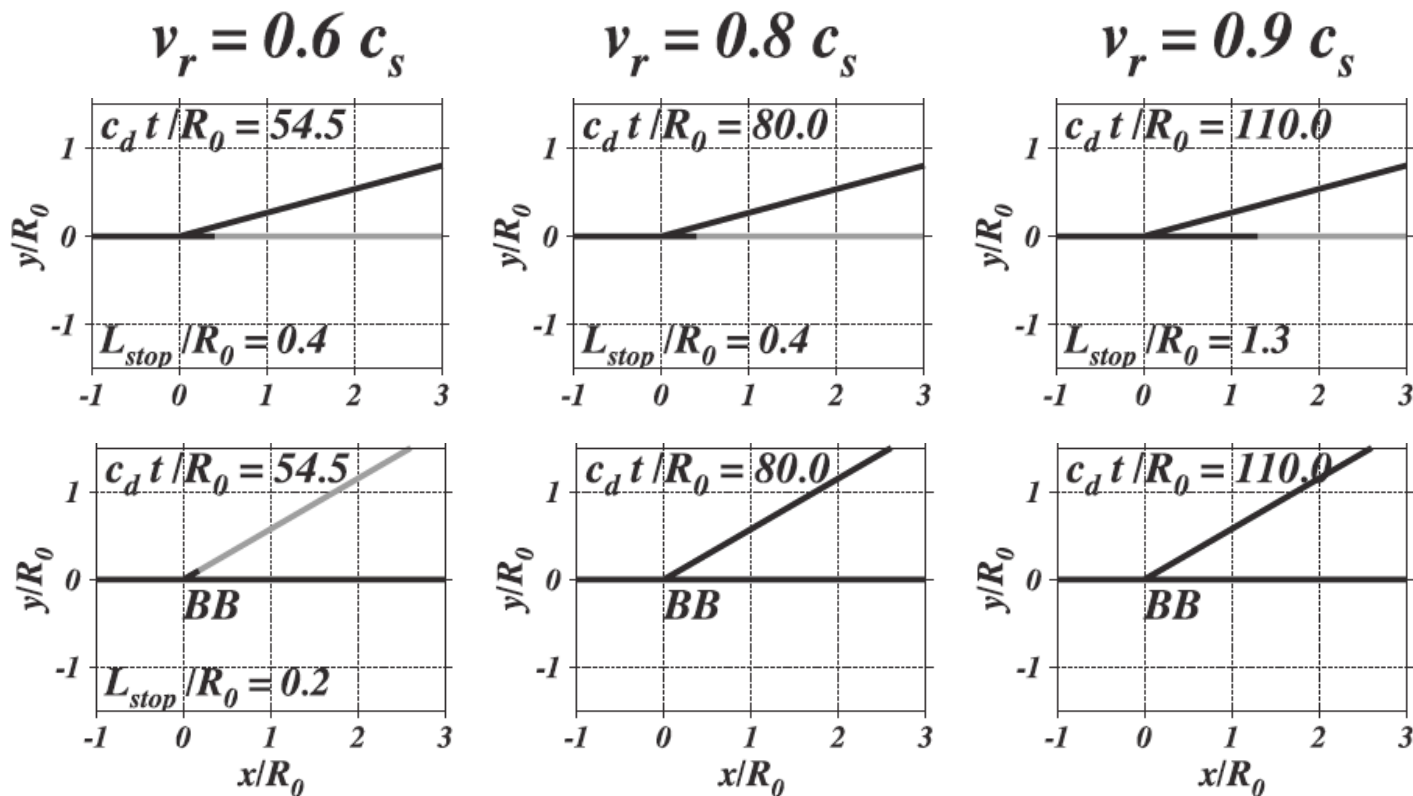
EPSL, 2007



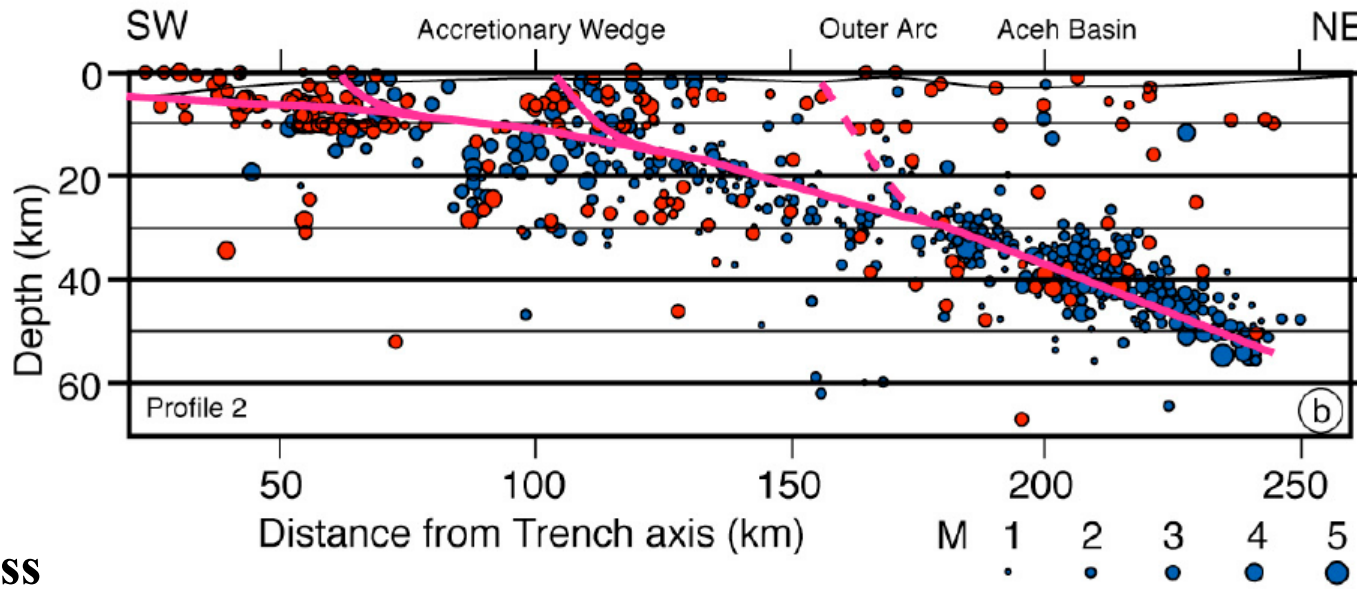


[Sibuet et al.,
EPSL, 2007]

Shallow
pre-stress
angle,
 $\Psi = 13^\circ$

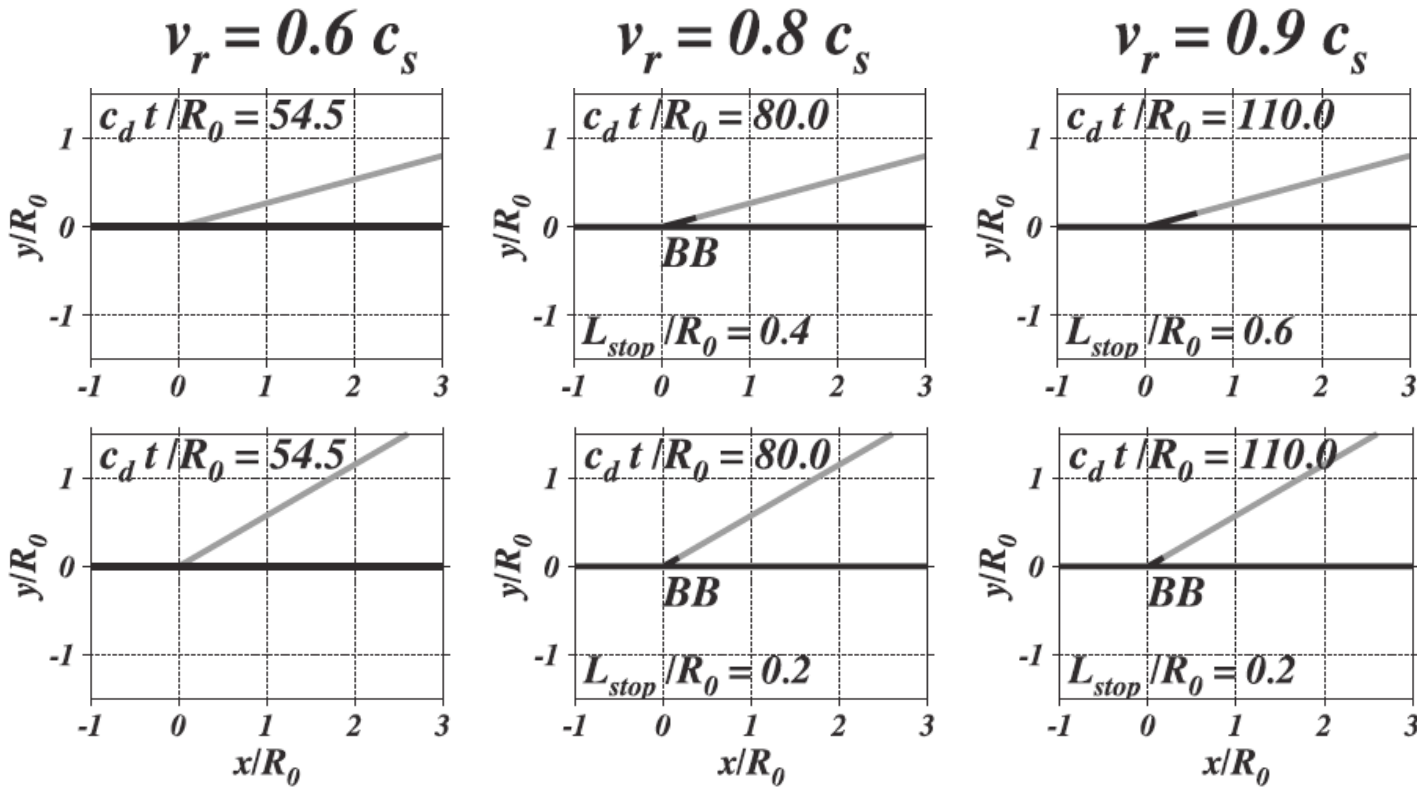


[Kame et al.,
JGR,
2003]



[Sibuet et al.,
EPSL, 2007]

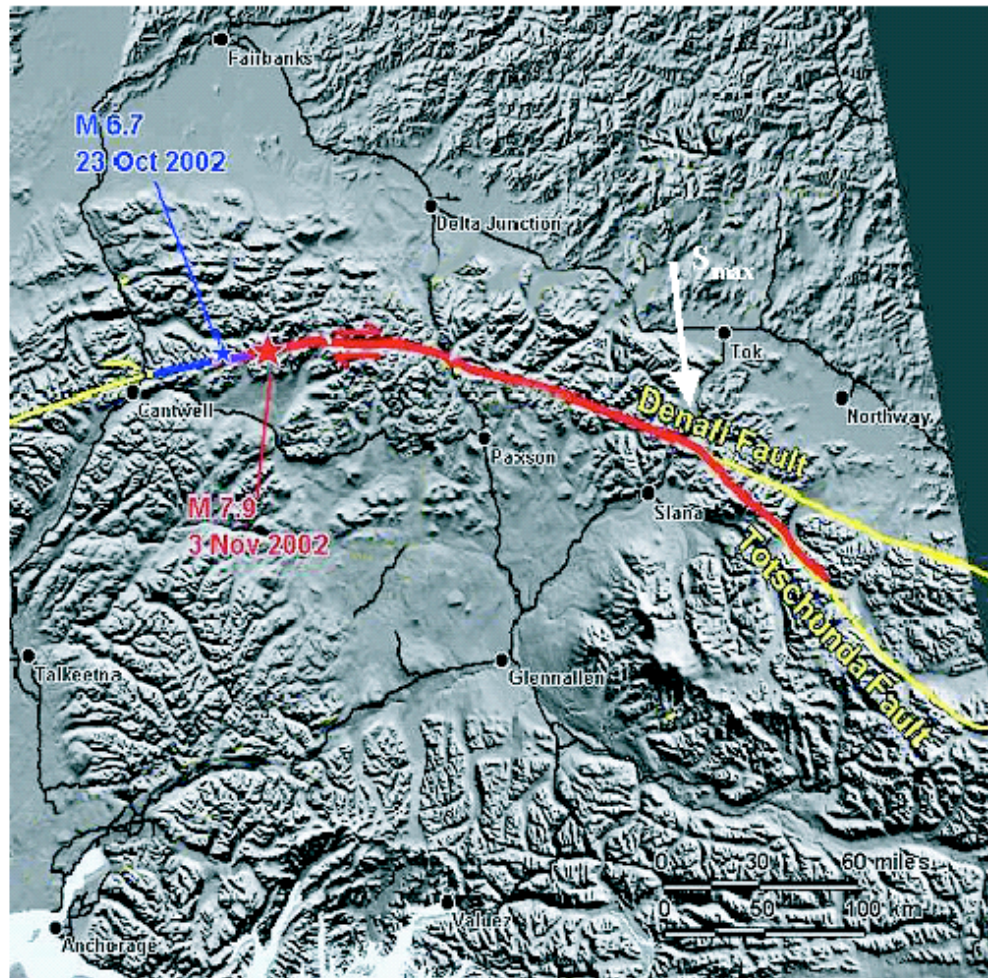
Steeper
pre-stress
angle,
 $\Psi = 25^\circ$



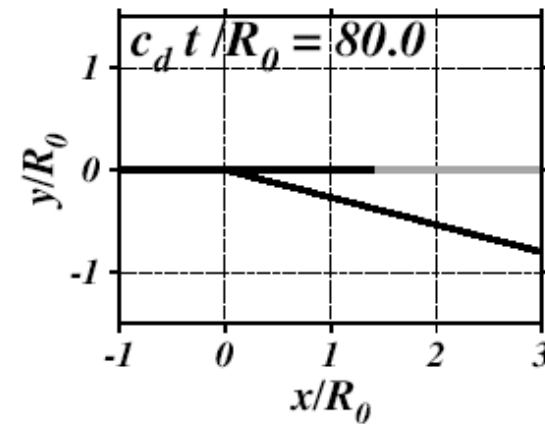
[Kame et al.,
JGR,
2003]

M 7.9 Denali, 3 November 2002 -- Branch from Denali Fault to Totschunda Fault

Bhat, Dmowska, Rice & Kame, *Bull. Seismol. Soc. Amer.*, 2004)



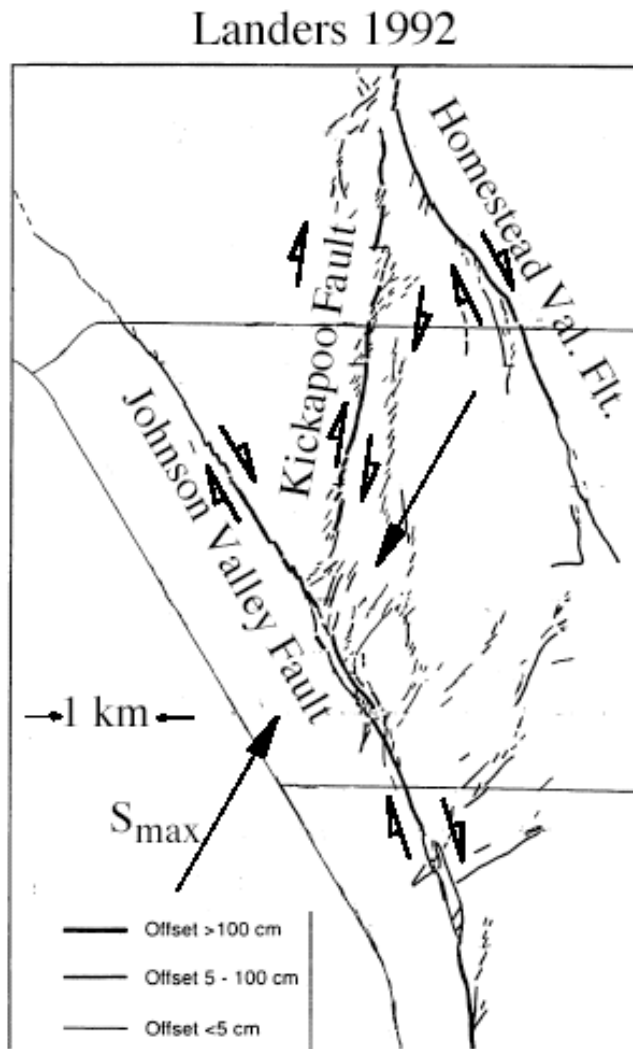
$$\Psi = 70^\circ, \quad v_r = 0.8 c_s$$



Stress direction from Ratchkovski and Hansen, 2002; Nakamura et. al., 1980; Estabrook and Davies, 1991.

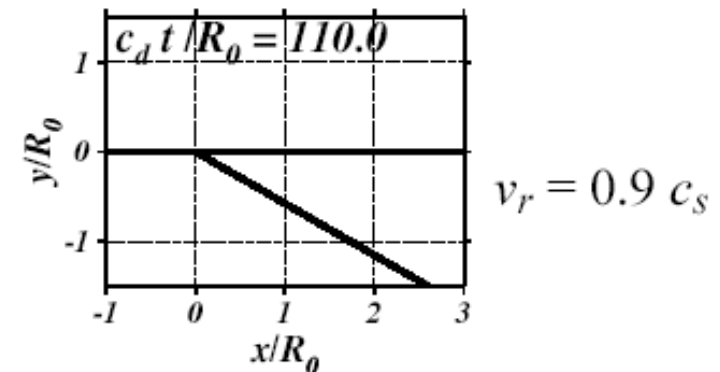
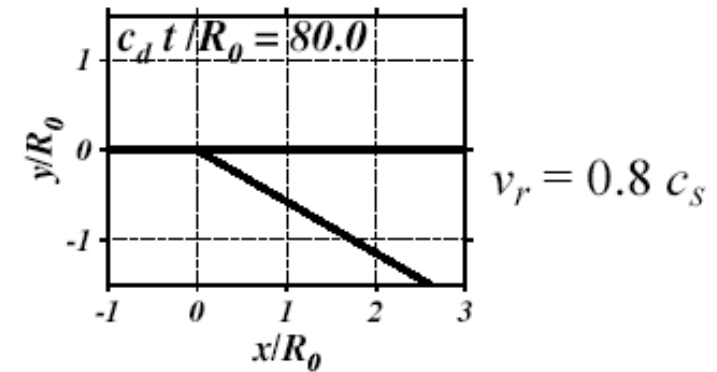
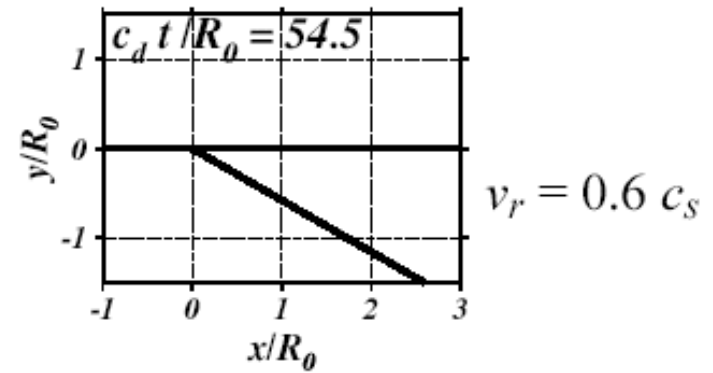
Fault map from Department of Natural Resources, Division of Geological and Geophysical Surveys, Alaska

(Kame et al., *JGR*, 2003)



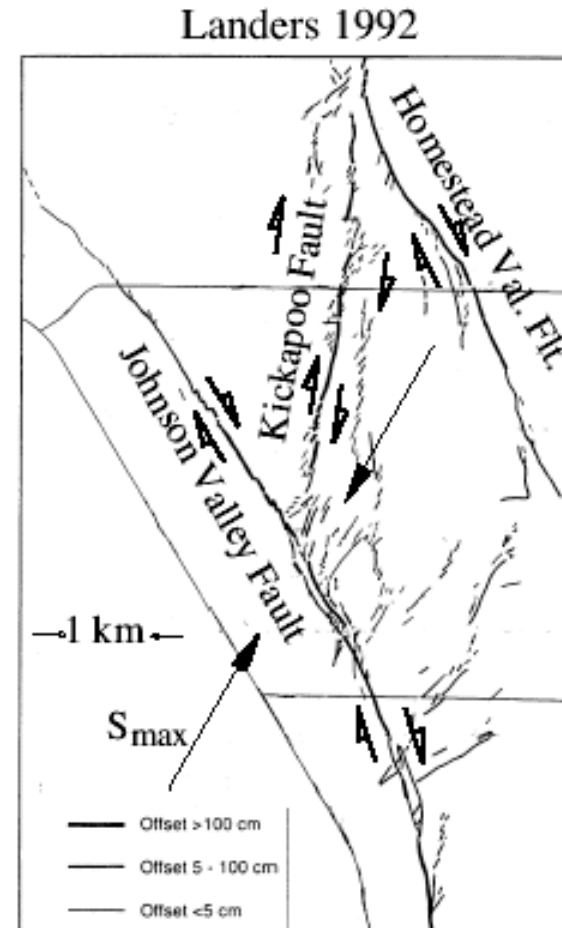
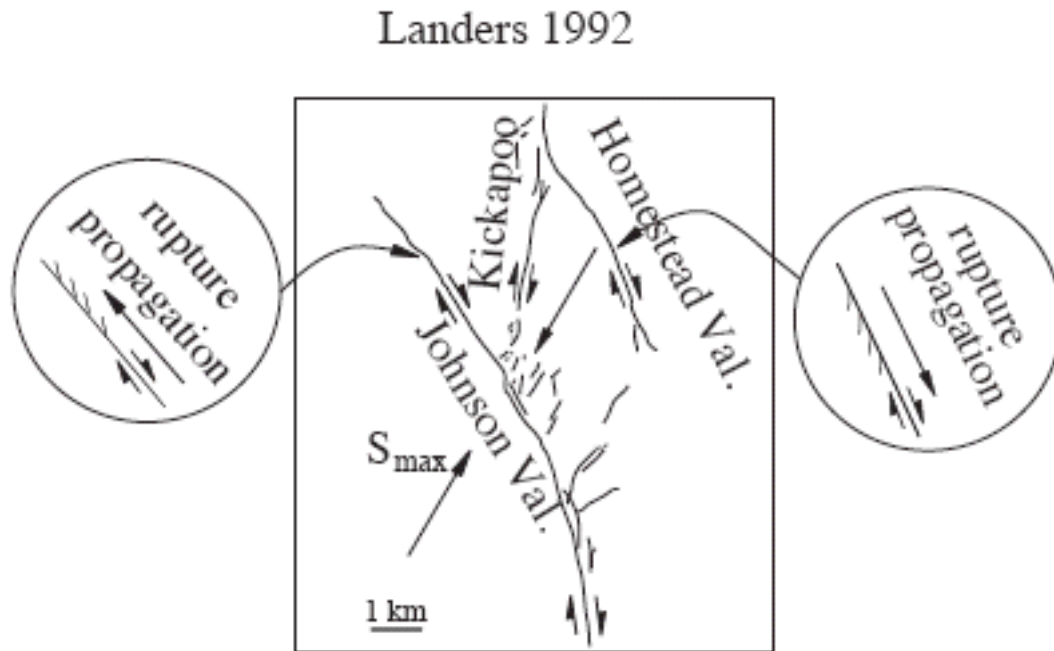
(fault map from Sowers et al., 1994;
stress from Hardebeck and Hauksson, 2001)

$$\Psi = 56^\circ$$



Small branching features show the direction of propagation
 [Poliakov, Dmowska & Rice, *JGR*, 2002]

Map view: Steep S_{\max} direction, $\Psi \approx 60^\circ$;
 secondary failures on *extensional* side:



(fault map from Sowers et al., 1994;
 stress from Hardebeck and Hauksson, 2001)

(Dmowska et al., *AGU*, 2002; Fliss et al., *JGR*, 2005)

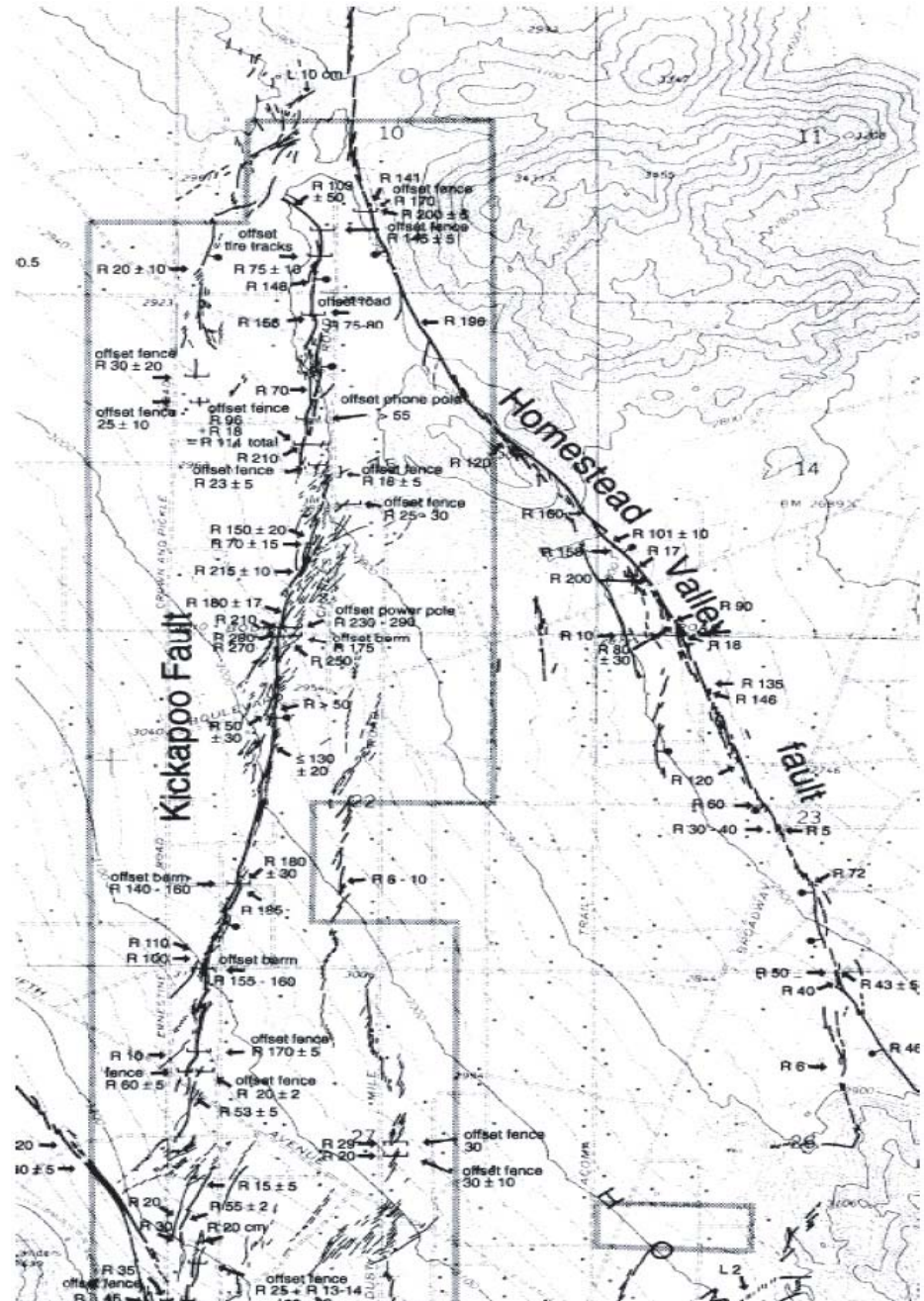
An example of *backward branching*:

Landers 1992 Earthquake

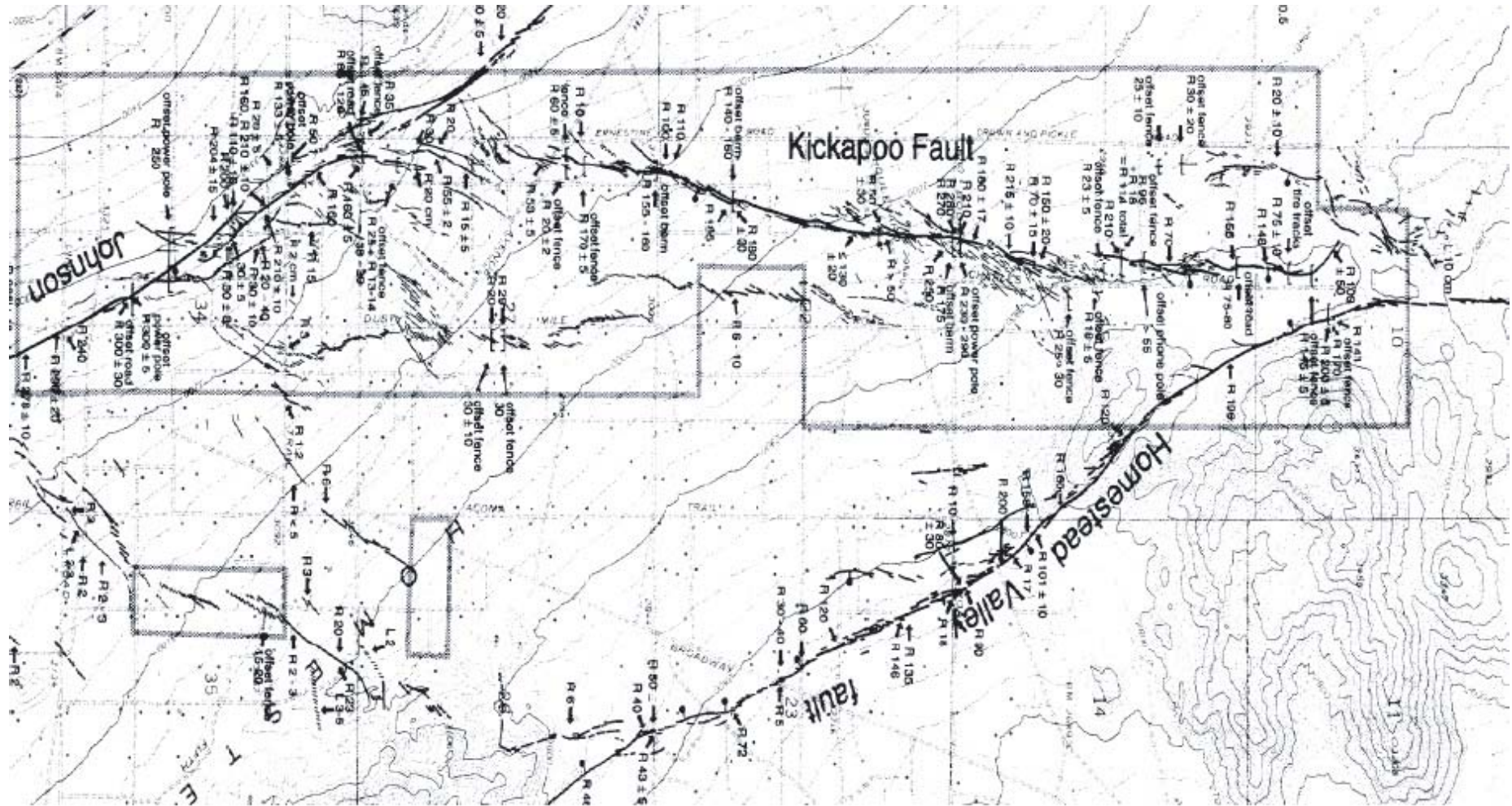
Rupture transition from
Kickapoo Fault to southern
part of Homestead Valley
Fault (which ruptured much
further to the north, off the
map here):

How does *backward
branching* happen?

(Fault map: Sowers et al., 1994.)



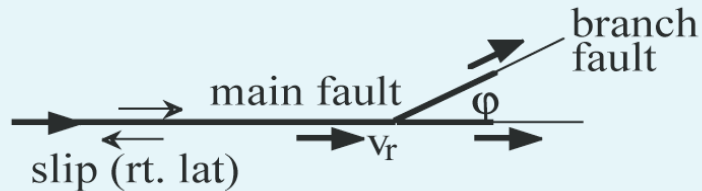
North →



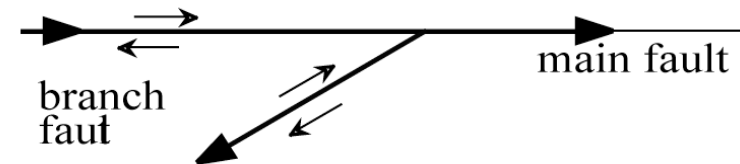
1 km

Backward Branching and Rupture Directivity

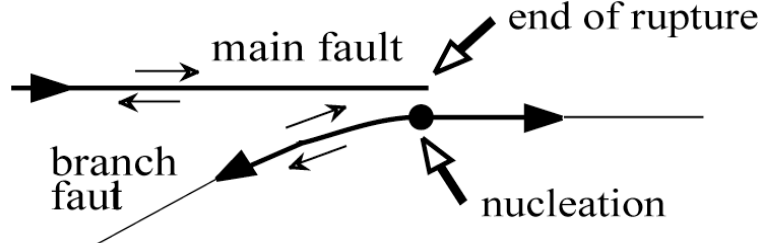
(a) Typical branching through acute angle $|\varphi| < 90^\circ$ (φ is most often negative)



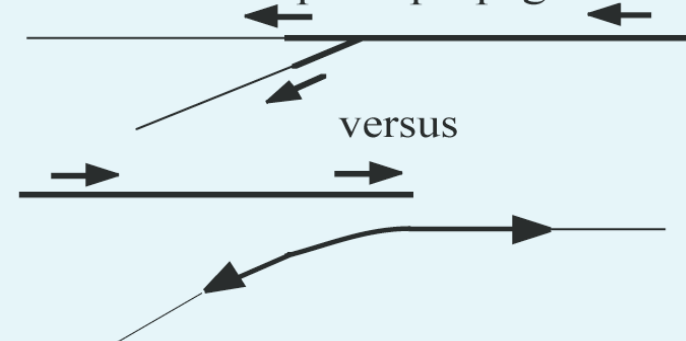
(b) Turn of rupture path through obtuse φ angle while continuing on main fault (never favored by stress field)



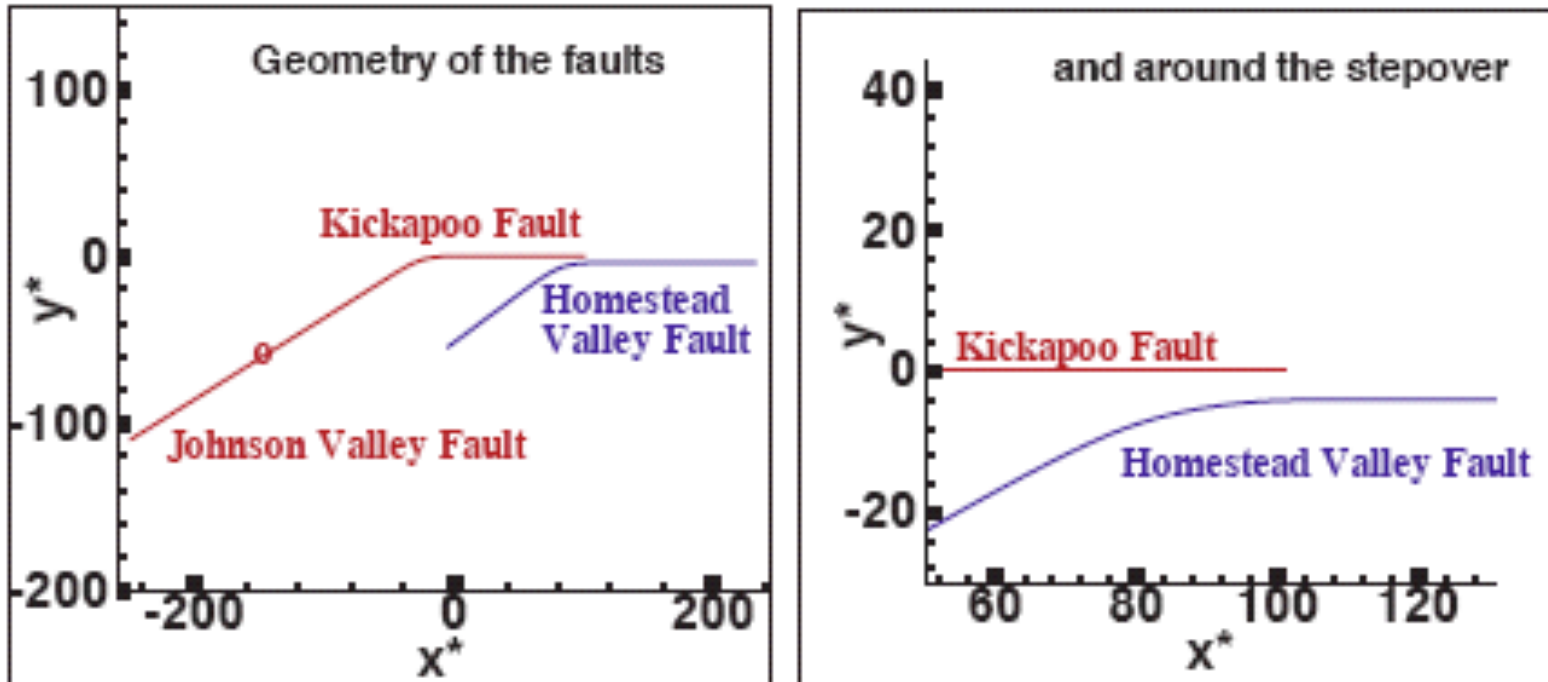
(c) Jumping mechanism; nucleation of bilateral rupture on a neighboring fault



(d) Given the branch geometry, what was the direction of rupture propagation?

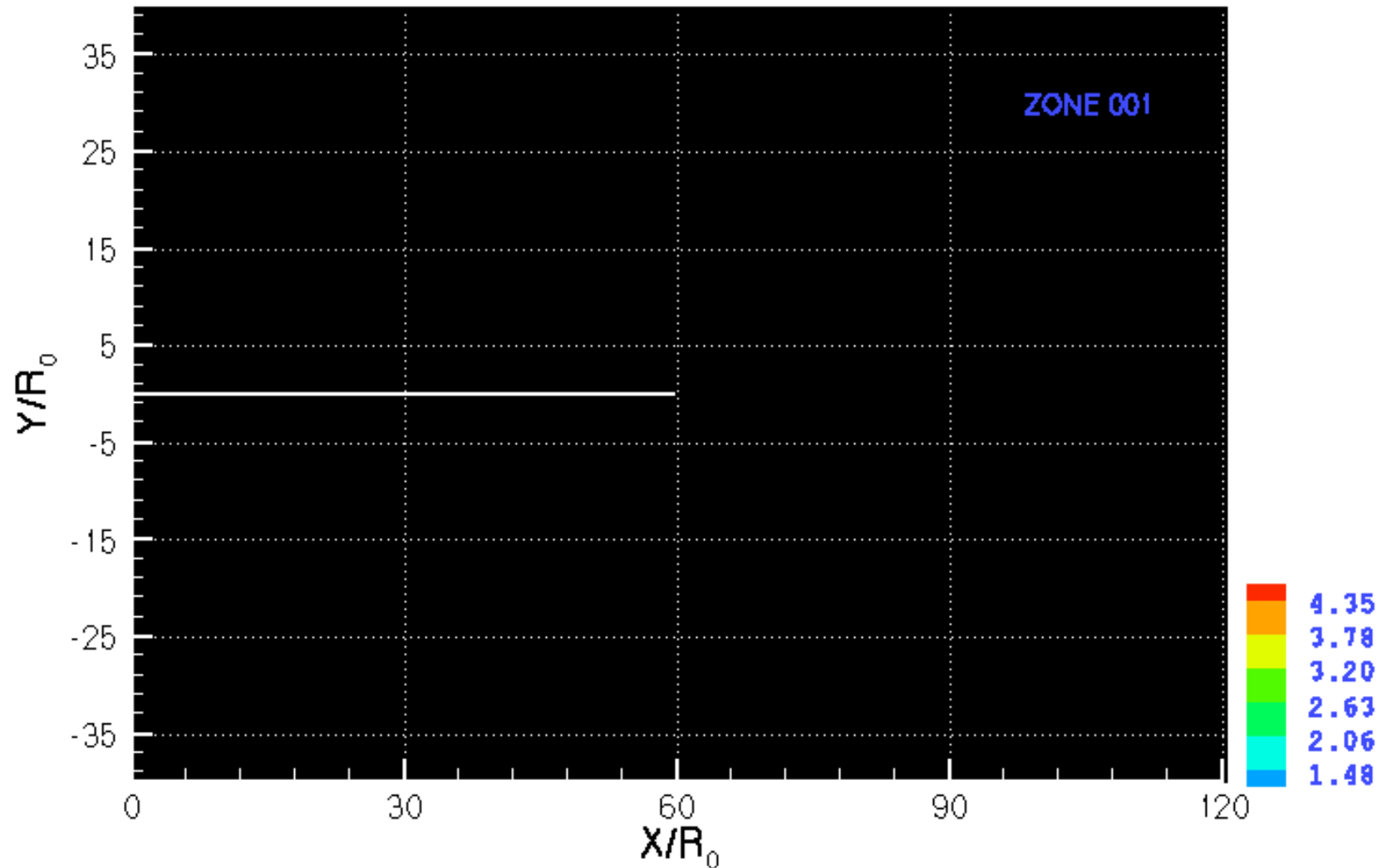


Fault geometry assumed for simulation



(Fliss, Bhat, et al., 2003; case with supershear propagation before arrest)

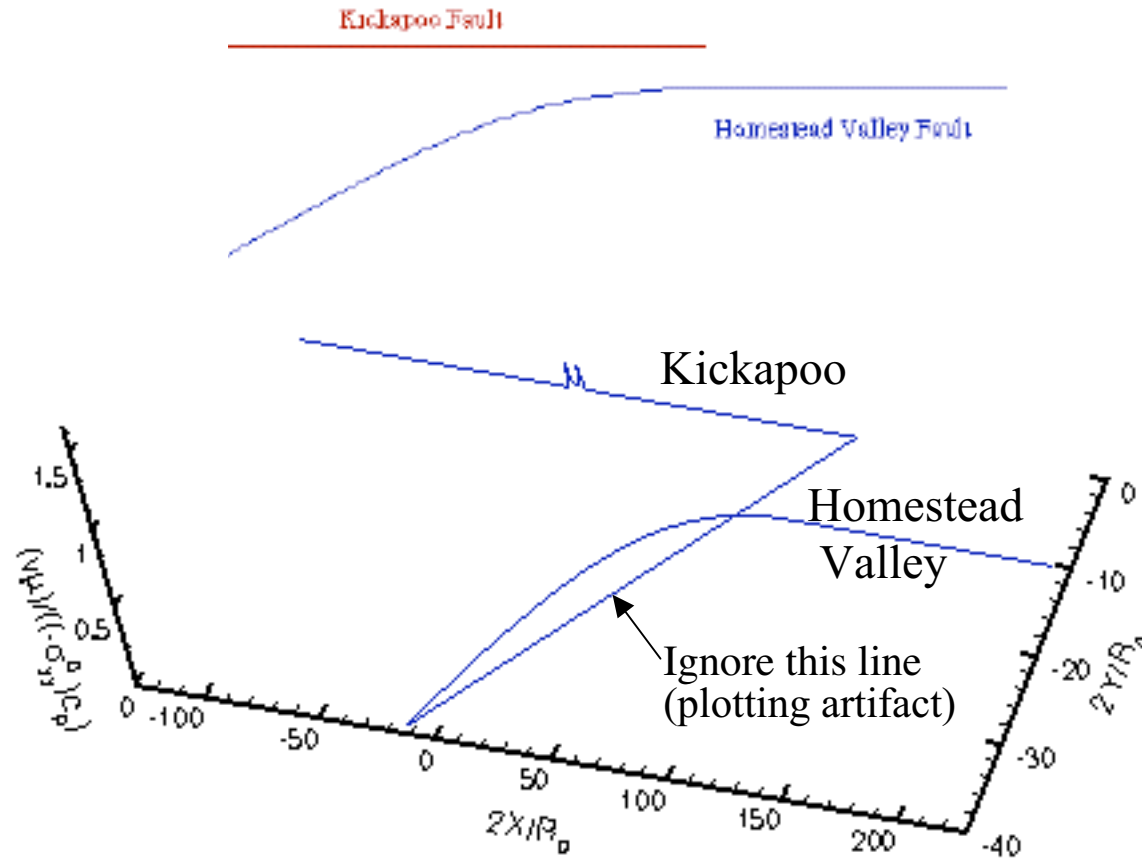
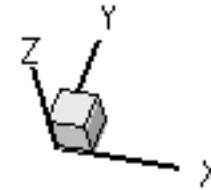
Contour plot of $T_{\text{coul}} = \tau_{xy} / \mu_s (-\sigma_{yy})$



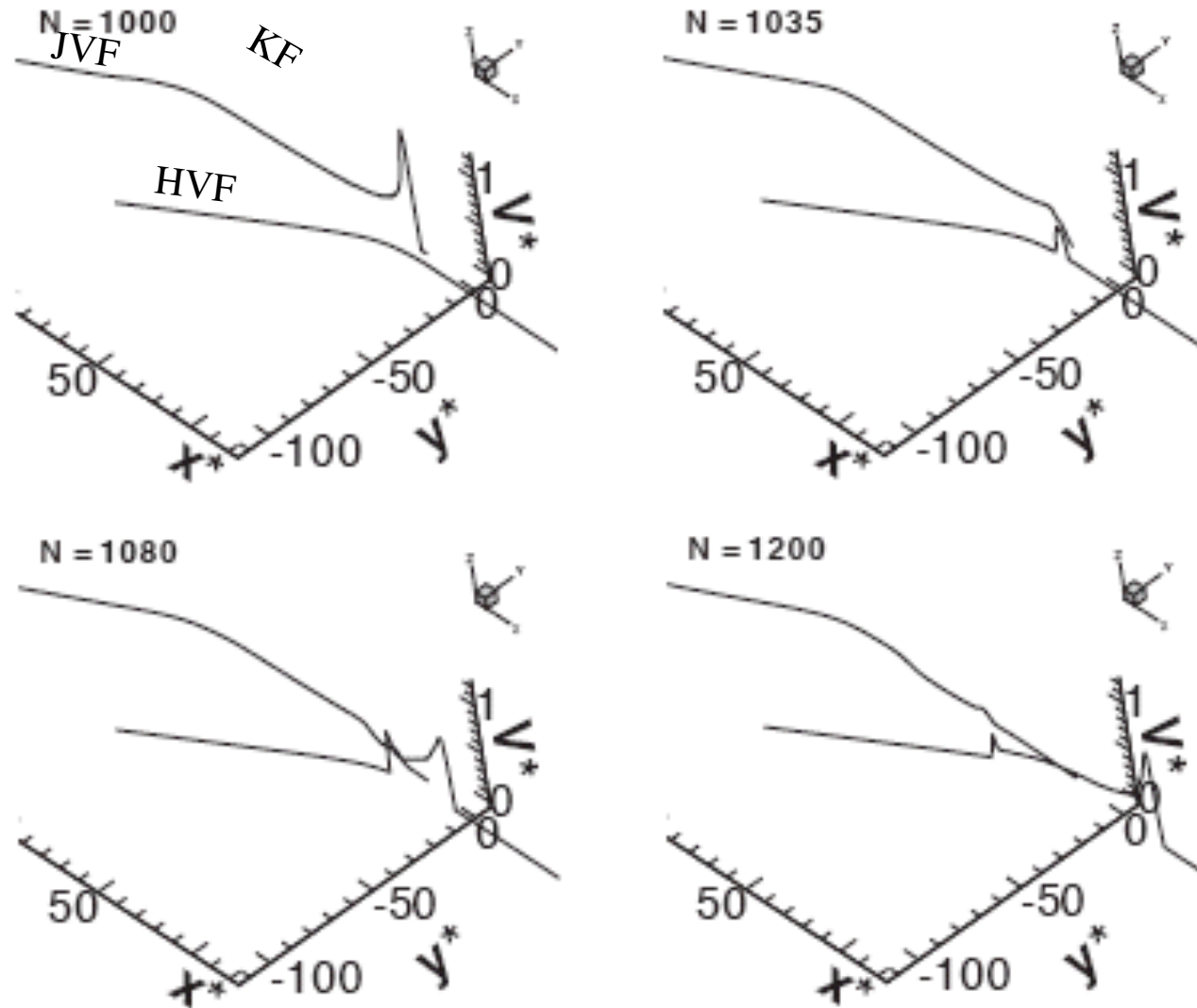
Only the region of potential failure is shown,
i.e. region where $T_{\text{coul}} > 1.0$;
Time elapsed between each zone = 0.2s

[Fliss, Bhat, Dmowska & Rice, *JGR*, 2005; this case with supershear propagation before arrest at end of KF]

Slip velocity for the 2 faults
for each 0.1 s



Fliss, Bhat, Dmowska & Rice [*JGR*, 2005]; simulation showing jump from the Kickapoo Fault (KF) to the Homestead Valley Fault (HVF), for a case with sub-Rayleigh v_r on the KF



Backward branching is most likely achieved as abrupt arrest on primary fault, followed by jump to a neighboring fault and bilateral propagation on it.

Such mechanism makes diagnosing directivity of a past earthquake difficult without detailed knowledge of the branching process.

SUMMARY OF BASICS OF RUPTURE BRANCHING

- If the branch would be taken or not depends on the geometry of the branch (on which side is the branch, how large is the angle between the main fault and the branch).
- It also depends on rupture velocity at the branching point: the larger the velocity, the more likely the rupture will deviate from its original direction.
- It also depends on the pre-stress field in the area of branching, in particular on the angle between the principal compressional stress direction and that of the rupturing fault.
- Backward branching complicates understanding which was the direction of the rupturing fault.

ROLE OF FINITE BRANCHES ON RUPTURE DYNAMICS ALONG THE MAIN FAULT

**2D numerical elastodynamic simulation using
boundary integral equation method and linear
slip-weakening failure criterion**

(Bhat et al., *JGR*, 2007)

Short branches (~few 10's to few 100's of meters) emanating from the main fault can lead to remarkable changes in rupture propagation characteristics on the main fault.

The interaction between the faults (not necessarily oriented optimally) depends on the pre-stress field, branch geometry and rupture velocity near the branch.

There are lots of *minor branch faults*.

How do they interact with rupture on the major fault strands?

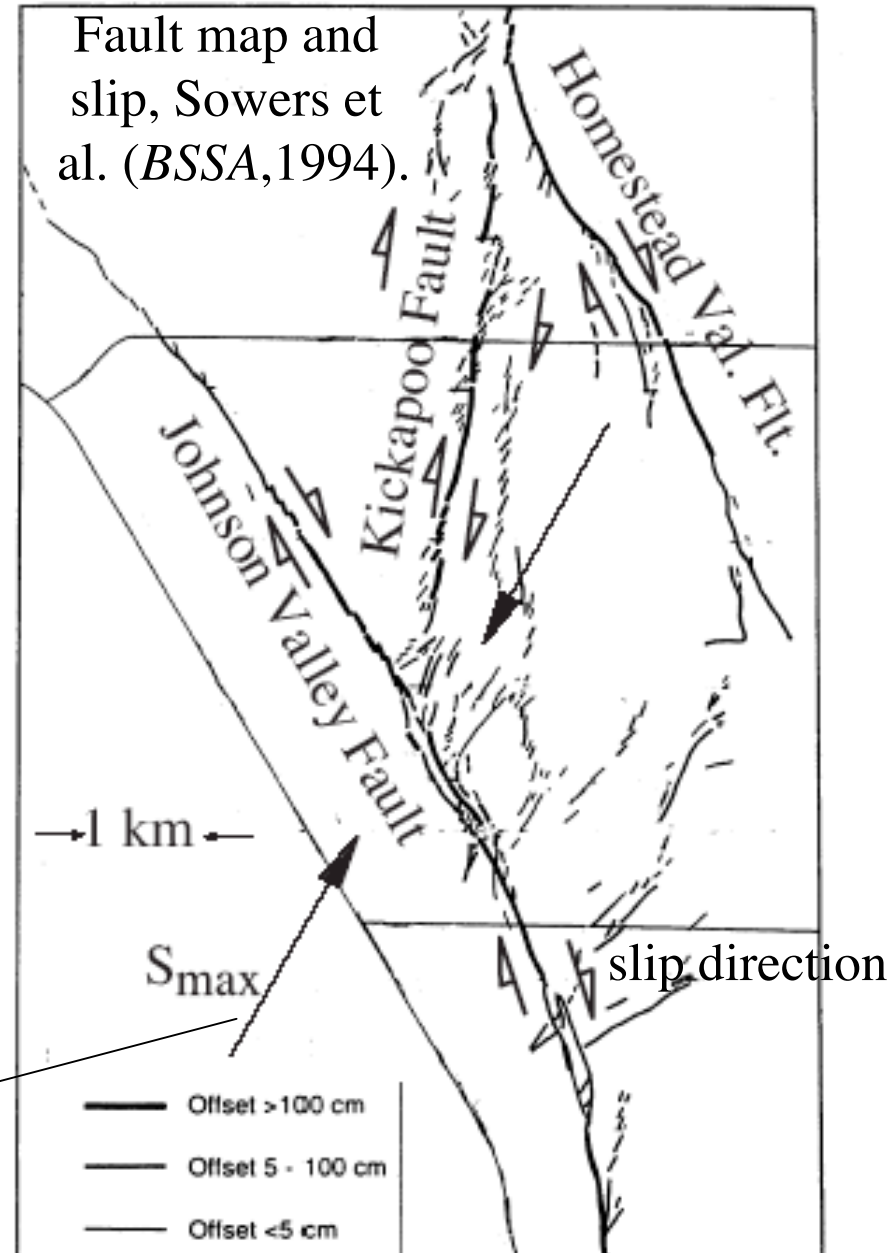
Could they make rupture propagation very nonuniform? -- and be a source of high-frequency ground motion?

Could they arrest rupture on a major fault strand?

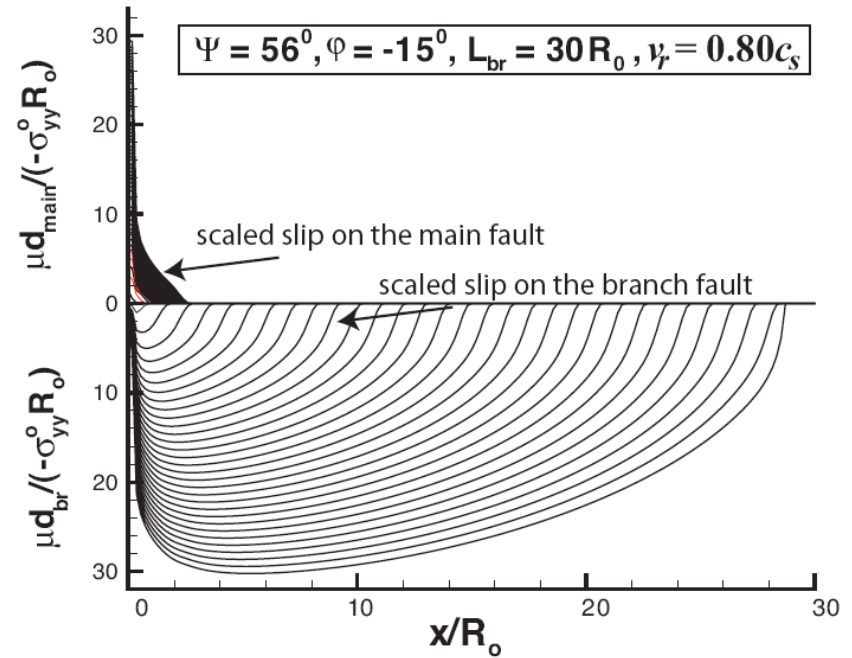
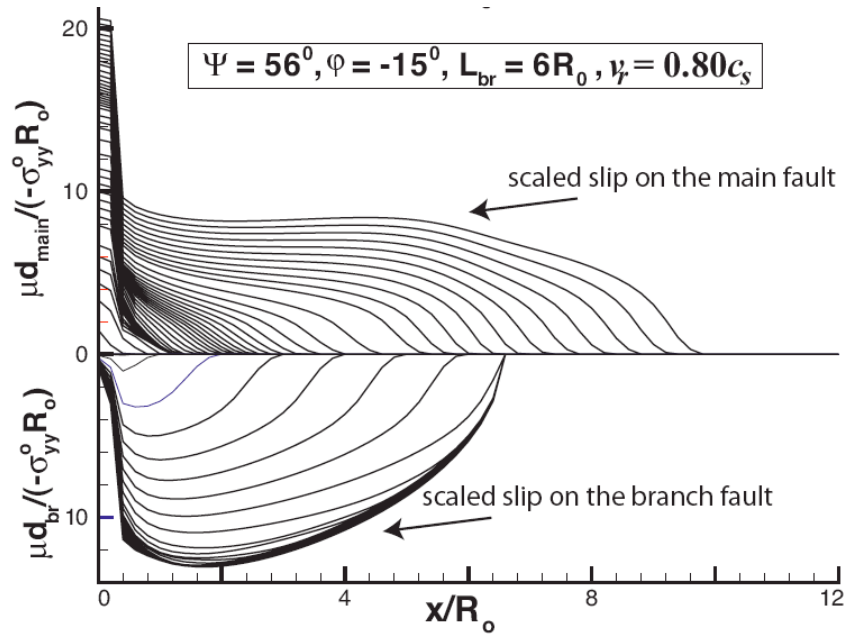
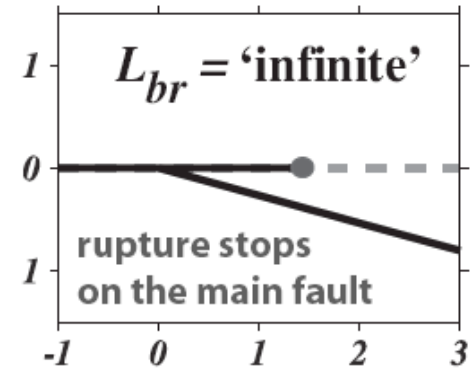
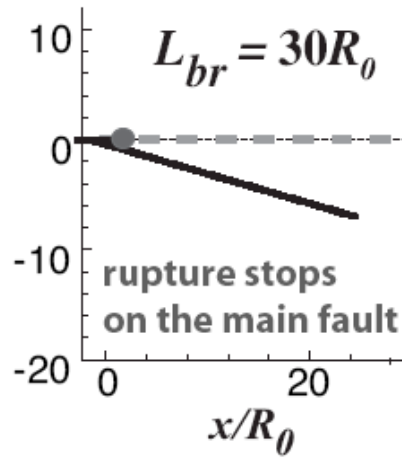
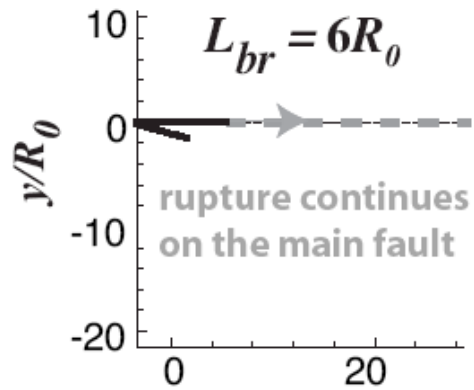
Examples given by Bhat, Olives, Dmowska & Rice [JGR 2007]

Pre-stress direction,
Hardebeck and
Hauksson (2001).

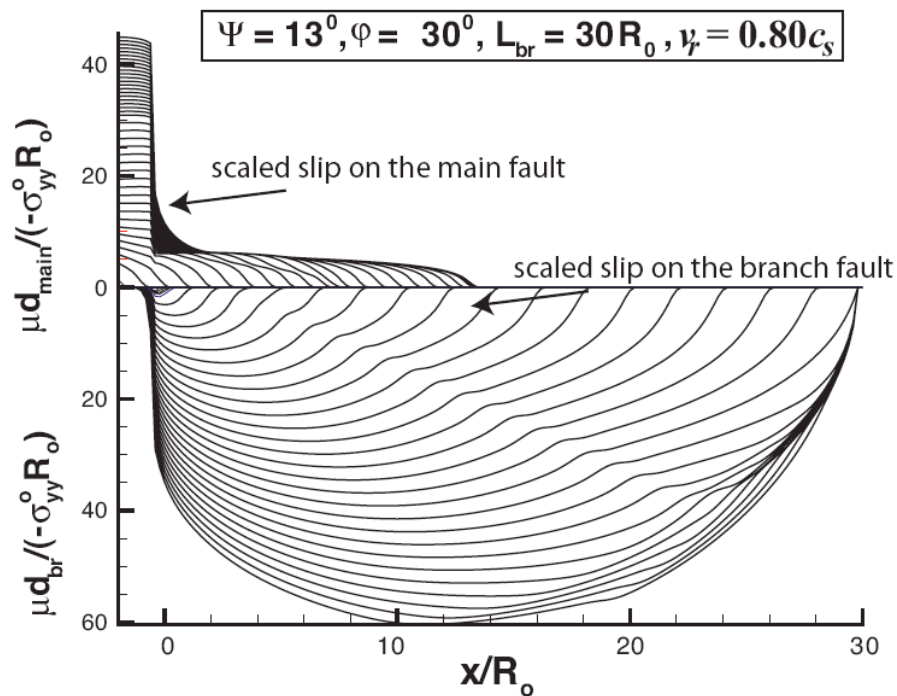
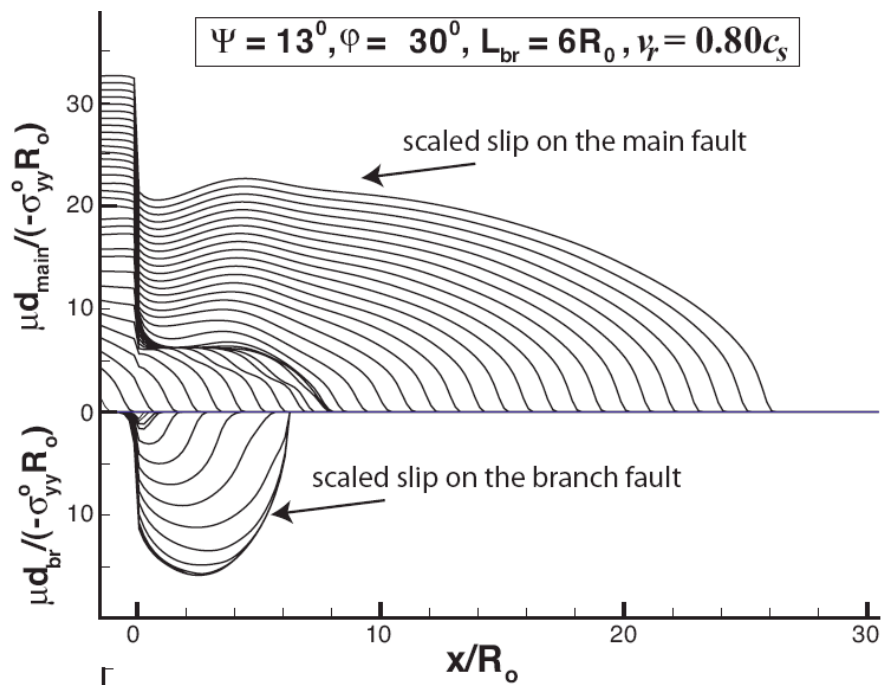
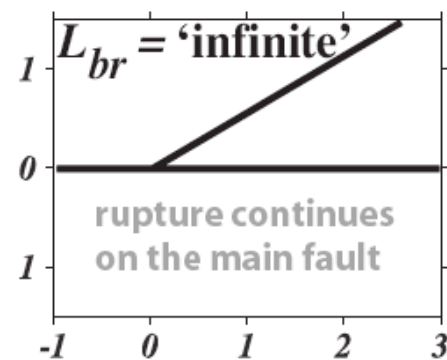
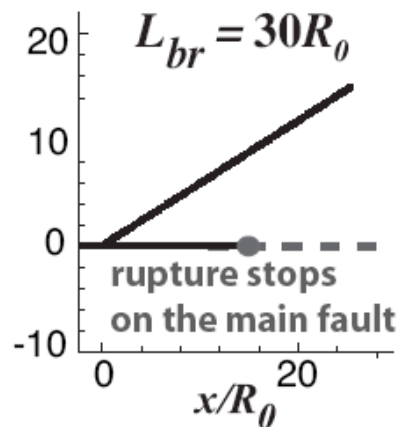
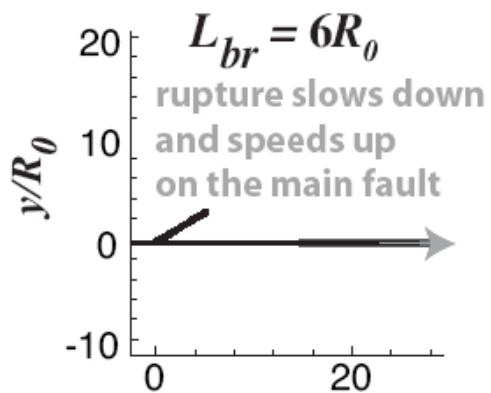
Landers 1992



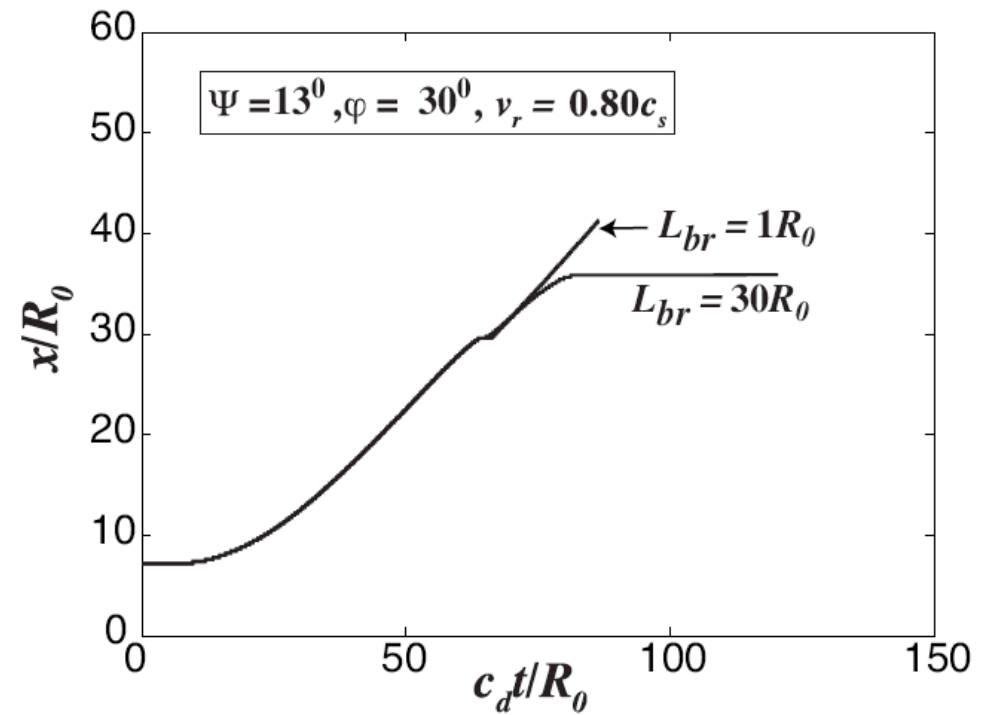
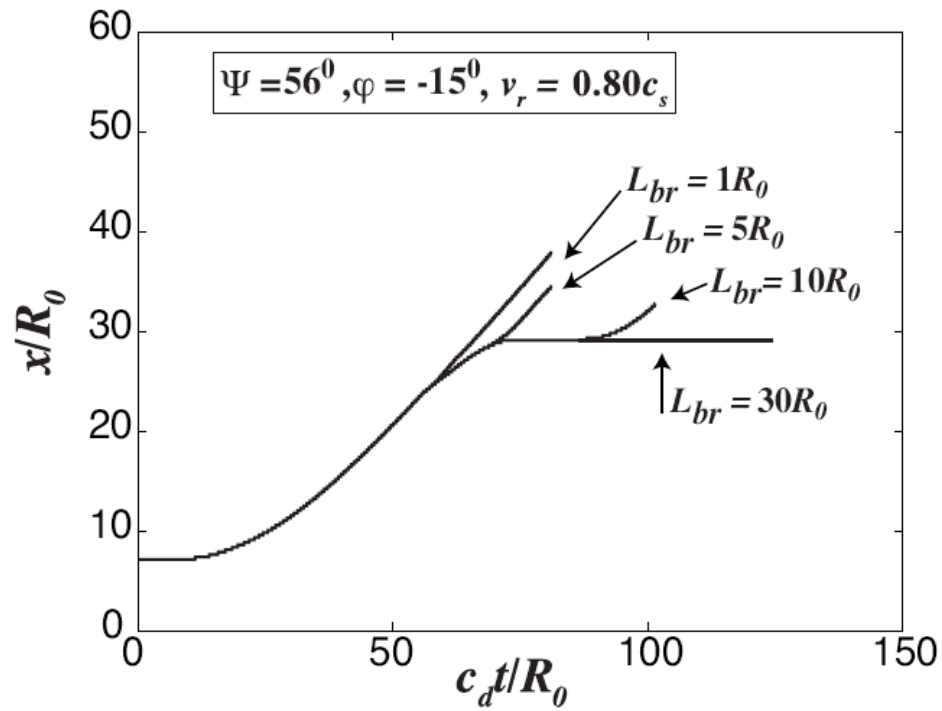
$$\Psi = 56^\circ; \varphi = -15^\circ; \nu_r = 0.80c_s$$



$$\Psi = 13^\circ; \varphi = 30^\circ; \nu_r = 0.80c_s$$



Length x of rupture on the main fault *versus* time t



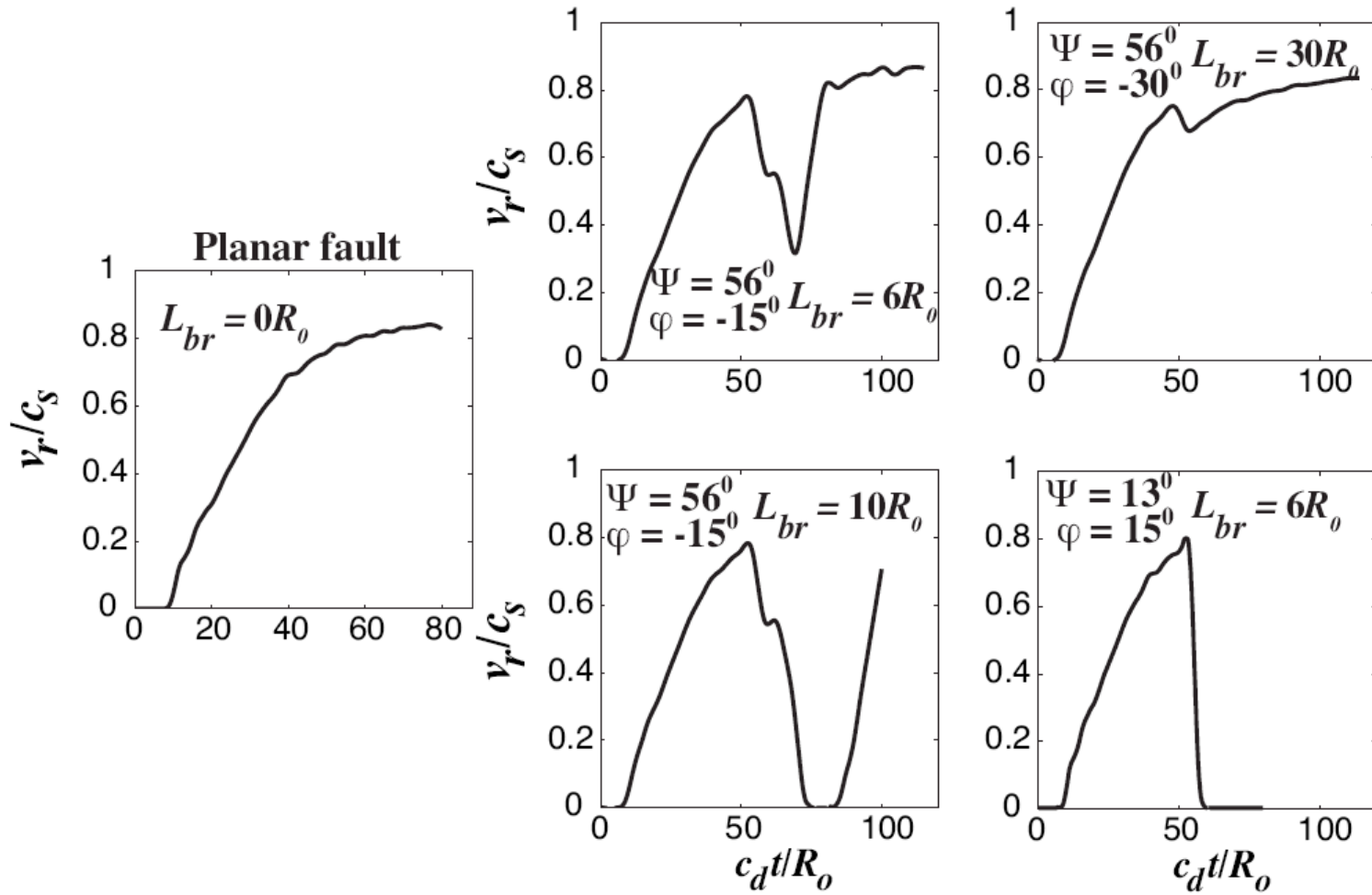


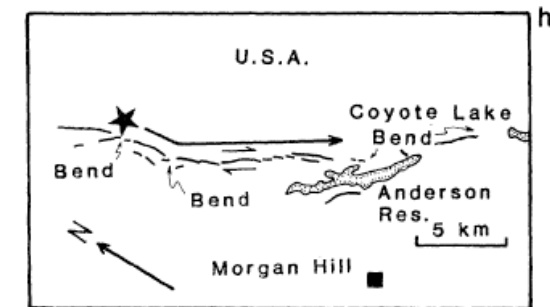
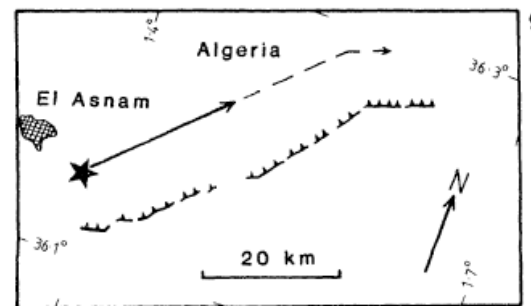
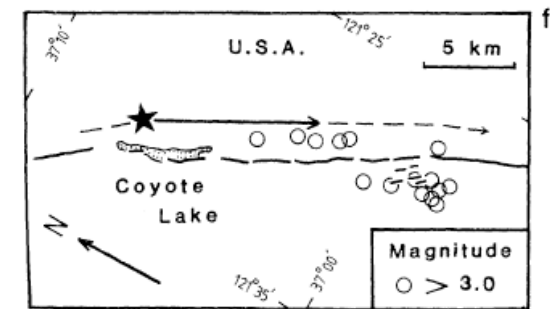
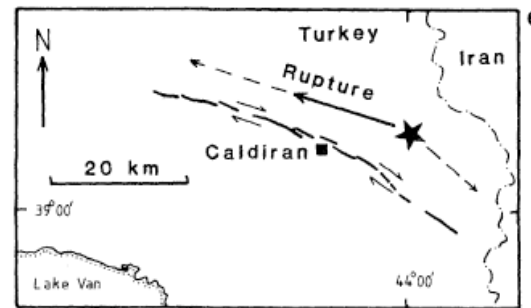
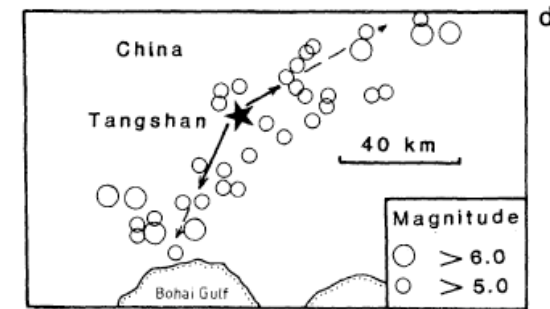
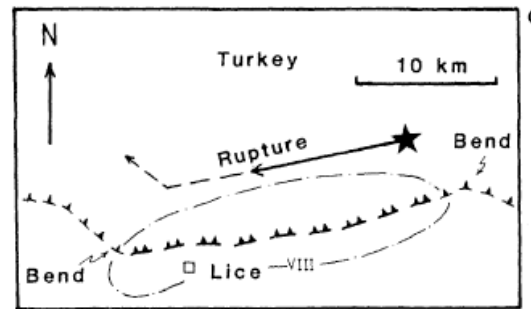
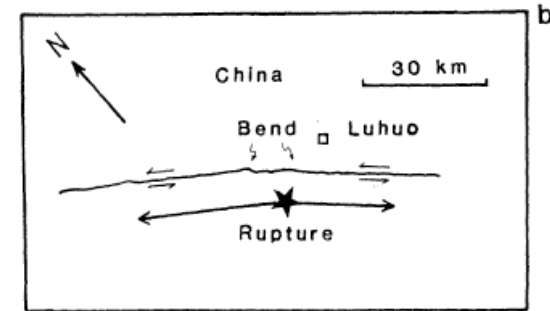
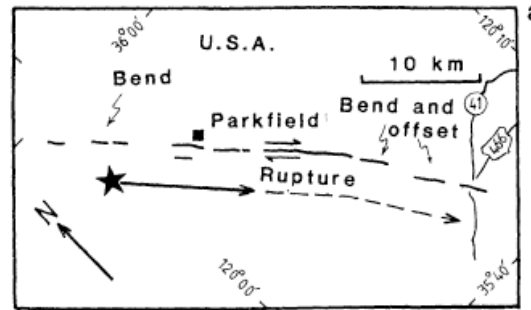
Figure 14: Complexities in rupture velocity, normalized by the shear wave speed (c_s), evolution with time for various configurations. Rupture velocity when approaching the branching junction, v_r , for all cases is $0.80c_s$.

- **Termination of rupture on the branch segment in some cases stops rupture propagation on the main fault.**
- **Complexities are introduced in rupture velocity pattern (rapid deceleration and acceleration) on the main fault.**
- **Finite branches also introduce complexities in the slip-pattern along the main fault.**
- **Finite branches introduce complexities in final stress distribution leading to potential locations of aftershocks.**

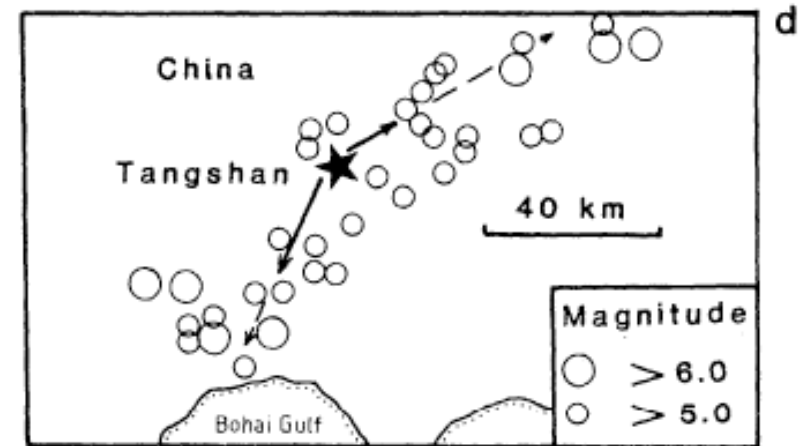
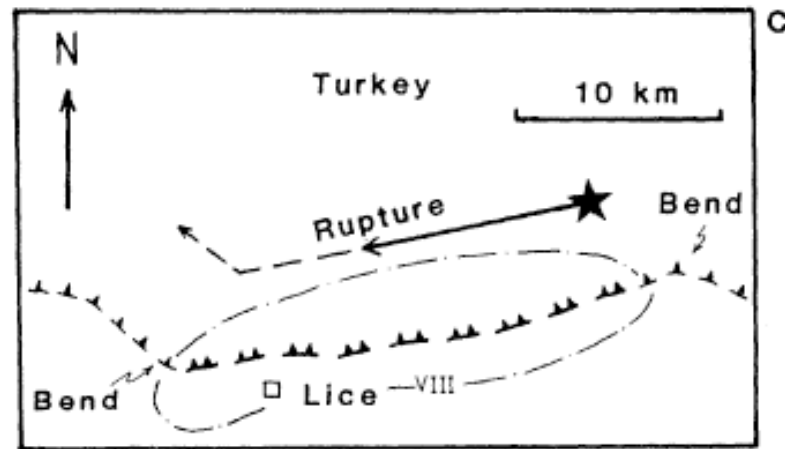
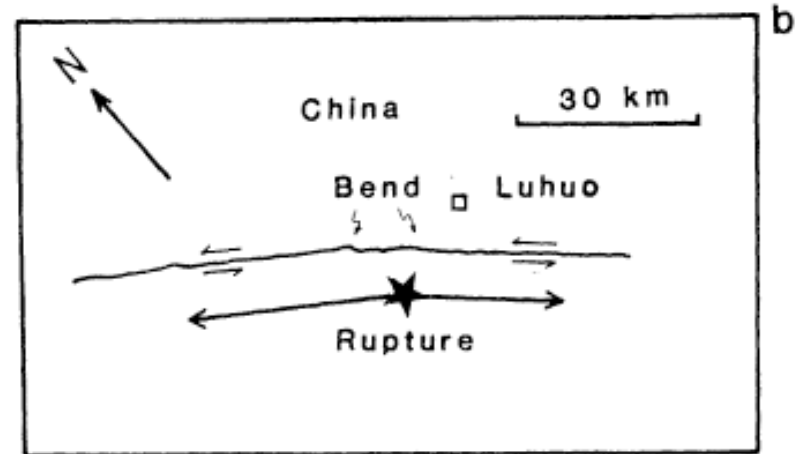
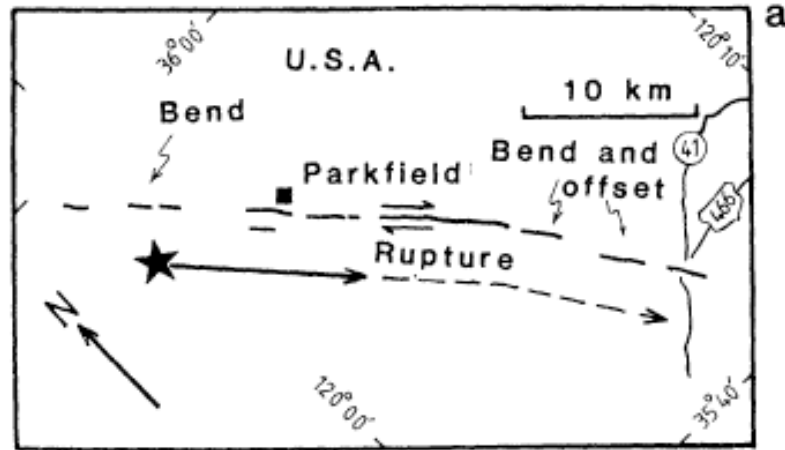
King & Nabelek,
Science, 1985:

Relation of bends in faulting to the initiation and termination of earthquake rupture for eight events:

- (a) Parkfield, California
- (b) Luhuo, China
- (c) Lice, Turkey
- (d) Tangshan, China
- (e) Caldiran, Turkey
- (f) Coyote Lake, Calif.
- (g) El Asnam, Algeria
- (h) Morgan Hill, Calif.



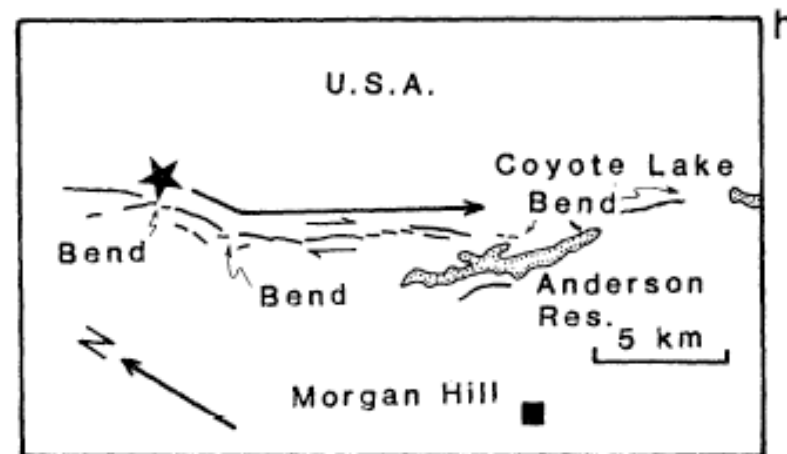
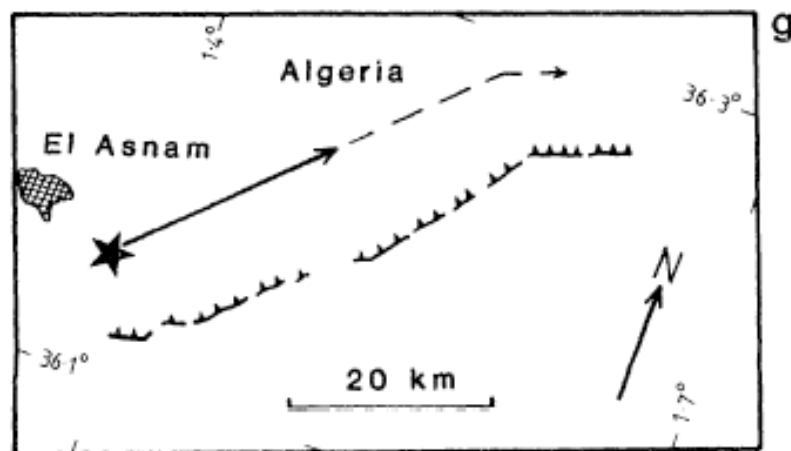
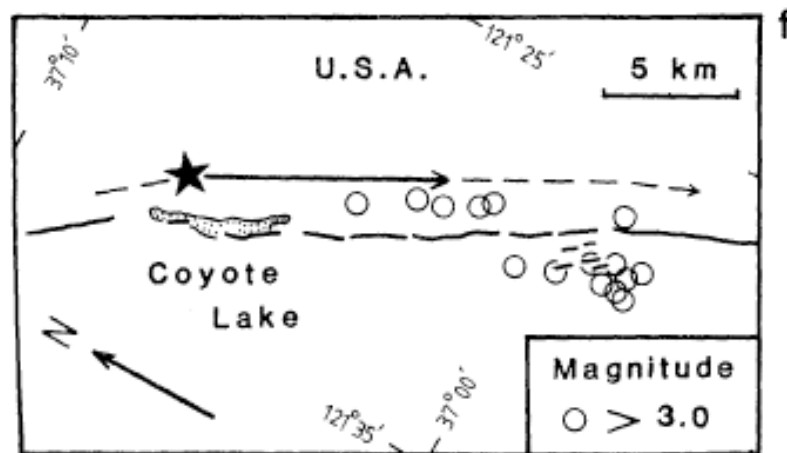
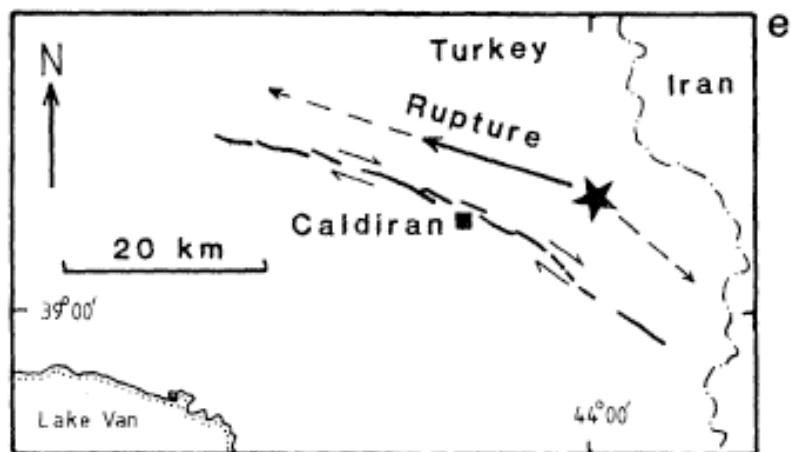
King & Nabelek, Science, 1985:



Relation of bends in faulting to the initiation and termination of earthquake rupture for eight events:

- (a) Parkfield, California
- (b) Luhuo, China
- (c) Lice, Turkey
- (d) Tangshan, China

King & Nabelek, Science, 1985:



Relation of bends in faulting to the initiation and termination of earthquake rupture for eight events:

- (e) Caldiran, Turkey
- (f) Coyote Lake, Calif.
- (g) El Asnam, Algeria
- (h) Morgan Hill, Calif.

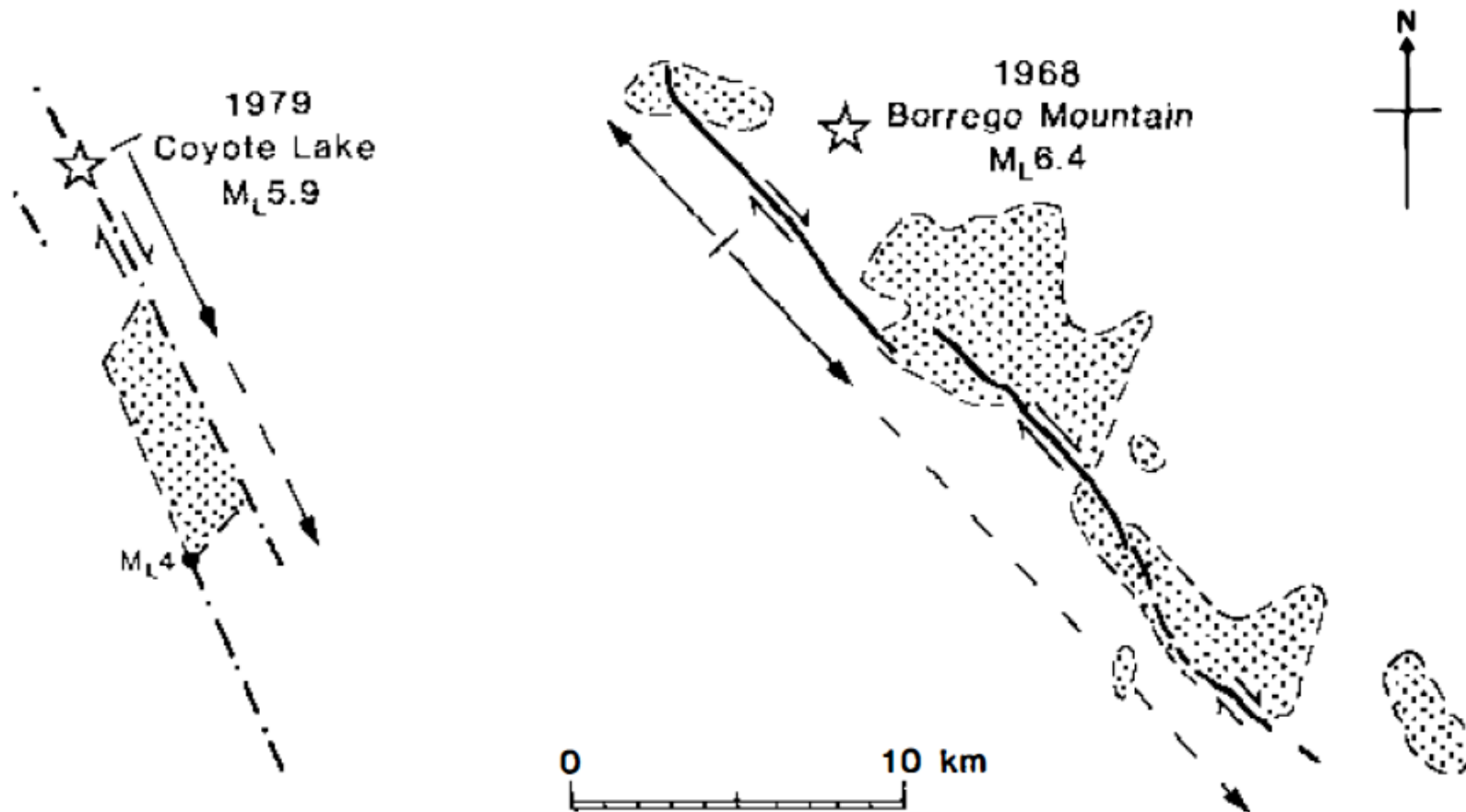


Figure 3 Seismotectonic maps illustrating aftershock concentrations associated with right-lateral strike-slip rupturing within the San Andreas fault system, California (after Sibson 1985). (Left) The 1979 $M_L = 5.9$ Coyote Lake earthquake rupture, which terminated in a dilational fault jog; (Right) The 1968 $M_L = 6.4$ Borrego Mountain rupture, which was at least partly arrested at an antidilational jog. (Epicenters represented by stars, propagation direction and extent of mainshock ruptures by arrows, surface breaks by broad lines, microearthquake lineaments by dash-dot lines, areas of intense aftershock activity by stippling.)

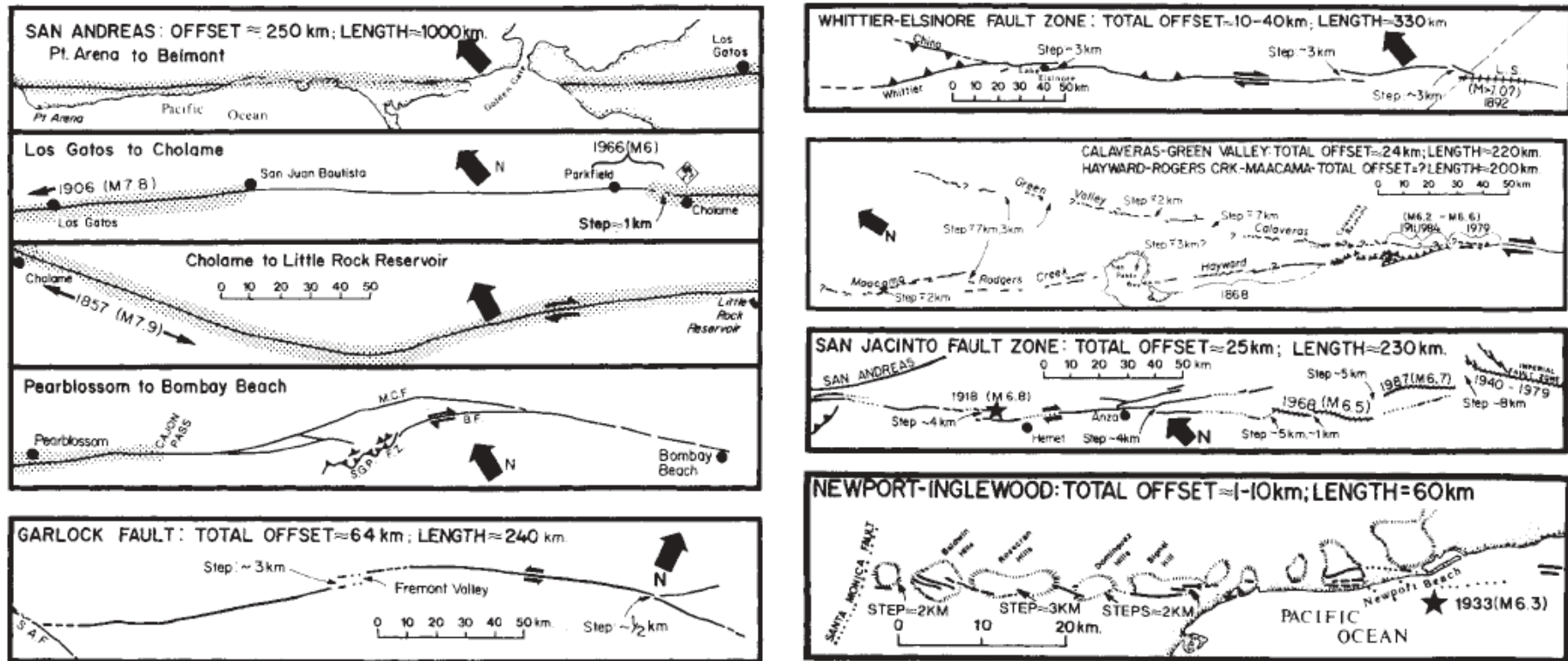
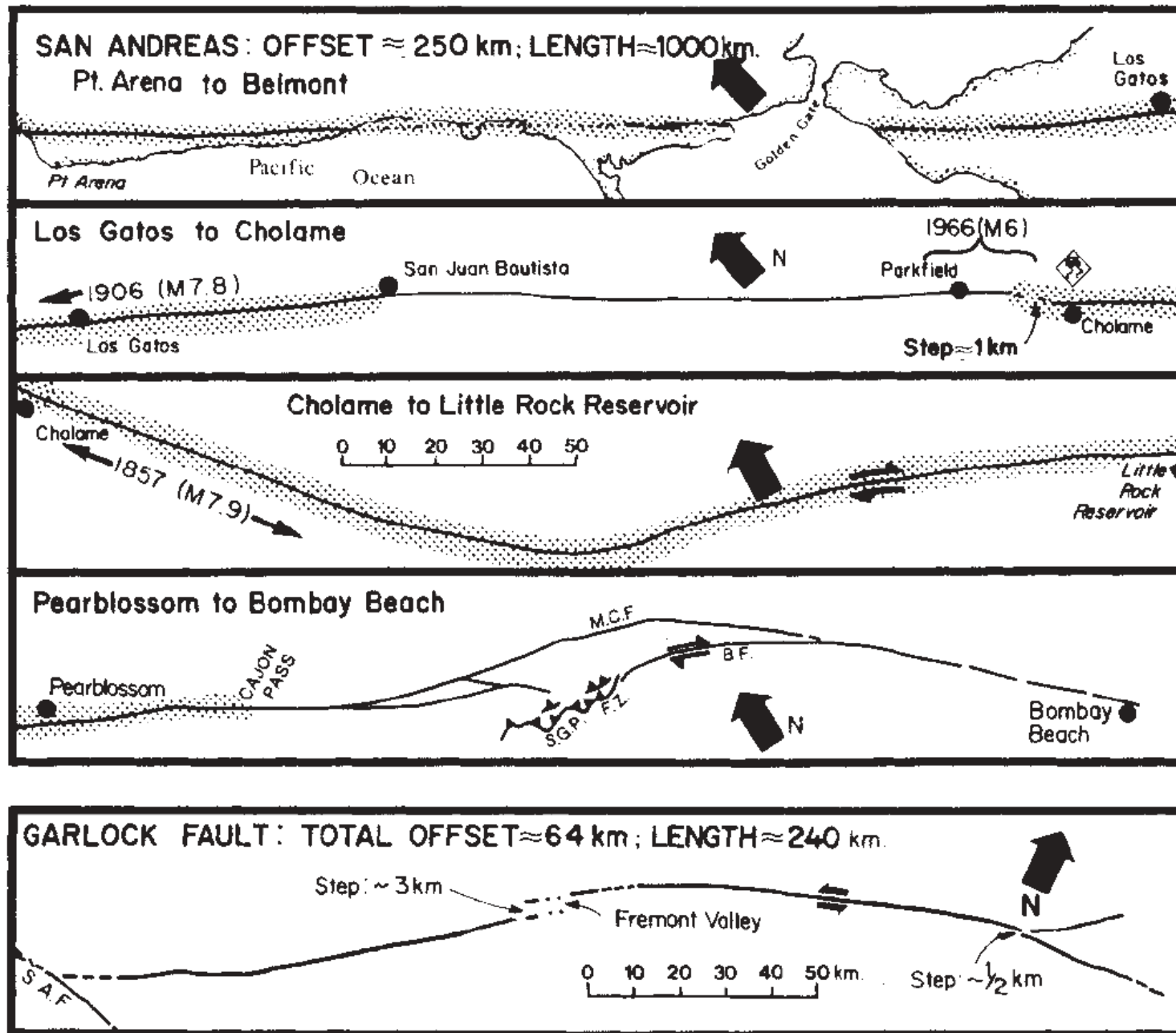
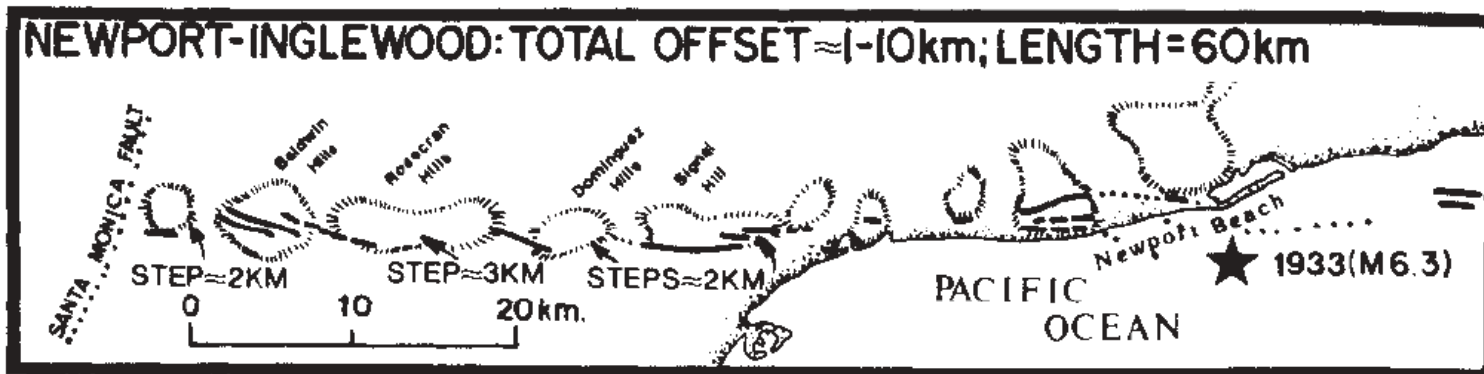
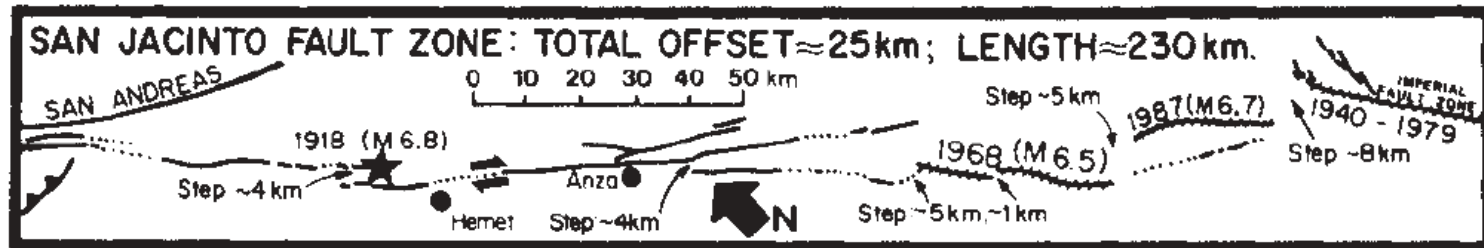
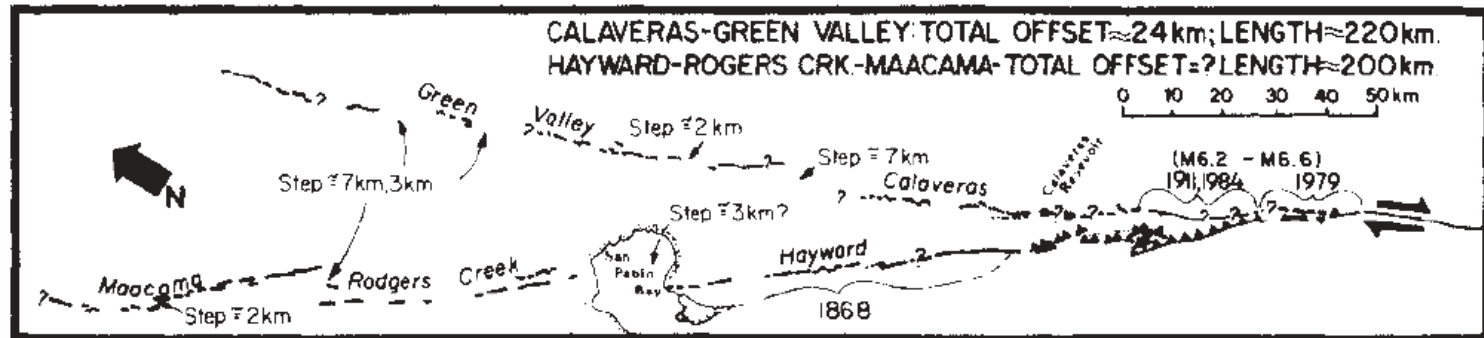


Fig. 1 Maps of the San Andreas¹⁶⁻²², Garlock²³, Whittier-Elsinore²⁴, Calaveras-Green Valley²⁵, San Jacinto²⁶ and Newport-Inglewood¹³ fault zones of California showing the location of steps in fault traces which are characterized by stepover widths $W_s \geq 1$ km. Segments of fault which have ruptured during historical earthquakes are marked by hachures, stippling or brackets, and the dates and magnitudes of the respective earthquakes. Epicentre of 1933 Long Beach earthquake is marked by star and half-sided arrows indicate sense of displacement along faults.

Wesnousky, Nature, 1988



Wesnousky, Nature, 1988



Wesnousky, Nature, 1988

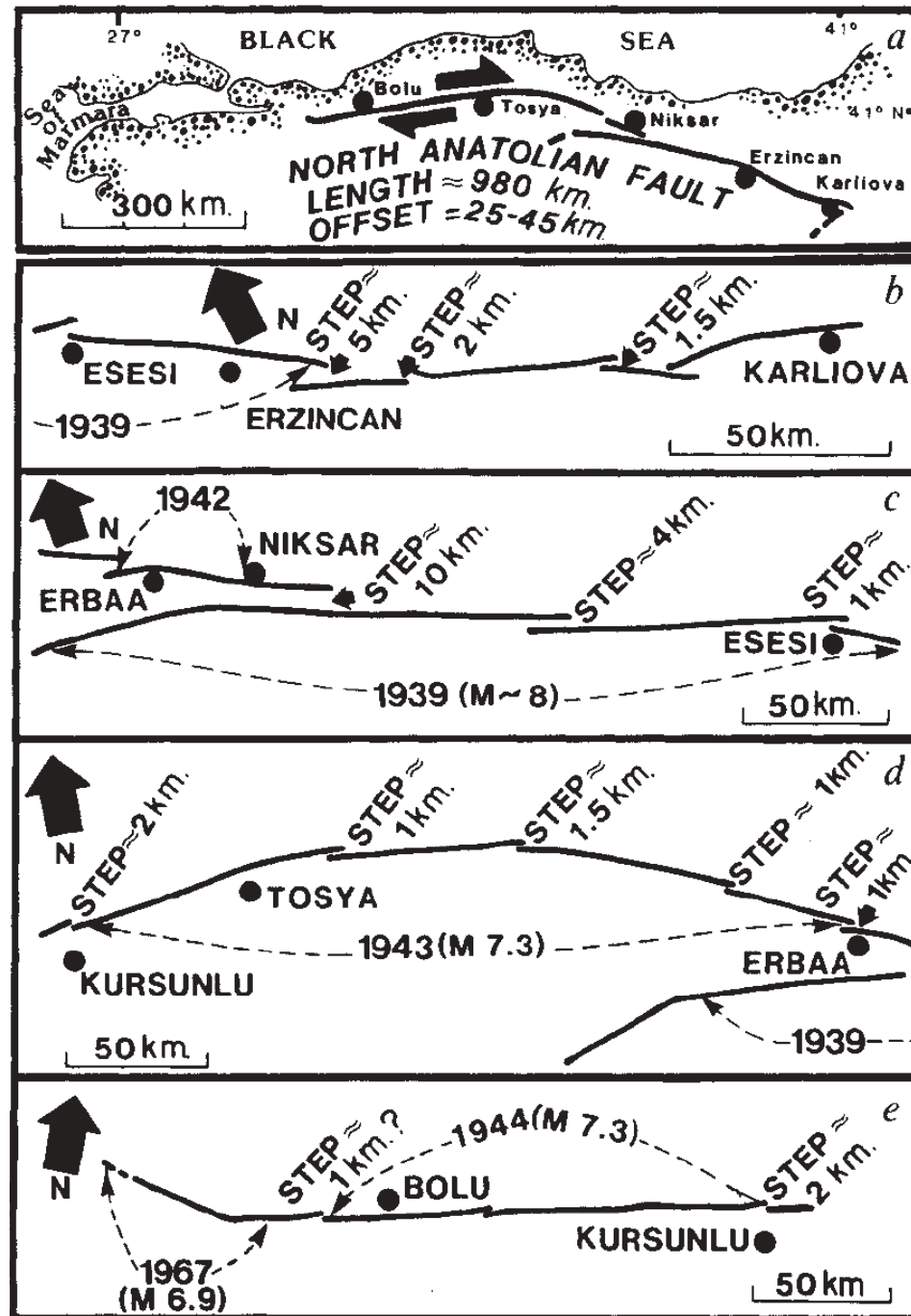
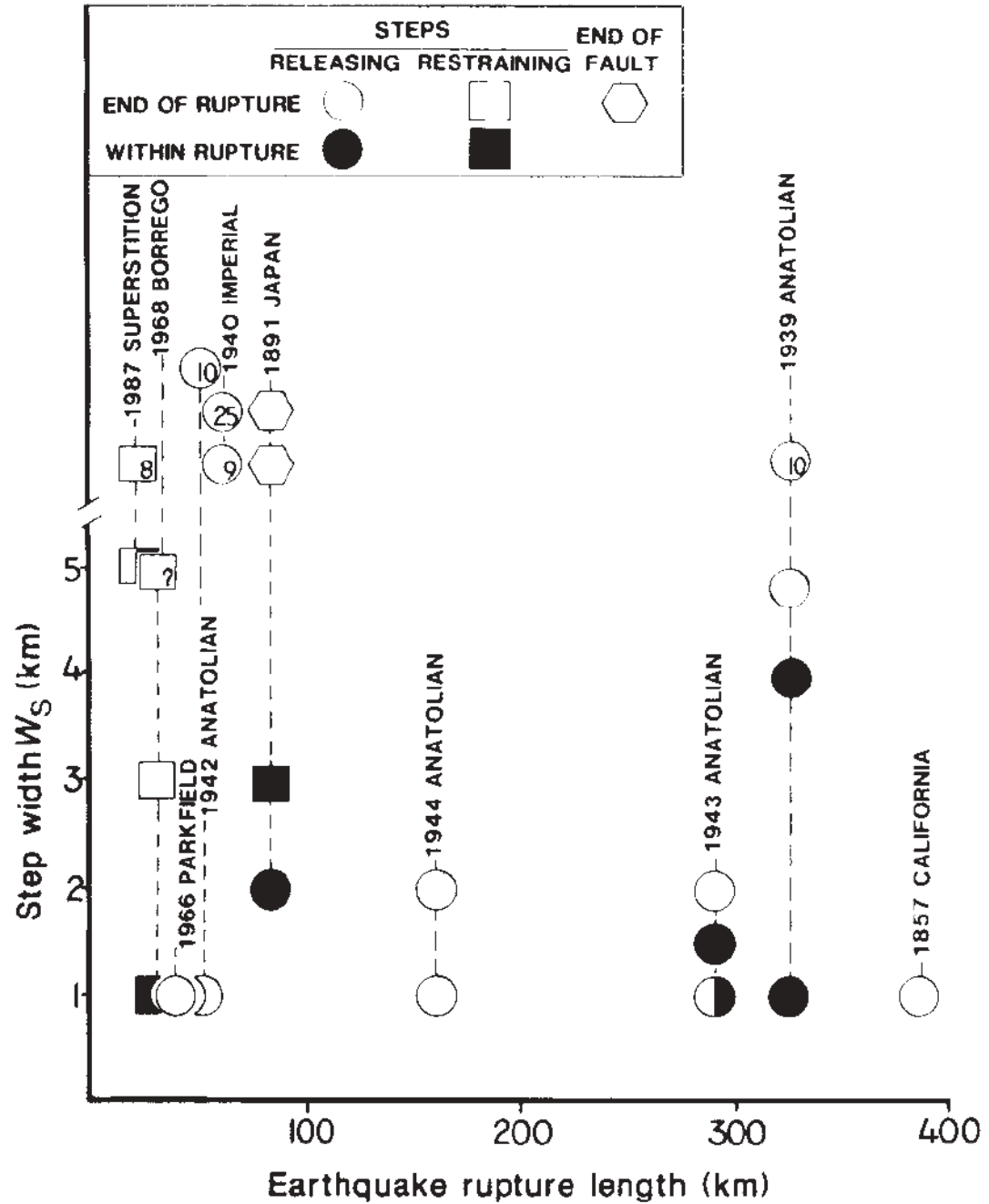


Fig. 2 a, The North Anatolian fault shows right-lateral movement and strikes westward across Turkey from a point near Karliova to west of Bolu. Larger-scale and overlapping strip maps of the fault (b-e) are taken from Barka and Kadinsky-Case5 and show location of steps greater than about 1 km in size. Dates and arrows show the year and extent of rupture during large historical earthquakes, respectively.

Wesnousky,
Nature, 1988

Fig. 3 Earthquake rupture length versus the size W_s of steps in mapped fault trace observed at the endpoints (open symbols) and within (solid symbols) the rupture zone of large Anatolian and California earthquakes. Half-filled symbol indicates that steps of similar size occurred both within and at endpoint of rupture. Steps in fault trace are also subdivided according to whether they are restraining (squares) or releasing (circles) in nature.



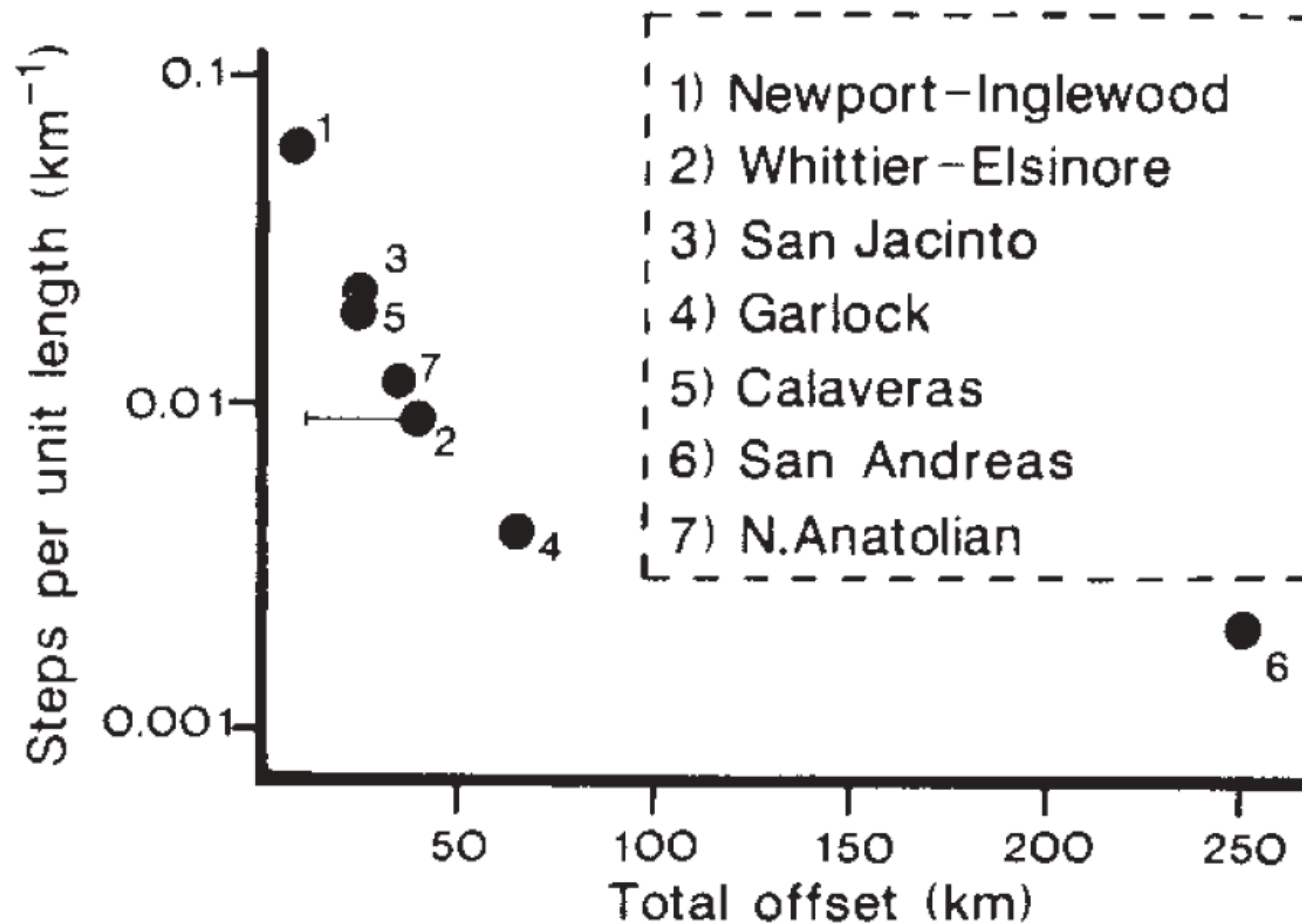


Fig. 4 The number of steps ($W_s \geq 1$ km) per unit length of mapped fault trace versus cumulative geological offset along major strike-slip faults in California and Turkey.

FAULT STEPS

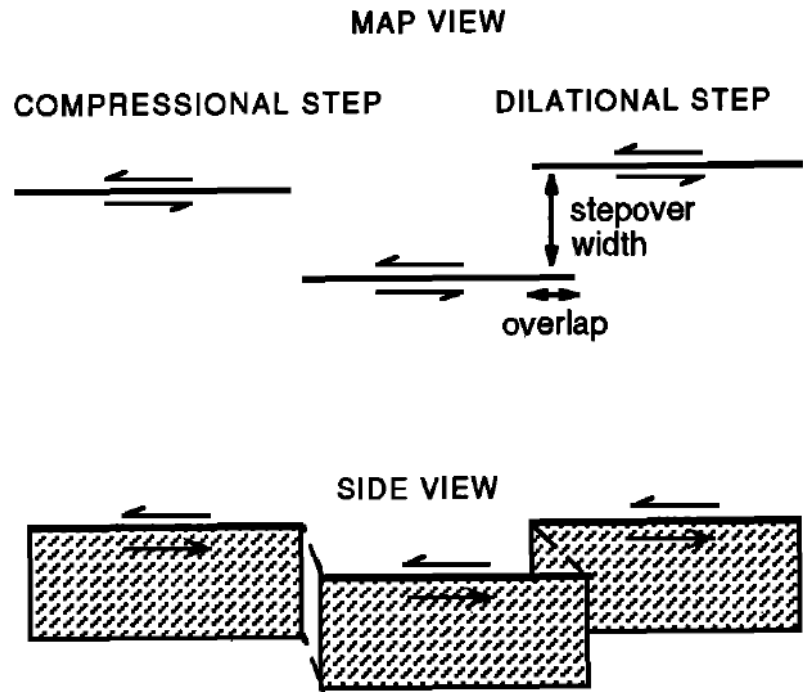


Fig 1. Right and left steps in a left-lateral vertical strike-slip fault. When two of the fault segments are slipping at the same time, a right step is a compressional step and a left step is a dilational step. For right-lateral faults, right steps are dilational and left steps are compressional. The stepover width is the perpendicular distance between the two faults and the overlap is the along-strike distance of fault crossover. When the two fault ends do not pass each other the overlap is negative, as shown for the compressional step.

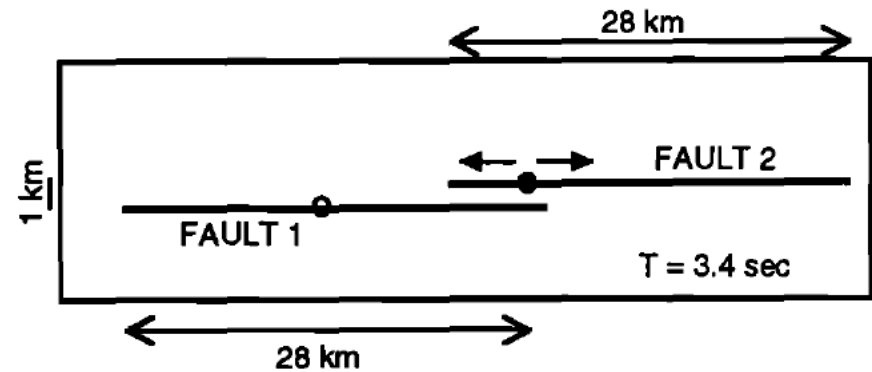
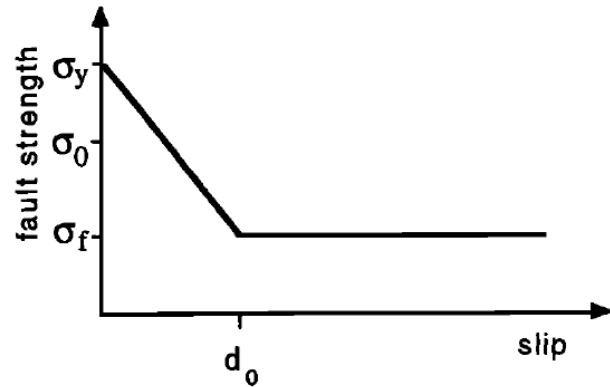


Fig 2. Map view of two faults at 3.4 s for the case of a dilational step (left step in left-lateral shear) and the parameters listed in Table 1, Case A. Both faults are 28 km long. Stepover width is 1 km, overlap is 5 km. Open circle indicates point where rupture first nucleated on fault 1 at 0 seconds. At 2.9 s the rupture first reached the end of fault 1. At 3.4 seconds the point marked by the solid circle on fault 2 starts to rupture. After 3.4 s, the rupture propagates bilaterally on fault 2.

Slip-weakening Fracture Criterion



- d_0 = slip-weakening critical distance
- σ_y = static yield stress = $-\mu_{stat} \sigma_{normal}$
- σ_0 = initial shear stress
- σ_f = dynamic yield stress = $-\mu_{dyn} \sigma_{normal}$

Fig 3. The slip-weakening fracture criterion defines the strength of the fault as a function of slip on the fault. Initially the fault strength is the static yield strength. When the fault first begins to slip the strength linearly decreases to the dynamic friction strength. Once the fault has slipped a critical distance, d_0 , the fault strength is equal to the dynamic strength.

Rupture nodes

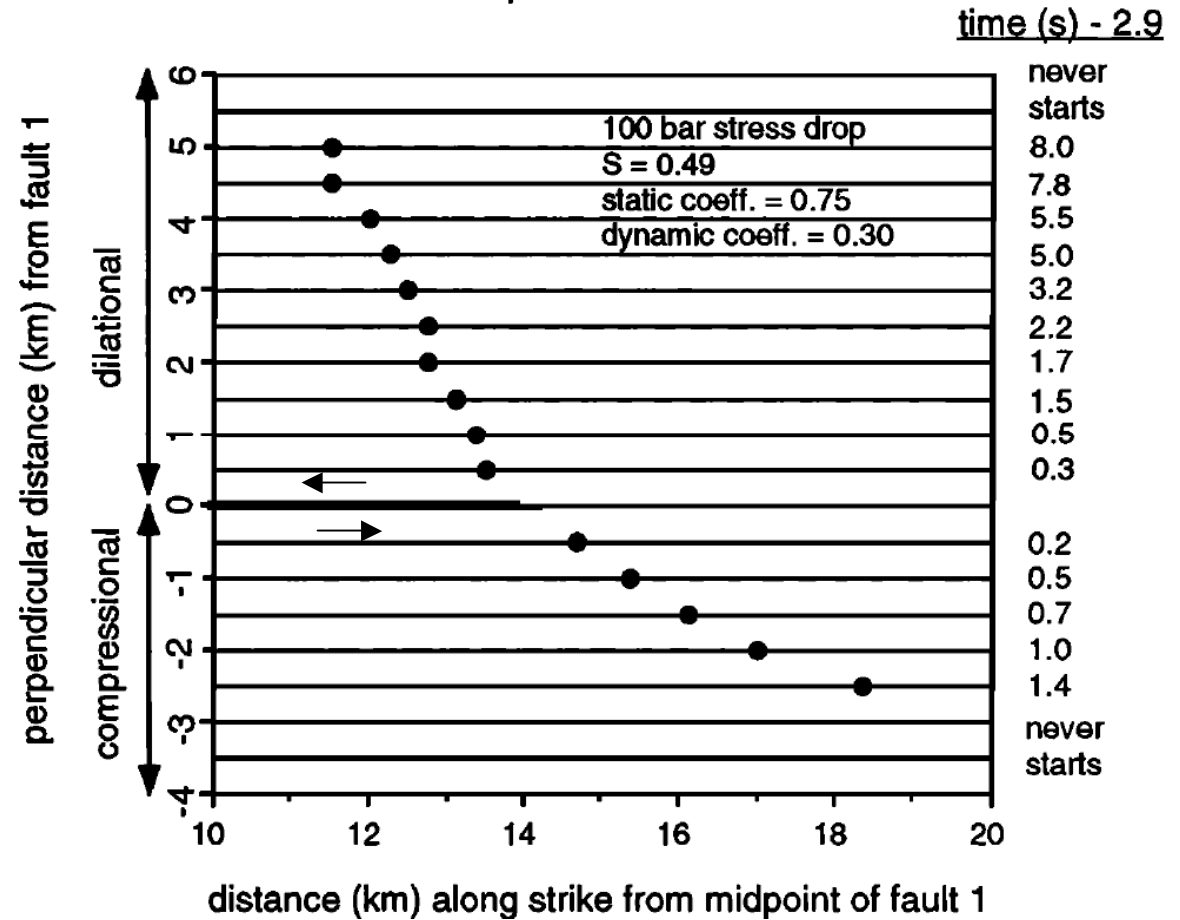


Fig 6. Case A. Summary (map view) of the results from 20 simulations of fault steps in left-lateral shear. Table 1, Case A lists the variables used in this simulation. For each simulation only two faults exist, as depicted in Figure 2. Fault 1 is drawn with a heavy dark line. The rupture first reached the end of fault 1 at 2.9 seconds. All of the fault 2's are shown by the light parallel lines. Faults with positive stepover widths are dilational steps, negative stepover widths are compressional steps. Each solid circle indicates the point where a fault 2 is initially triggered. The times to the right of the figure are the trigger times for each fault 2. The parameter S is defined in equation (1) in the text.

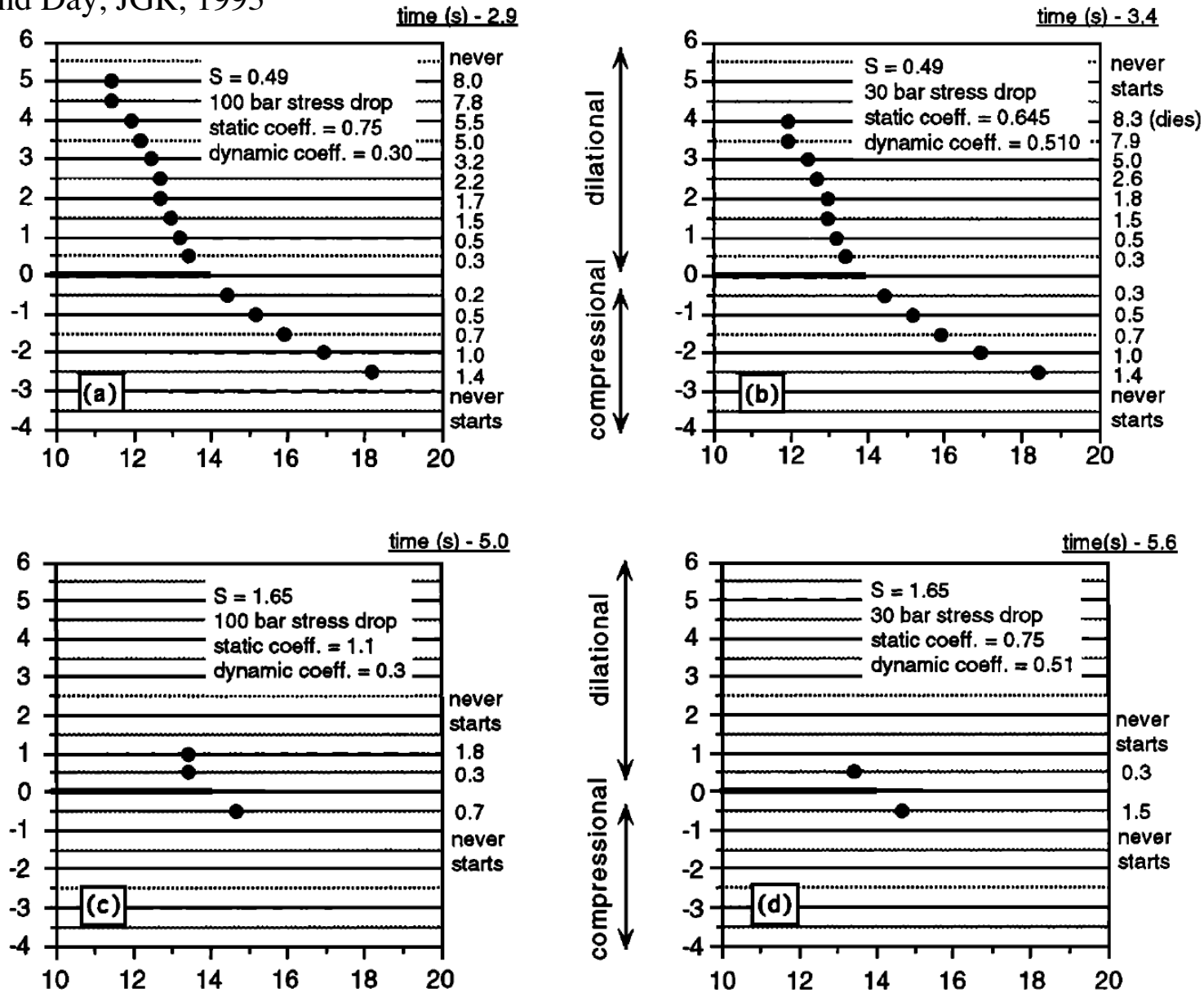


Fig. 7. Summary (map view) of the results from 20 simulations of fault steps in left-lateral shear. This figure shows the results for Cases A-D. See Table 1 for a listing of the variables used in each case, and the text for a discussion. (a) Case A - same as Figure 6, this case is shown again for comparison. (b) Case B. (c) Case C. (d) Case D.

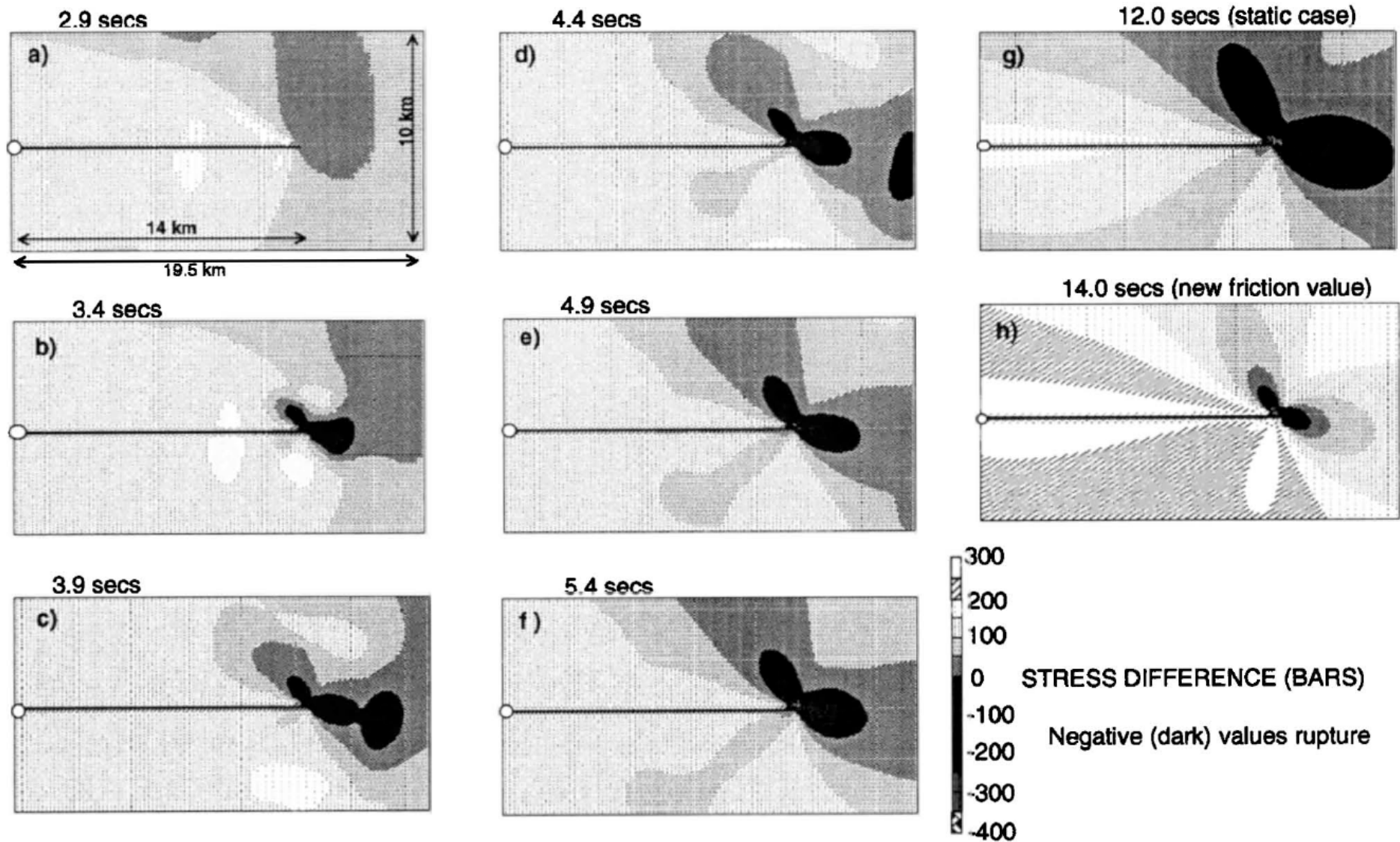


Fig. 8. Contoured map view of the stress difference (Δs) at 2.9 seconds due to rupture propagation on fault 1. Fault 1, a left-lateral fault, is the dark line. The map scale is 1:1. Negative values of Δs indicate regions where a second parallel fault could start but do not determine if the rupture would continue to propagate on the second fault (see text). At 2.9 seconds the rupture has just reached the end of fault 1. No negative regions exist so no parallel left-lateral strike-slip fault could trigger at this time. The parameters used in these simulations are listed

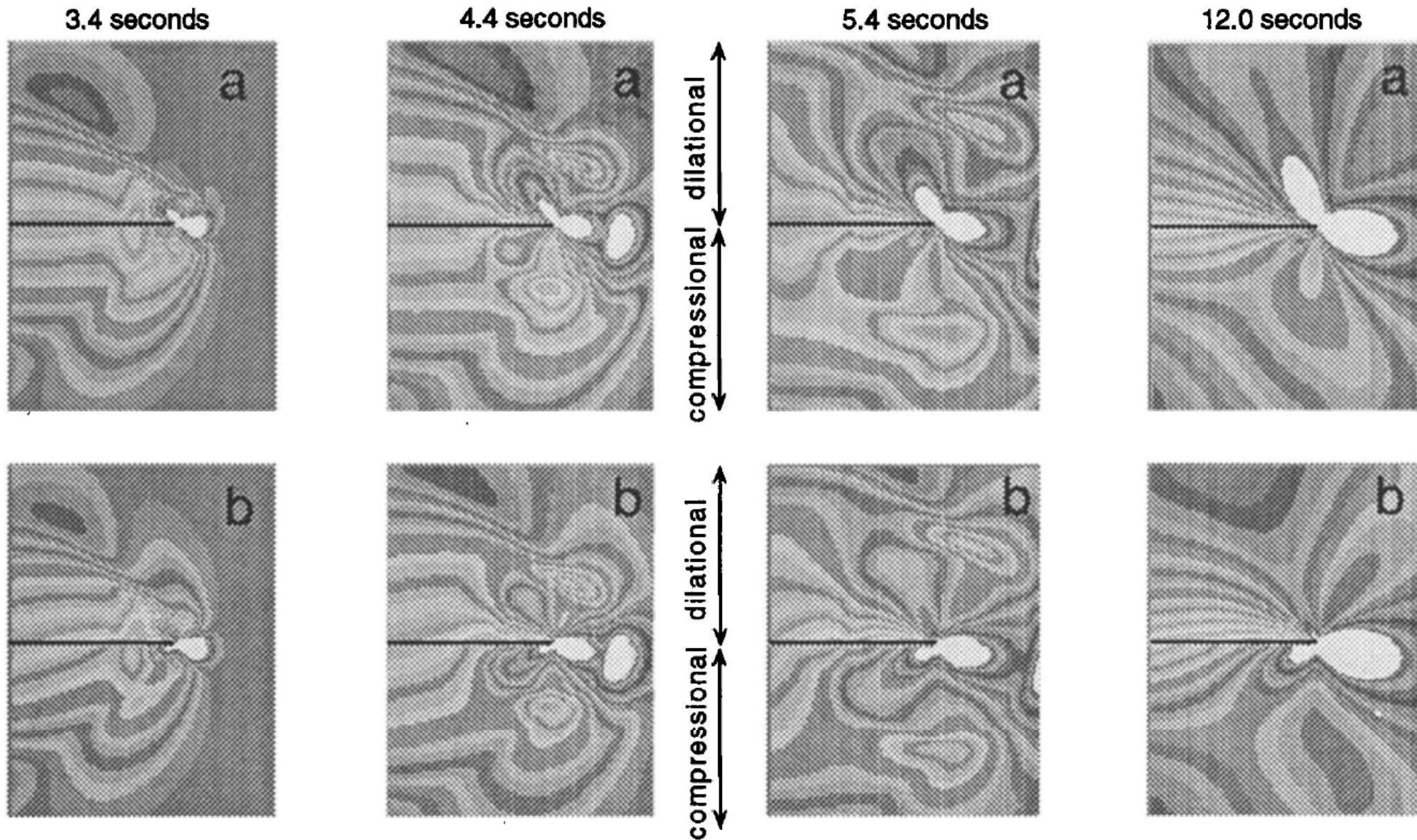


Fig. 10. Contoured map view of the stress difference (Δs) at 3.4, 4.4, 5.4, and 12.0 seconds for the case which (a) does not include the effects of changes in pore pressure (same as Figure 8), and (b) does include the effects of changes of pore pressure. Light regions indicate where a second parallel fault could trigger. Note that when the effects of changing pore pressure are included the rupture has difficulty jumping dilational steps.

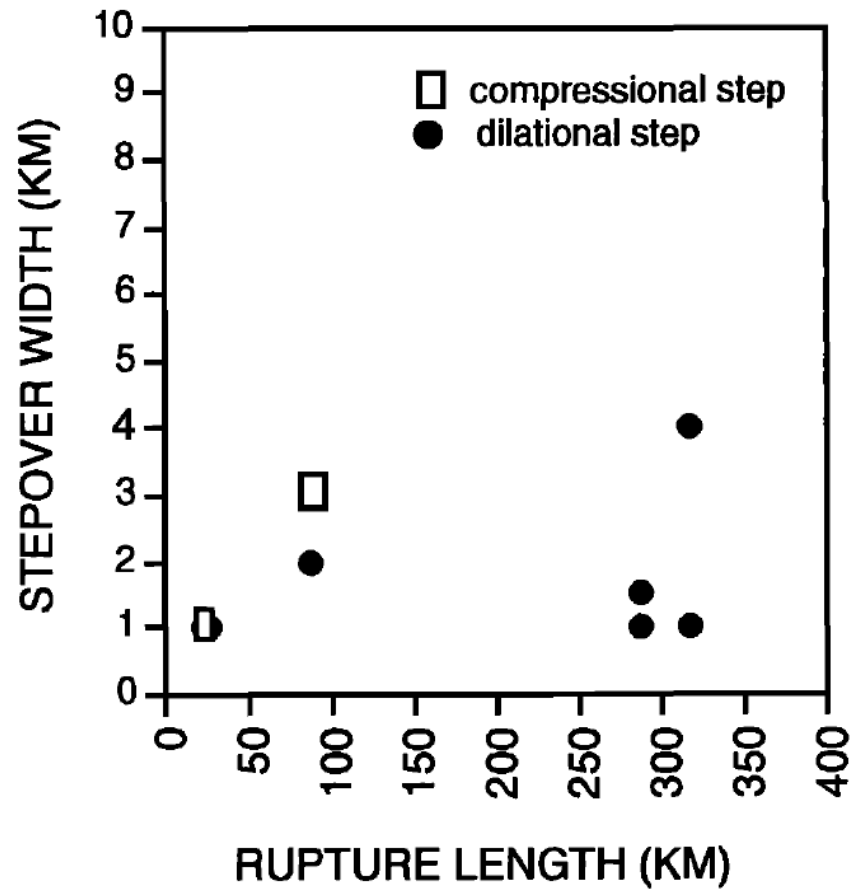


Fig. 9. Stepovert width versus rupture length, modified from *Wesnowsky* [1988]. Points indicate fault steps which were jumped during earthquakes. Data are from the 1968 Borrego Mountain, California, earthquake, 1966 Parkfield, California, earthquake, the 1891 Nobi Japan earthquake, the 1943 Northern Anatolian fault (Turkey) earthquake, and the great 1939 Erzincan earthquake, also on the Northern Anatolian fault. The earthquakes are listed in ascending order of rupture length.

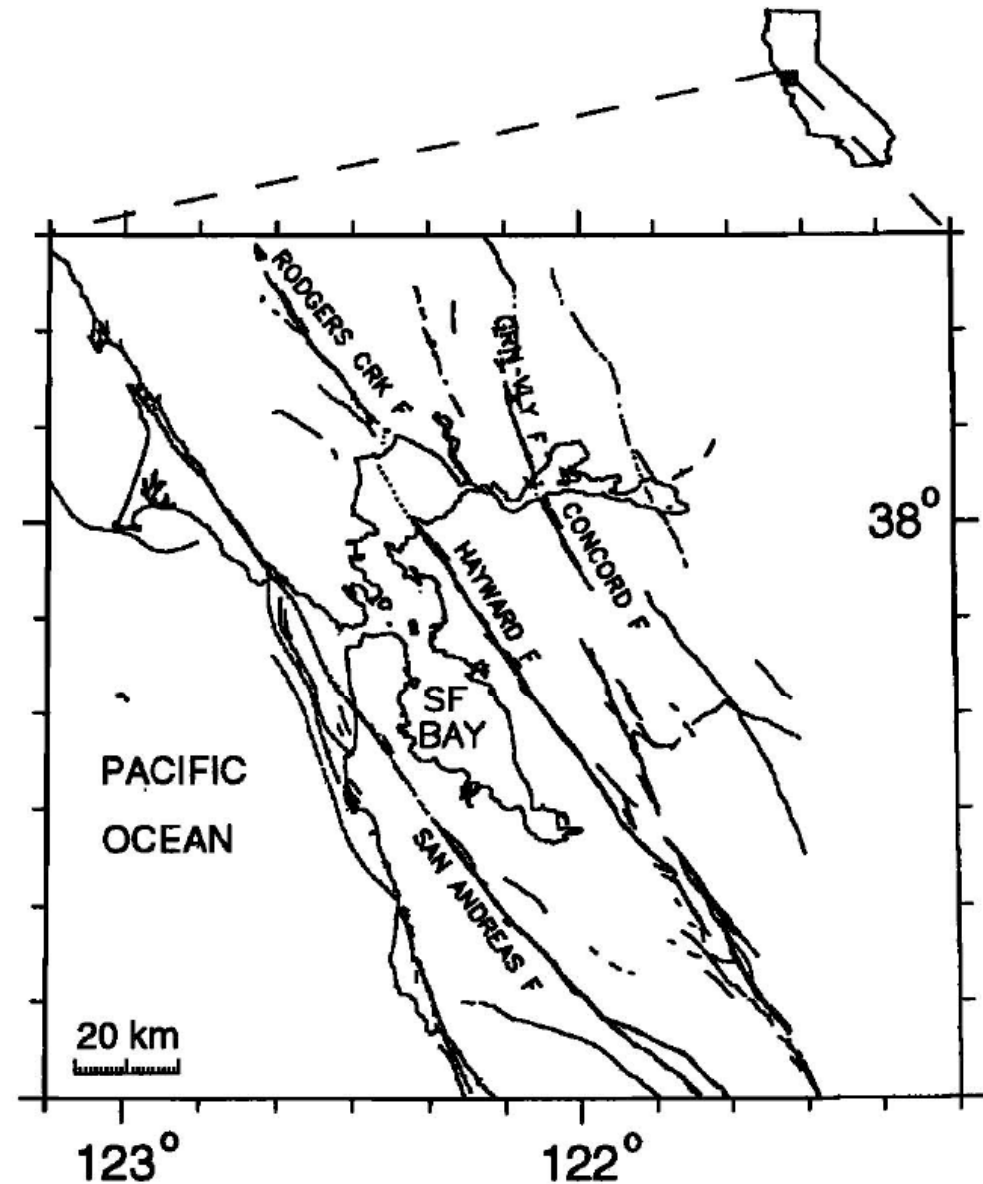


Fig. 11. Locations of fault steps in the San Francisco Bay region of California. The text discusses the right step between the right-lateral strike-slip Hayward and Rodgers Creek faults, and the right step between the right-lateral strike-slip Concord and Green Valley faults.

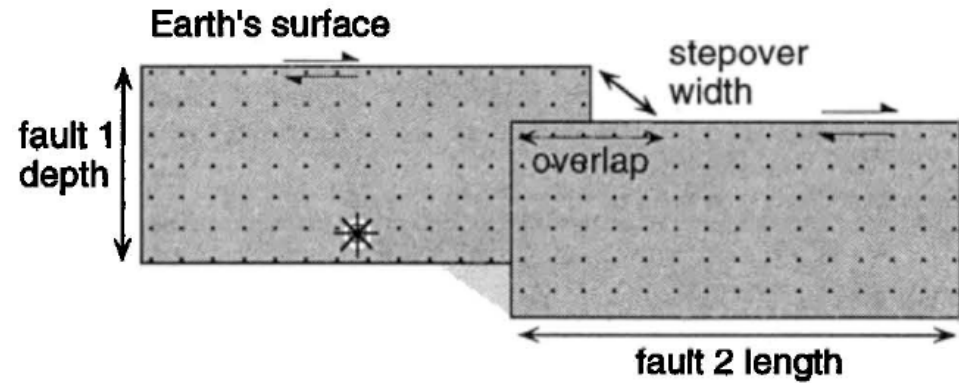
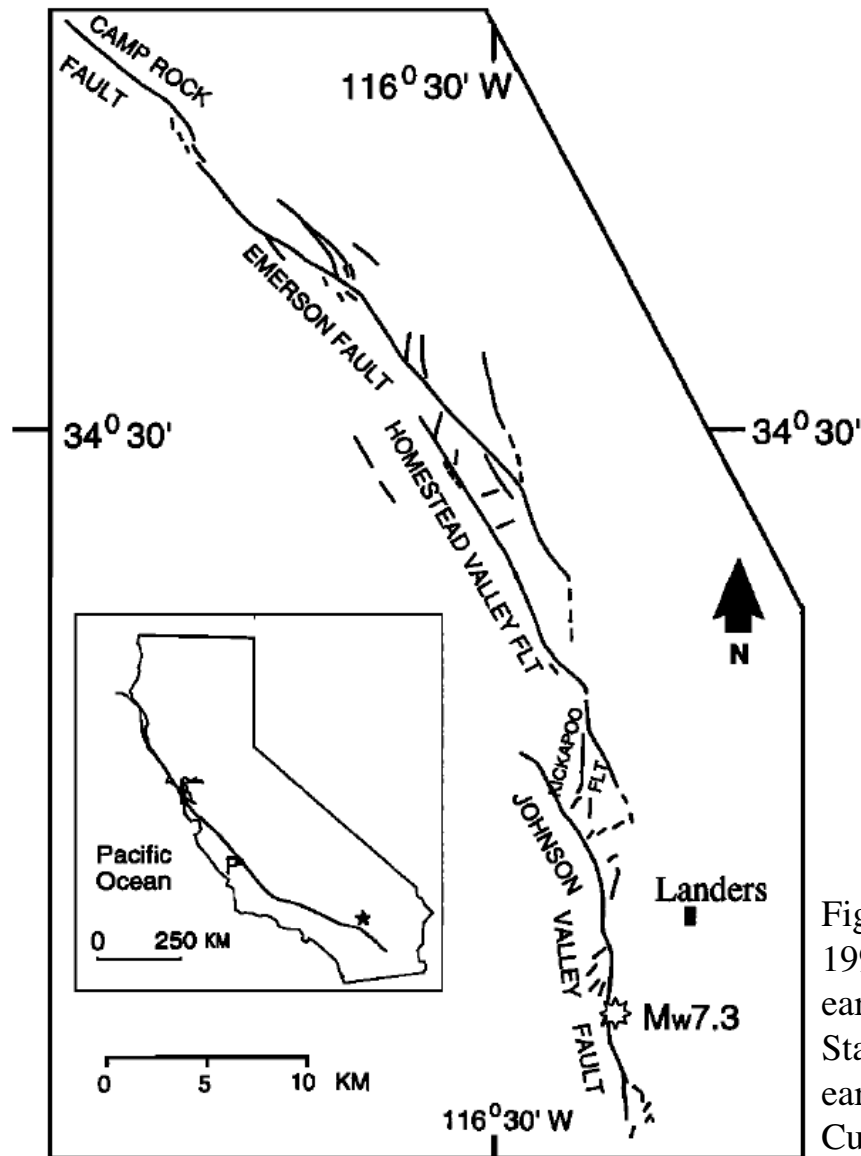
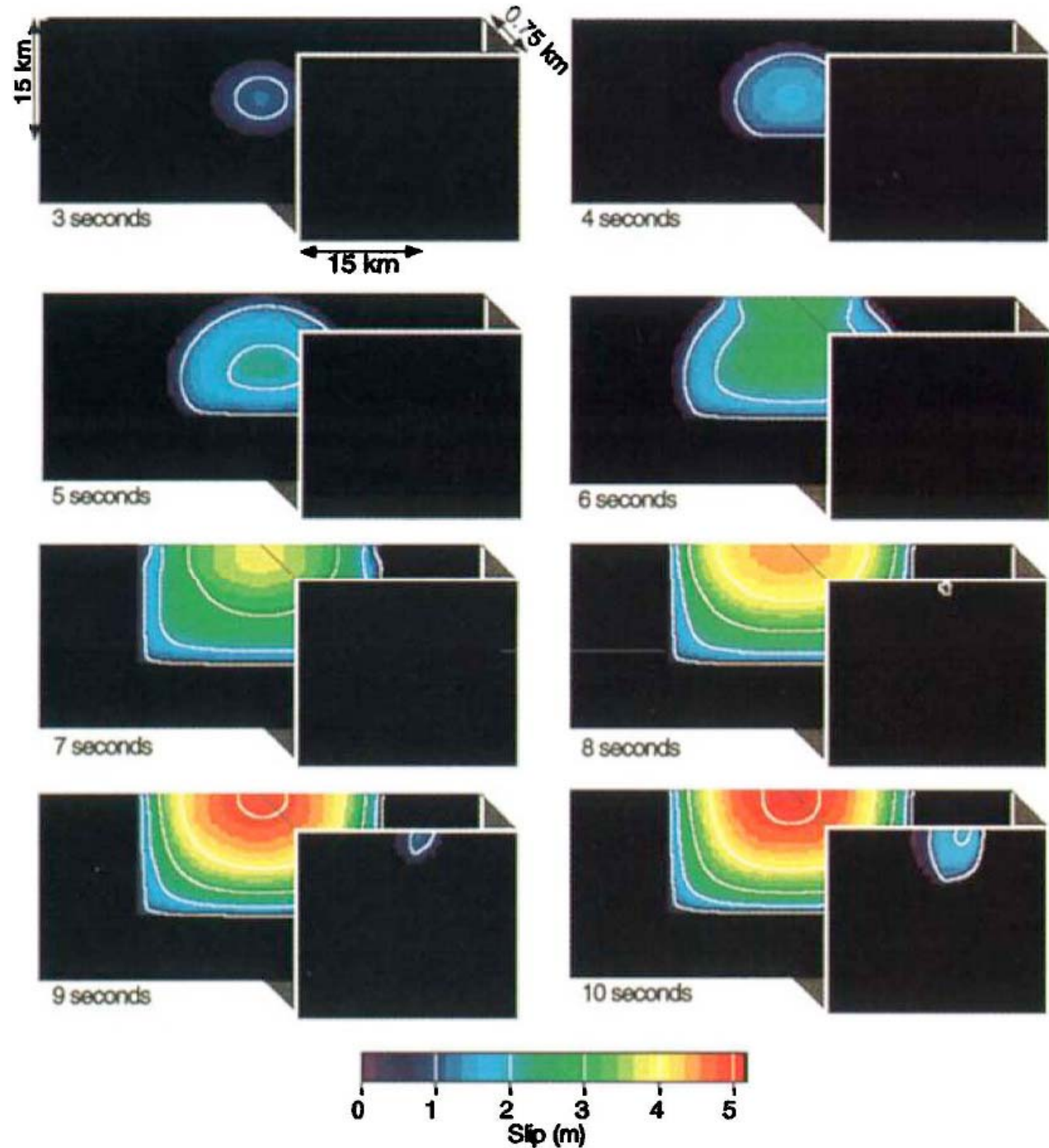


Figure 2. En echelon vertical strike-slip faults. A right step in a right-lateral strike-slip fault is a dilational stepover (depicted). A left step would be a compressional stepover. The perpendicular distance between the two faults is the stepover width, the overlap distance is measured along-strike. The simulated earthquake is nucleated in a region denoted by the star on the first fault plane, then allowed to spontaneously (unforced) propagate. Whether or not the earthquake can jump across the stepover between the faults depends on the fault geometry and the stress-conditions on the two faults.

Figure 1. Faults that ruptured during the 1992 Mw 7.3 Landers, California earthquake. Inset, outline of California. Star is the location of the Landers earthquake, P is the location of Parkfield. Curved line is the San Andreas fault.

Harris and Day, GRL, 1999

Figure 3. Simulation of a spontaneously propagating quake that nucleates on a fault near a 0.75 km-wide dilational step (Table I). Initial stresses are homogeneous over both 30-km long by 15-km deep fault planes; the material surrounding the faults is very strong so that the rupture cannot break into this 'intact rock'. Eight pictures show the slip on each fault plane, at 1 second intervals, starting 3 secs after nucleation. By 3 secs (upper left), the rupture has propagated outward, but is still far from the earth's surface and the ends of the first fault; no slip has occurred on the second fault. Soon after 5 secs the rupture has reached the earth's surface, by 7 secs the rupture has reached the ends of the first fault, but slip still has not occurred on the second fault. By 8 secs a very small patch of the second fault plane is slipping. The Jump occurred at 7.6 secs. By 9 secs a large patch is slipping on the second fault, and by 10 secs, it is clear that this is a successful jump, since a significant portion of the second fault is slipping.



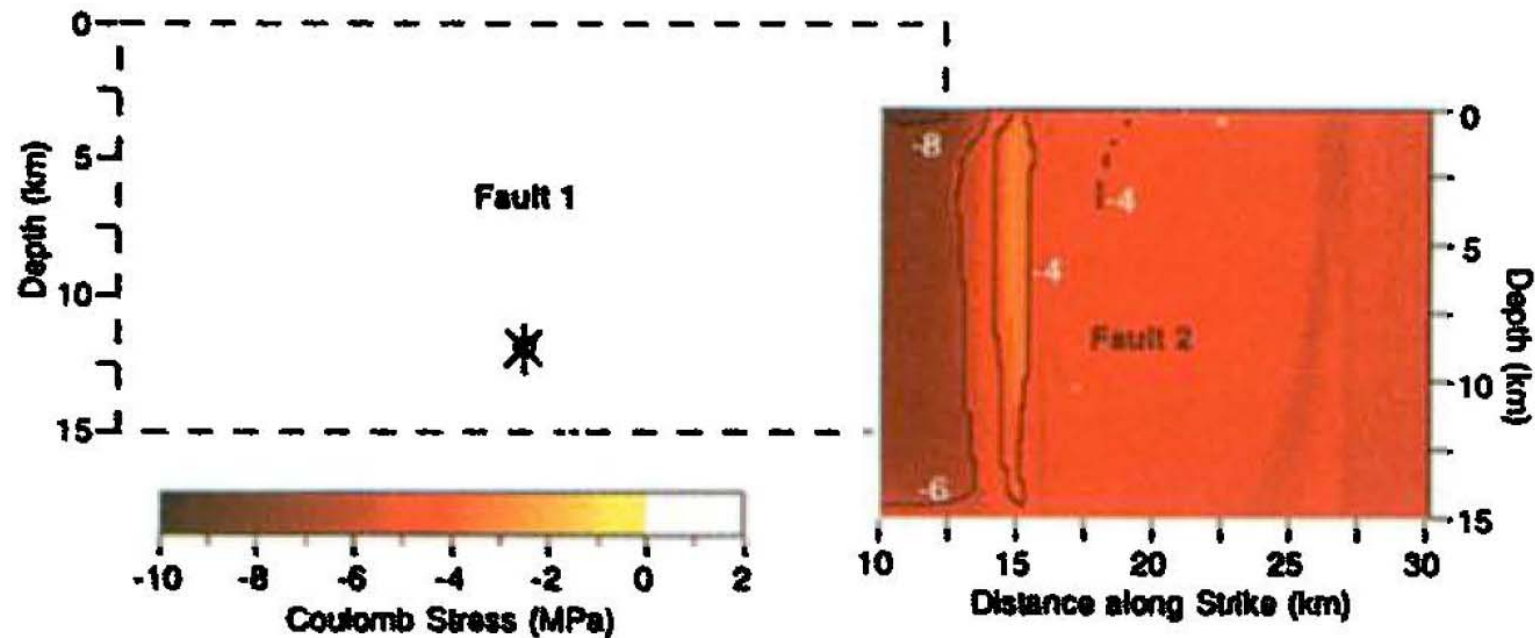


Figure 4. A 1 km stepover width at Parkfield [*Shedlock et al., 1990*] is consistent with seismicity modeling [*Eberhart-Phillips and Michael's, 1993, figure 8*]. Coulomb stress changes at 14 seconds after a simulated (2.4 MPa stress drop) 1934 earthquake show how this quake perturbs the stress field on the second fault plane (fault 2) even though it is unable to jump the step. A subsequent 1996-like quake is able to jump.

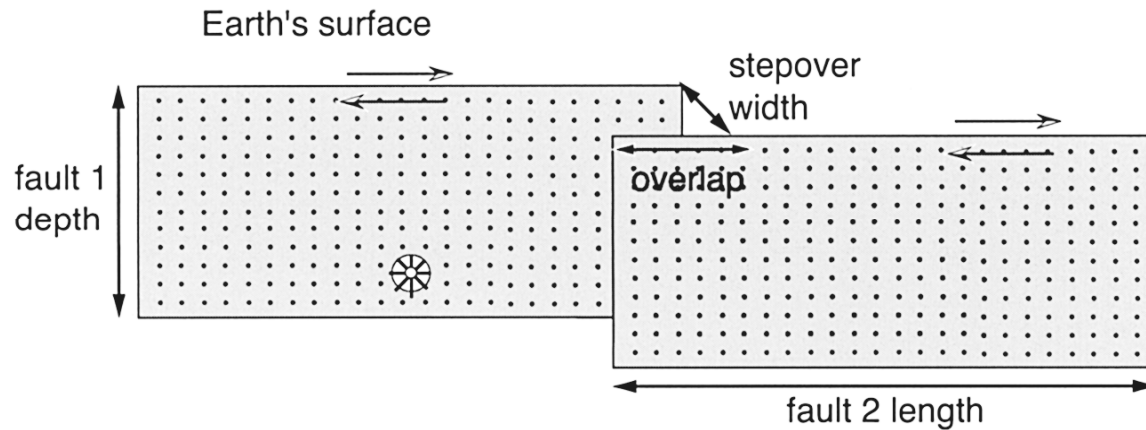


Figure 1. En-echelon vertical strike-slip faults. A right step in a right-lateral strike-slip fault is a dilational step-over (depicted). A left step would be a compressional step-over. The perpendicular distance between the two faults is the step-over width, and the overlap distance is measured along-strike. The simulated earthquake is artificially nucleated in a region, denoted by the star on the first fault plane, and is not forced, but is allowed to propagate spontaneously. Whether the earthquake can jump across the step-over between the faults depends on the fault geometry and the stress conditions on the two faults.

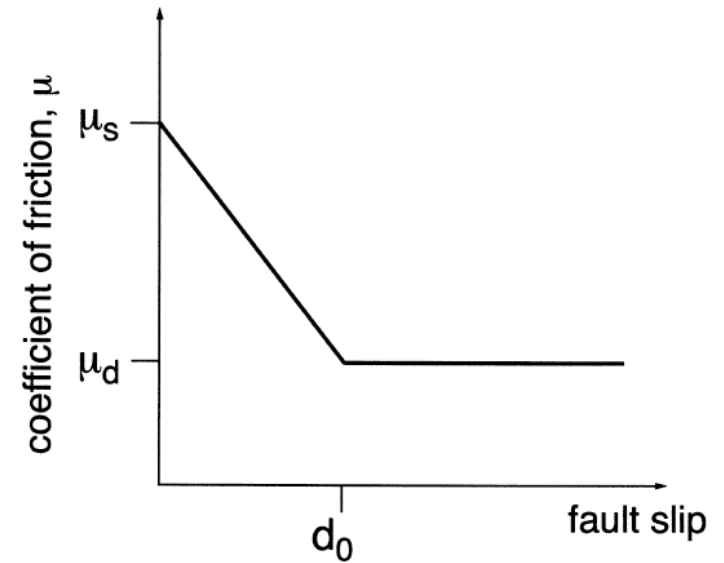


Figure 2. The slip-weakening fracture criterion (Ida, 1972; Andrews, 1976a,b; Day, 1982) determines when the fault can slip. The strength of a point on the fault is proportional to the time-dependent normal stress, with the proportional factor being the coefficient of friction, μ , which is determined by how much slip has occurred at that point. Initially, before any slip has occurred, μ equals μ_s , the static coefficient of friction. When the fault starts to slip, μ linearly decreases until the fault has slipped a distance called the critical distance, d_0 . After the fault has slipped d_0 , μ equals μ_d , the dynamic, or sliding friction. Table 1 lists the values of μ that we used in our simulations.

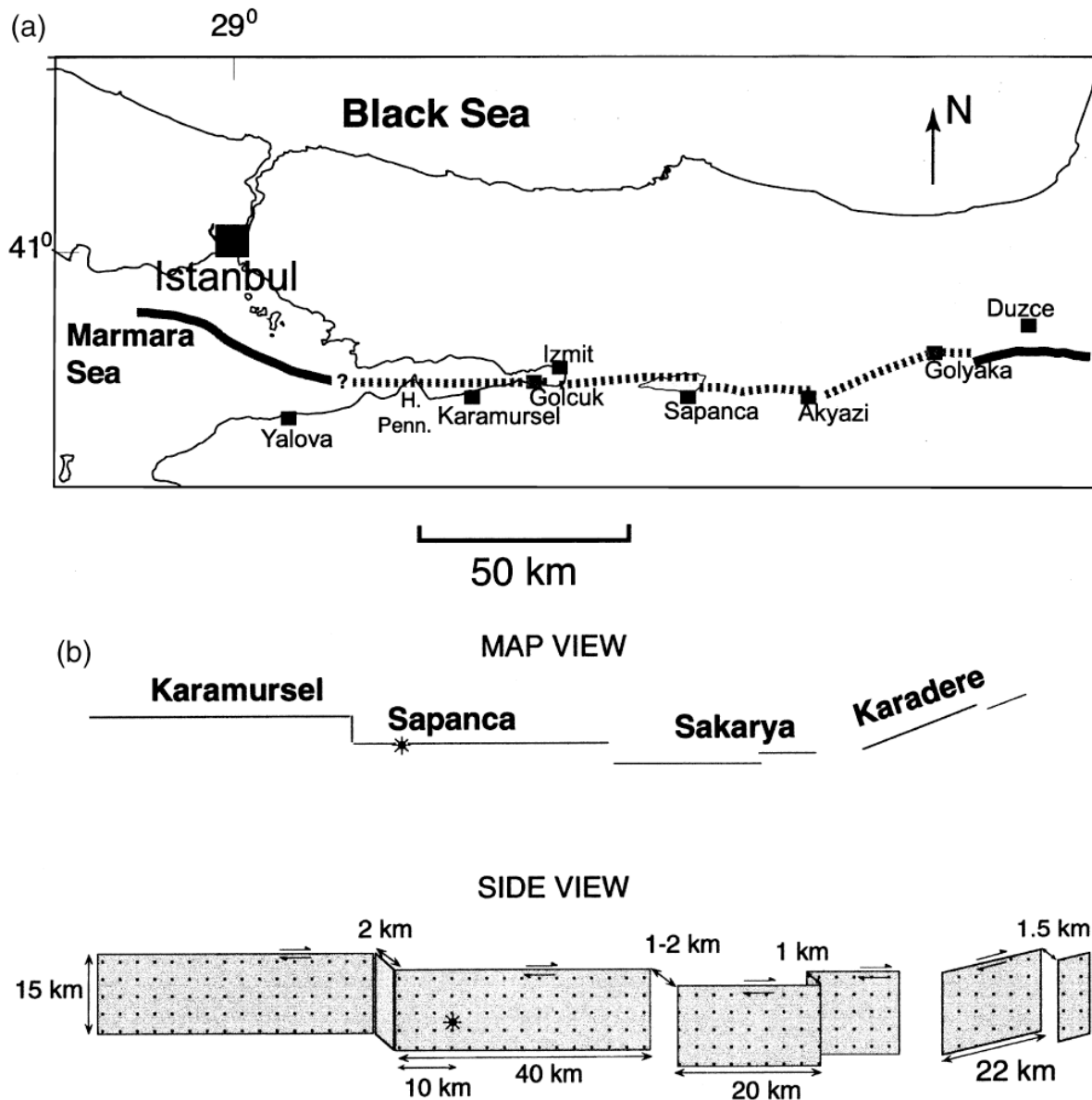
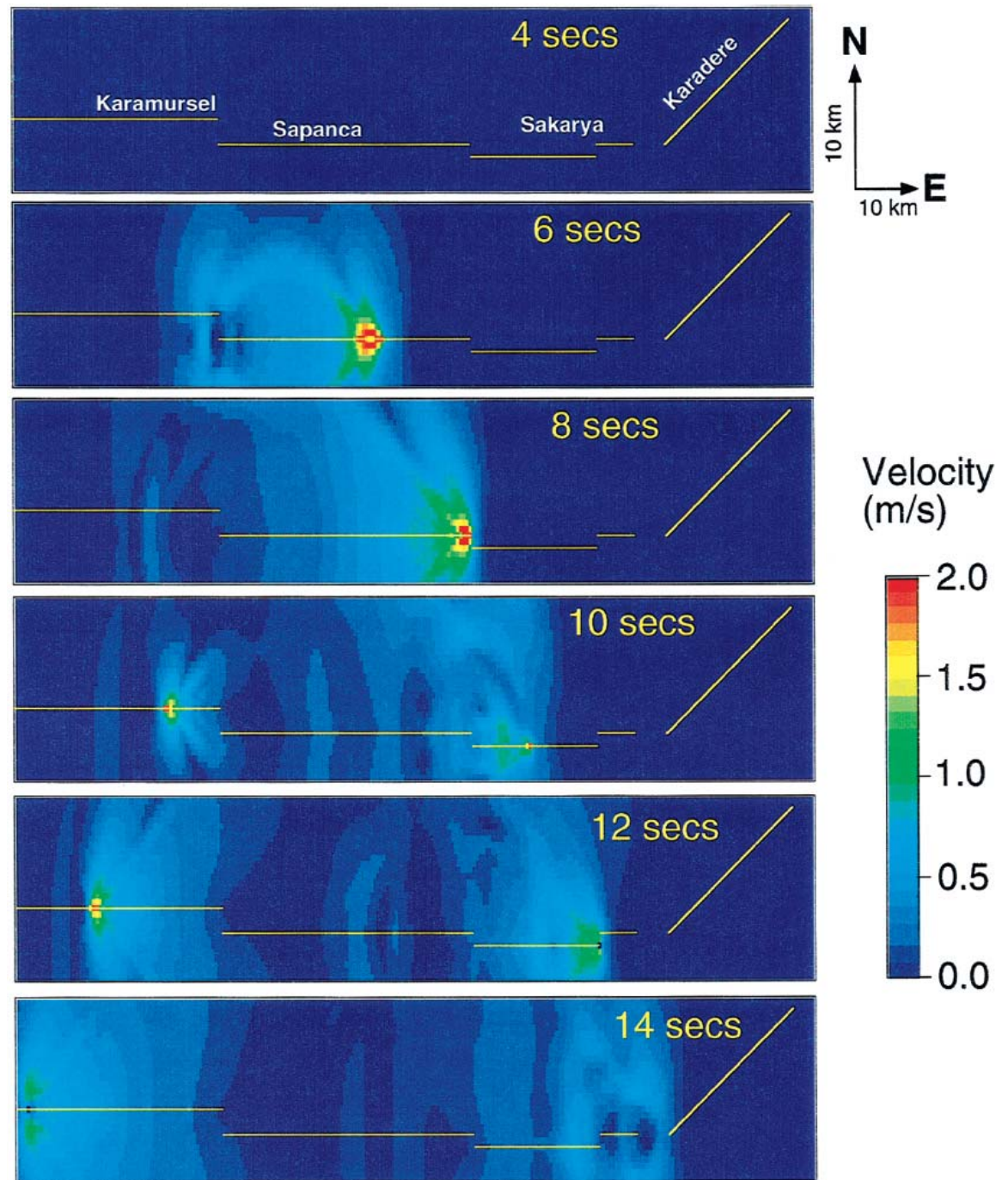


Figure 3. (a) Location of the 1999 Izmit earthquake rupture in Turkey is shown by the dashed gray fault segments (figure is modified from Barka, 1999; Parke *et al.*, 1999; Kusçu *et al.*, 2000; Okay *et al.*, 2000). The eastern solid dark gray fault segment shows the part of the North Anatolian fault that ruptured in the November 1999 M 7.2 Düzce earthquake. The western solid dark gray fault segment striking toward Istanbul is called the Princes Island strand of the North Anatolian fault. This portion of the fault probably did not rupture in 1999. The question mark indicates that we do not know exactly how the Karamursel fault segment connects to the Princes Island strand. H. Peninsula is the Hersek peninsula. The squares show locations of cities. (b) We use a simplified version of the coseismically active fault trace mapped by the geologists and inferred by the geodesists (Fig. 3a) and assume that the faults are primarily west–east-trending and extend vertically from the Earth’s surface down to 15-km depth. The Karadere segment is assigned a 22.5° change in strike from the other faults to the west. The simulated earthquake nucleates on the Sapanca segment, at 9-km depth, following the seismological observations.

Harris, Dolan, Hartleb
& Day, BSSA, 2002

Figure 4. The slip velocities at the Earth's surface resulting from a simulated earthquake that nucleates at 9-km depth along the Sapanca segment and then spontaneously propagates. In this example the step-over width at Sapanca Lake is assumed to be 1 km wide. At 4 sec after nucleation, the rupture has not yet made it to the Earth's surface but is propagating at depth in the updip, downdip, and along-strike directions on the Sapanca segment. At 6.04 sec the rupture makes the jump at the Earth's surface from the Sapanca to the Karamürsel segment (in this case there is no transfer fault). The rupture continues its progression westward on the Karamürsel segment and propagates until it reaches the (western) end of the Karamürsel segment. To the east, the rupture jumps to the Sakarya segment at depth at 8.08 sec and at the Earth's surface at 8.64 sec. The rupture jumps the compressional step-over within the Sakarya segment at 12.20 sec. The Karadere segment is first triggered at 14.16 sec (not shown in this figure).



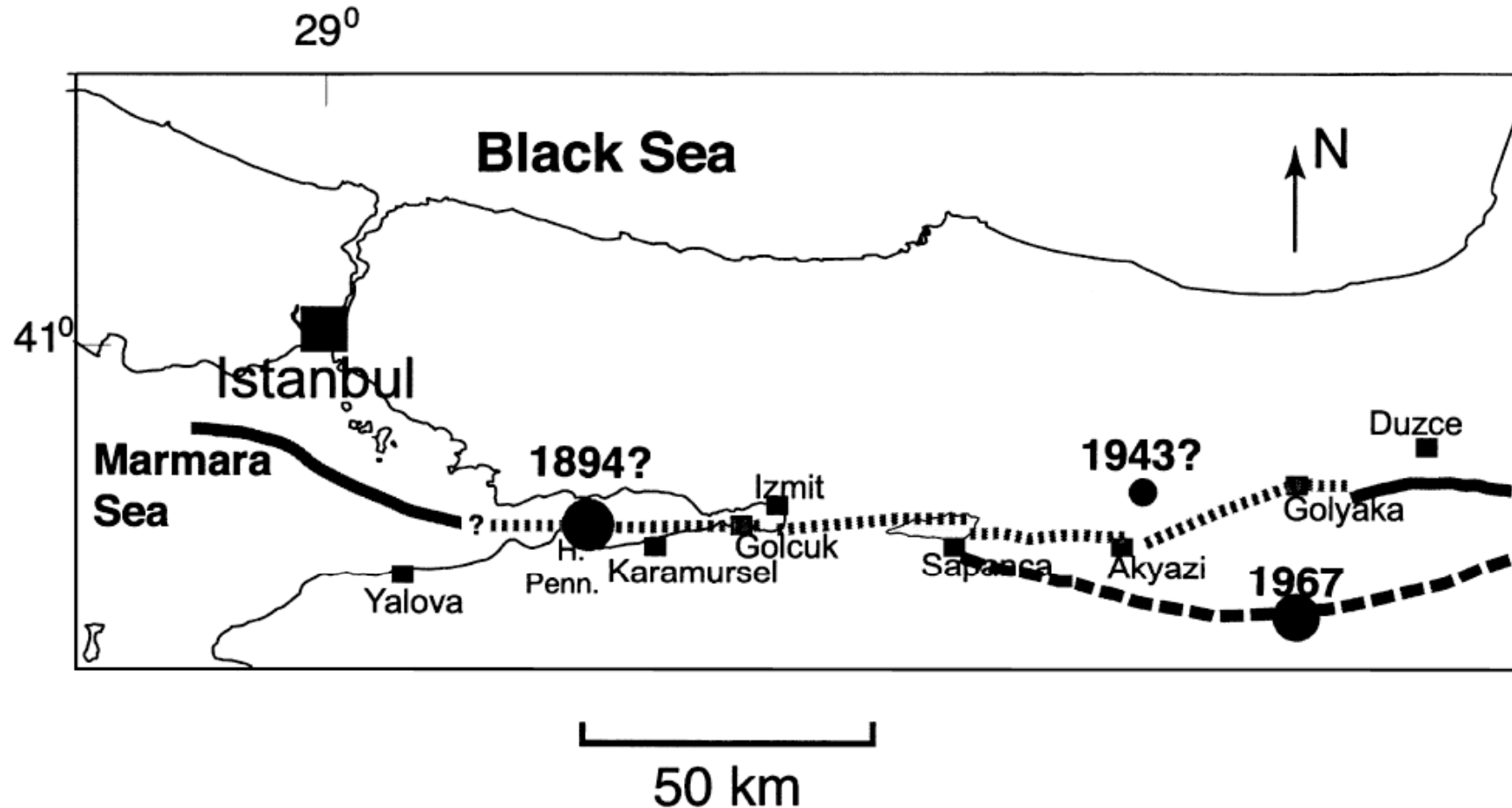
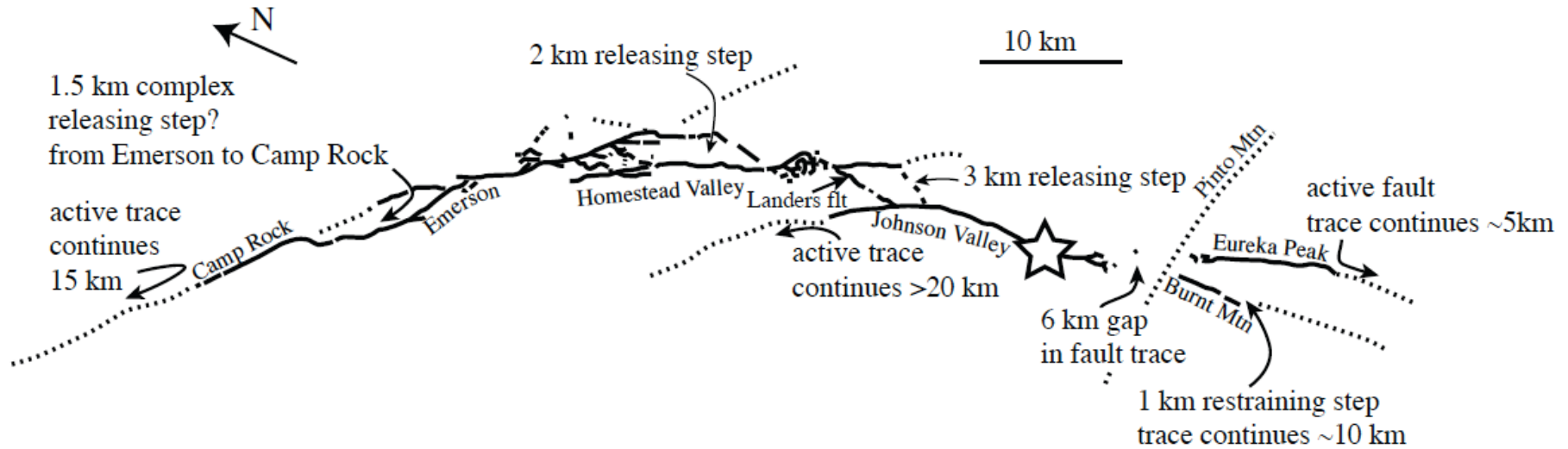
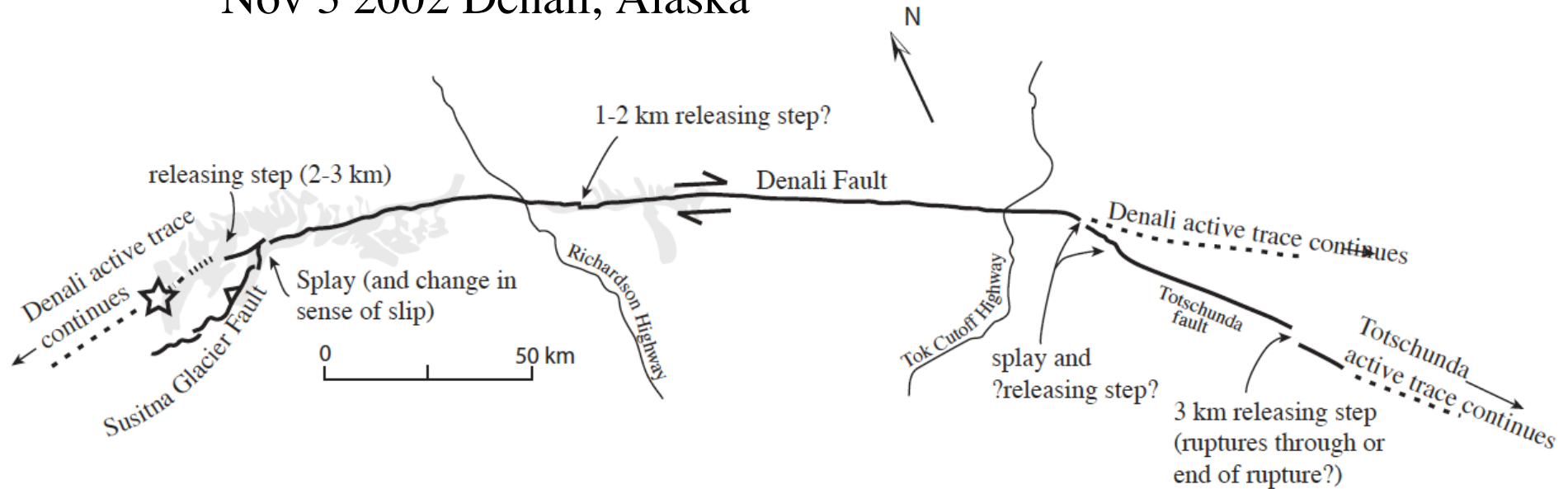


Figure 5. The 1943 Hendek-Adapazari and 1967 Mudurnu earthquakes occurred close to the 1999 İzmit earthquake, but the exact location of the 1943 earthquake is poorly known (Nalbant *et al.*, 1998). (Figure modified from Barka, 1999; Parke *et al.*, 1999; Kuşçu *et al.*, 2000; Okay *et al.*, 2000.) The 1894 earthquake occurred in the Marmara Sea (Ambraseys, 2001; Ambraseys and Jackson, 2000) and may have affected the westward rupture extent of the 1999 İzmit earthquake. H. Penn. is the Hersek peninsula.

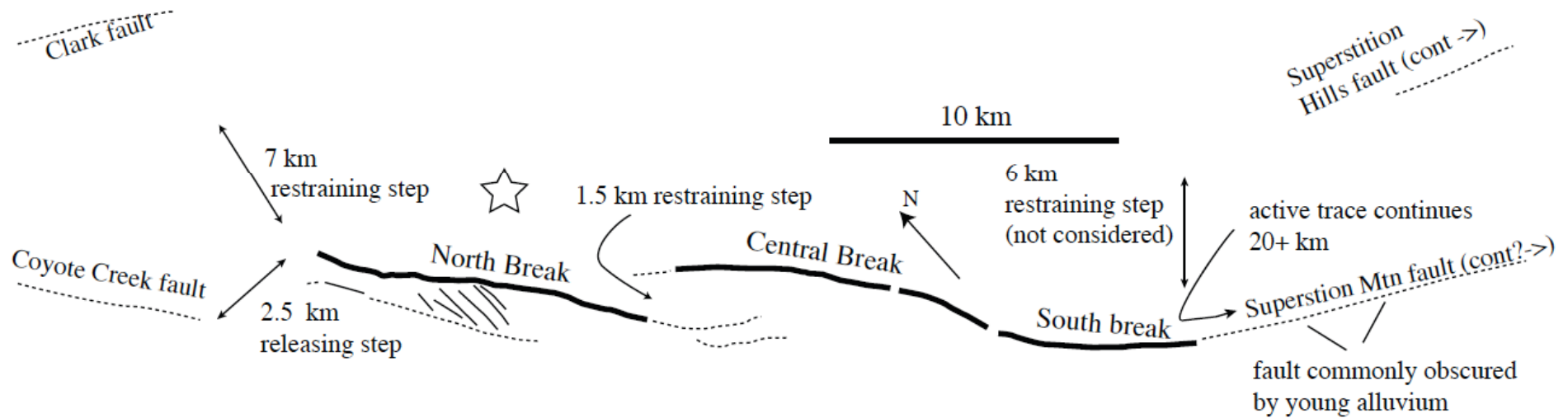
Jun 28 1992 Landers, California



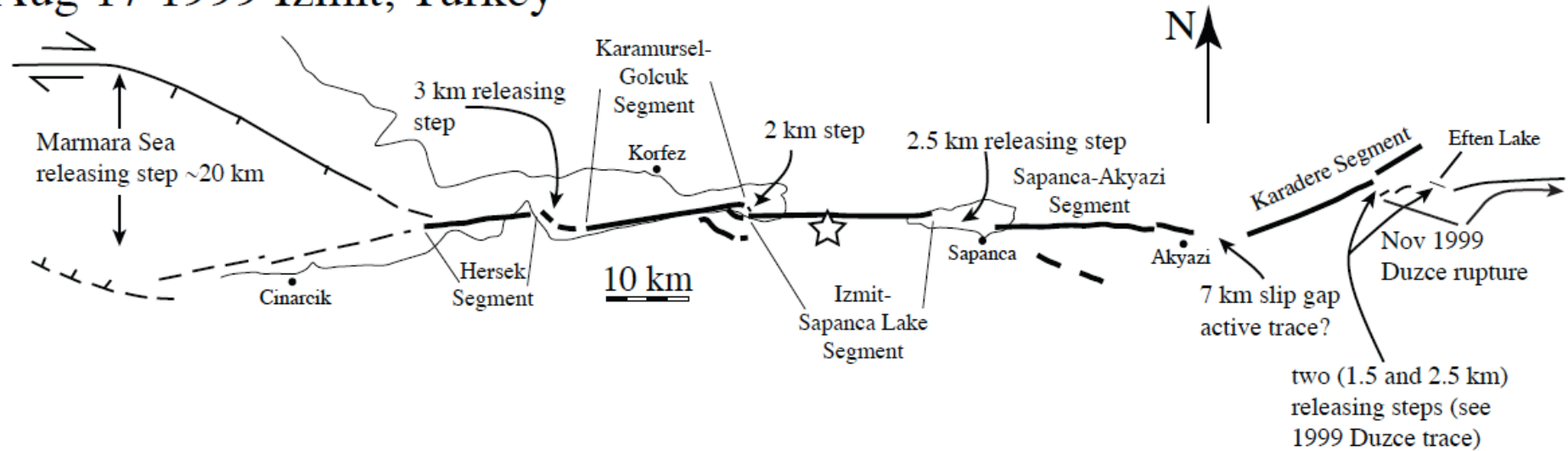
Nov 3 2002 Denali, Alaska



Apr 09 1968 Borrego Mountain, California



Aug 17 1999 Izmit, Turkey



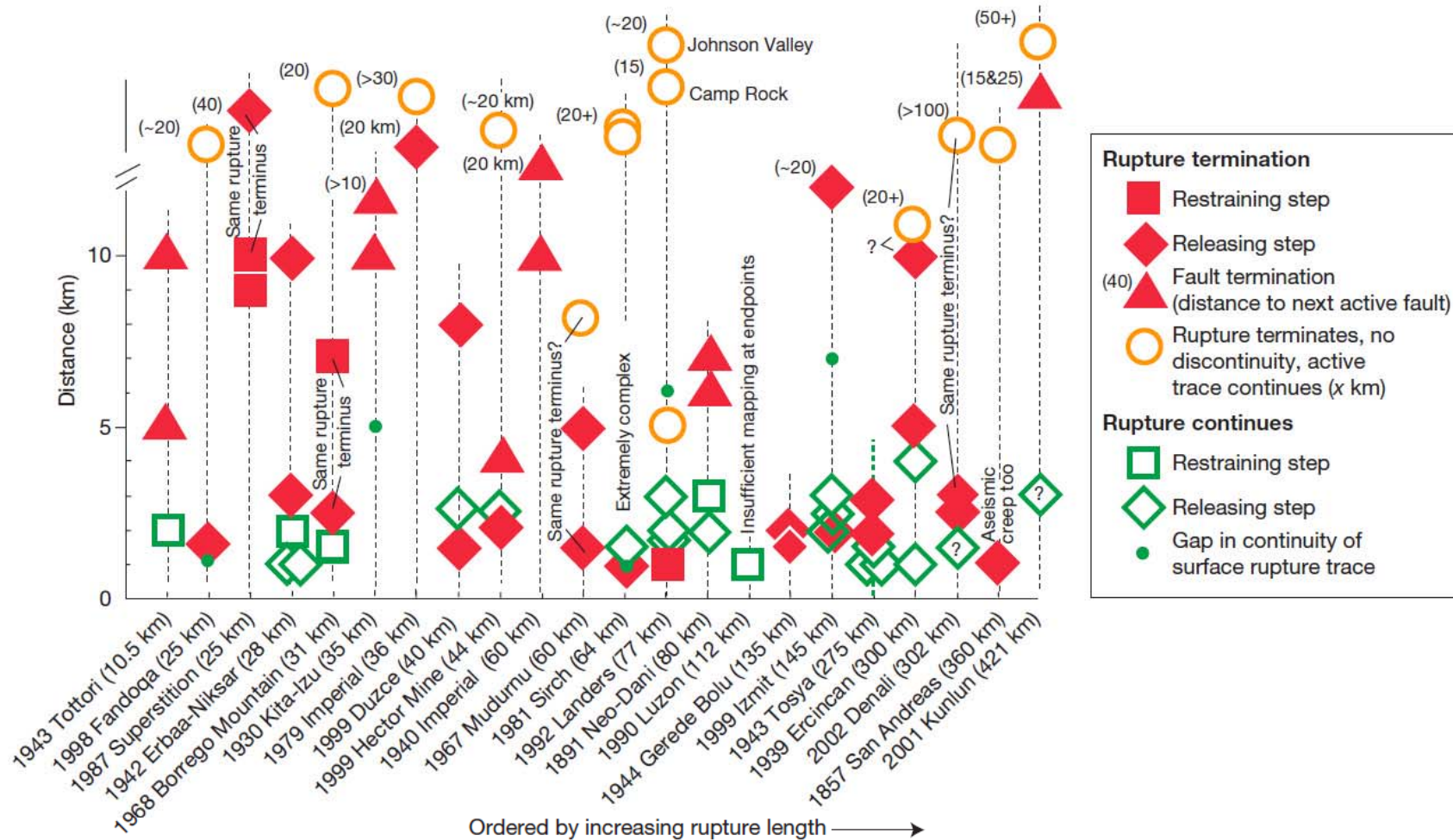
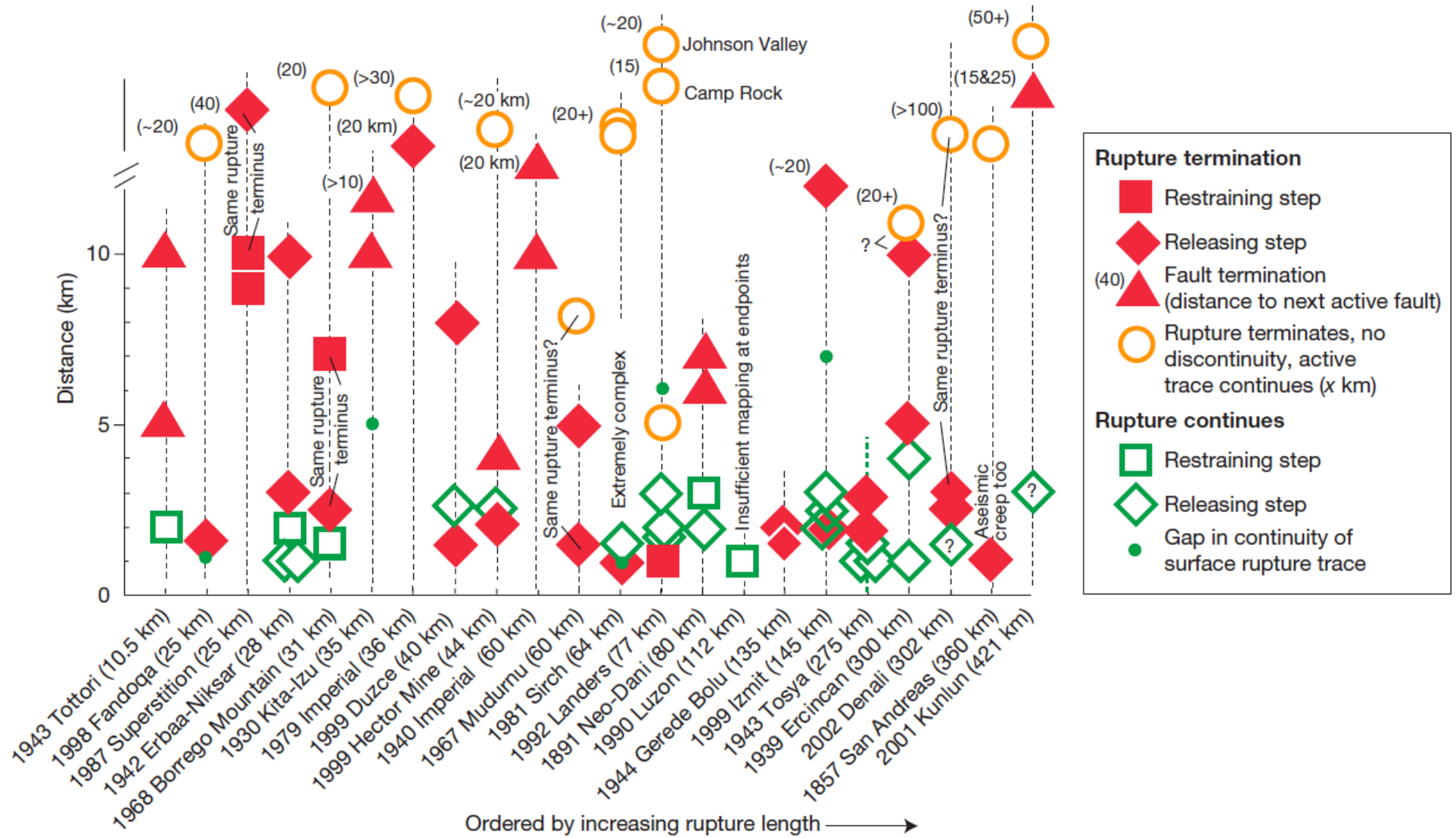


Figure 2 | Synopsis of observations bearing on relationship of geometrical discontinuities along fault strike to the endpoints of historical earthquake ruptures. Earthquake date, name and rupture length listed on horizontal axis. The earthquakes are ordered by increasing rupture length (but not scaled to distance along-axis). Above the label of each earthquake is a vertical line and symbols along line represent dimension of discontinuities within and at endpoints of each rupture. The dimension of discontinuities are measured as distance across fault step approximately perpendicular to fault

strike or the distance from rupture terminus to nearest-neighbouring active fault trace. Discontinuities through which ruptures passed (broke through) are green open squares and diamonds. Discontinuities located at ends of ruptures are red solid squares, triangles and diamonds. The orange open circles represent the endpoints or earthquake ruptures which are not associated with a geometrical discontinuity and the value next to each is an indicator of the distance along which the active trace continues past the endpoint of the historical rupture.

Wesnousky, Nature, 2006



Wesnousky, Nature, 2006

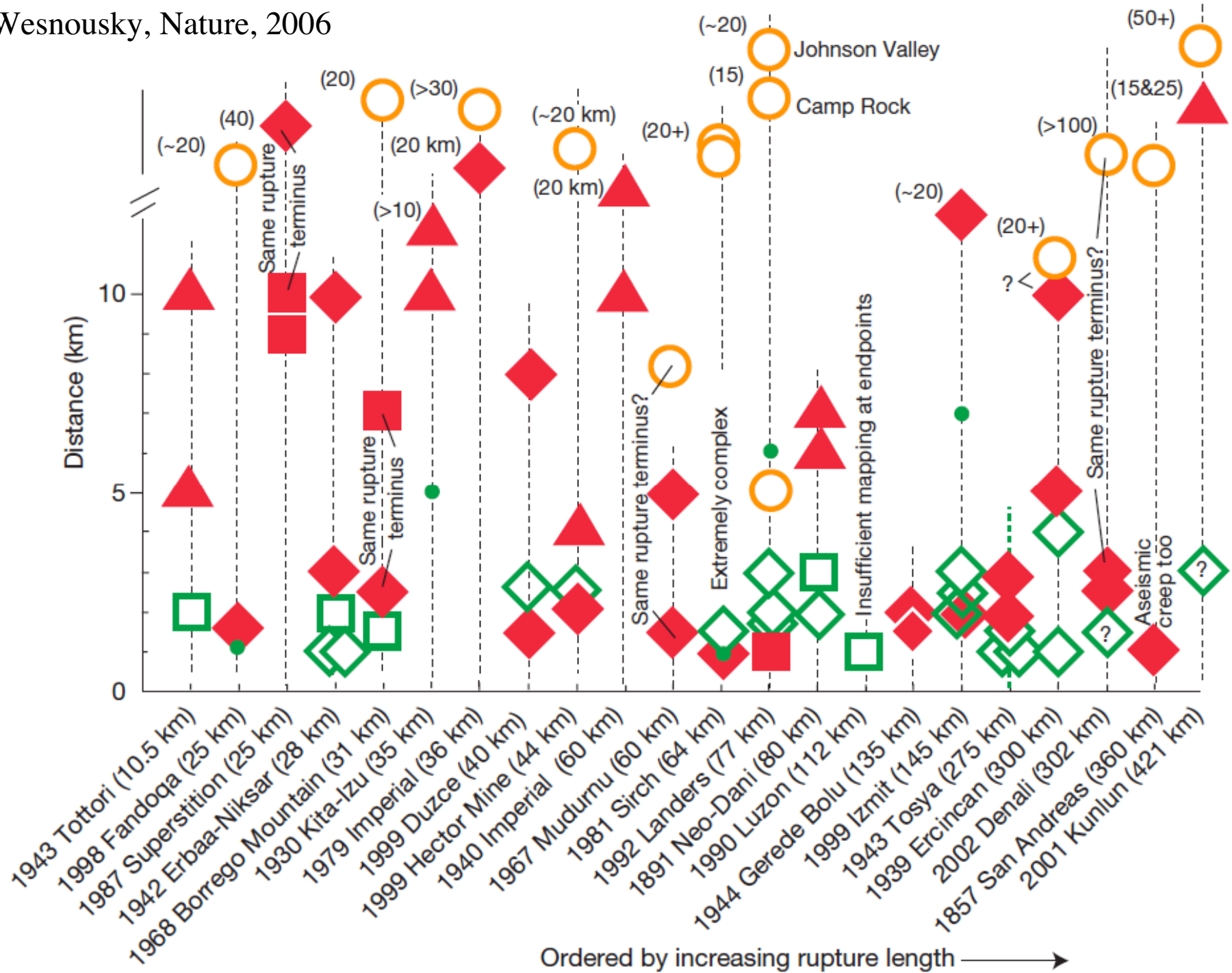
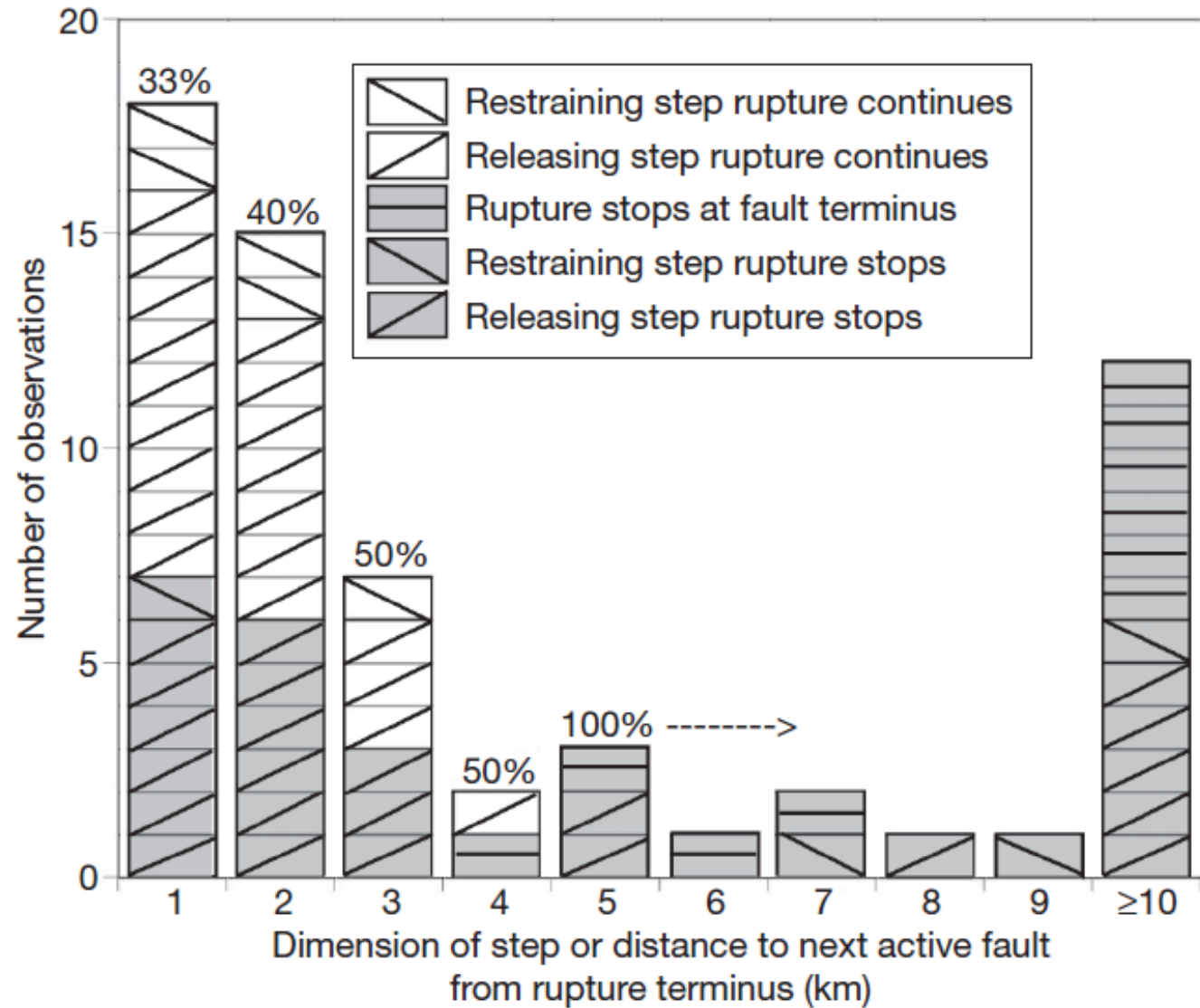


Figure 3 Geometrical discontinuities as a function of size. Histogram of the total number of geometrical discontinuities located along historical strike-slip ruptures binned as a function of size (≥ 1 , ≥ 2 , ...) and shaded according to whether the particular step occurred at the endpoint of rupture (shaded) or was broken through by the rupture.



TOPICS ADDRESSED

- **Forward branching**
- **Backward branching**
- **Role of finite branches**
- **Stepovers and jumping**

Papers and download links (page 1 of 2):

A. N. B. Poliakov, R. Dmowska and J. R. Rice, 2002: Dynamic shear rupture interactions with fault bends and off-axis secondary faulting. *Journal of Geophysical Research*, **107** (B11), *cn*:2295, *doi*:10.1029/2001JB000572, pp. ESE 6-1 to 6-18.

http://esag.harvard.edu/dmowska/PoliakovDmowskaRice_JGR02.pdf

N. Kame, J. R. Rice and R. Dmowska, 2003: Effects of pre-stress state and rupture velocity on dynamic fault branching. *Journal of Geophysical Research*, **108**(B5), *cn*: 2265, *doi*: 10.1029/2002JB002189, pp. ESE 13-1 to 13-21.

http://esag.harvard.edu/dmowska/KameRiceDmowska_JGR03.pdf

H. S. Bhat, R. Dmowska, J. R. Rice and N. Kame, 2004: Dynamic slip transfer from the Denali to Totschunda Faults, Alaska: Testing theory for fault branching. *Bulletin of the Seismological Society of America*, **94**(6B), pp. S202-S213.

http://esag.harvard.edu/dmowska/BhatDmRiKa_Denali_BSSA04.pdf

S. Fliss, H. S. Bhat, R. Dmowska and J. R. Rice, 2005: Fault branching and rupture directivity. *Journal of Geophysical Research*, 110, B06312, *doi*:10.1029/2004JB003368, 22 pages.

http://esag.harvard.edu/dmowska/FlissBhatDmRi_JGR05.pdf

Papers and download links (page 2 of 2):

H. S. Bhat, R. Dmowska, G. C. P. King, Y. Klinger and J. R. Rice, 2007: Off-fault damage patterns due to supershear ruptures with application to the 2001 Mw 8.1 Kokoxili (Kunlun) Tibet earthquake, *Journal of Geophysical Research*, 112, B06301, doi: 10.1029/2006JB004425, 19 pages.

http://esag.harvard.edu/dmowska/BhatDmKiKlRi_supershear_JGR07.pdf

H. S. Bhat, M. Olives, R. Dmowska and J. R. Rice, 2007: Role of fault branches in earthquake rupture dynamics, *Journal of Geophysical Research*, 112, B11309, doi: 10.1029/2007JB005027, 16 pages.

http://esag.harvard.edu/dmowska/BhatOlDmRi_FiniteBranch_JGR07.pdf

Templeton, E. L., A. Baudet, H. S. Bhat, R. Dmowska, J. R. Rice, A. J. Rosakis, and C.-E. Rousseau, 2009: Finite element simulations of dynamic shear rupture experiments and dynamic path selection along kinked and branched faults", *Journal of Geophysical Research*, doi:10.1029/2008JB006174, 17 pages.

http://esag.harvard.edu/dmowska/TempletonEtAl_BranchKink_JGR09.pdf

Templeton, E. L., H. S. Bhat, R. Dmowska, and J. R. Rice, 2010: Dynamic rupture through a branched fault configuration at Yucca Mountain and resulting ground motions, *Bulletin of the Seismological Society of America*, in press.

http://esag.harvard.edu/dmowska/TempletonBhDmRi_BranchYM_BSSA10.pdf